HYPOID GEAR NOISE AND VIBRATION CONTROL IN AUTOMOTIVE REAR AXLE SYSTEMS

by

CHIA-CHING LIN

DISSERTATION

Submitted in partial fulfillment of the requirements

for the degree of

DOCTOR OF PHILOSOPHY

in Aerospace Engineering

Committee Chair: Dr. Teik C. Lim

Members: Dr. Kent L. Lawrence

Dr. Robert L. Woods

Dr. Yawen Wang

Dr. Shih-Ho Chao

The University of Texas at Arlington

August 2020

ACKNOWLEDGEMENTS

I would like to express my sincere appreciation to my advisor, Dr. Teik C. Lim, who served as my academic advisor and committee chair, for his guidance and support throughout my graduate study. I am also very thankful to Dr. Robert L. Woods, Dr. Kent Lawrence, Dr. Yawen Wang, and Dr. Shih-Ho Chao for serving as my committee members and providing valuable instructions.

I would also like to show gratitude for the financial support provided by the National Chung-Shan Institute of Science and Technology. This research is also supported by the Hypoid and Bevel Gear Mesh and Dynamic Modeling Consortium and an individual project with Jian’an.

I wish to thank all my colleagues at the Vibro-Acoustic and Sound Quality Research Laboratory at the University of Texas at Arlington. I’m very appreciative of my mentor, Dr. Yawen Wang, who gave me his insightful suggestions and instructions. I also want to thank Dr. Weiqing Zhang for sharing his knowledge of gear manufacture. My special regards go to Dr. Sandeep Vijayakar at Advanced Numerical Solutions for his help and technical wisdom.

Finally, I would like to thank my mom and my wife En-Yu for their unconditional support and love.

ABSTRACT

HYPOID GEAR NOISE AND VIBRATION CONTROL IN AUTOMOTIVE REAR AXLE SYSTEMS

Chia-Ching Lin, Ph.D.

The University of Texas at Arlington, 2020

Supervising Professor: Teik C. Lim

Gear whine is a key issue for the vehicle powertrain system, and the design of a quiet, reliable driveline system is highly desirable for the automotive industry. From past studies, the main source of excitation for gear vibration and noise is the transmission error (TE), which generates the dynamic mesh force between the gear teeth. Then the vibration transmits through the flexible axle components and radiates off from the surface of the axle housing structure. The dynamic responses of the hypoid geared rotor system in the rear axle have a significant effect on the performance of noise, vibration, and harshness (NVH) for the vehicle design.

Hypoid gear noise and vibration reduction can be achieved by controlling the excitation source and the path transmissibility. However, the gear design optimization usually relies on the experience of gear engineers or trial-and-error approaches. Therefore, a robust method is needed to consider all the hypoid gear design parameters of both macro-geometry and micro-geometry, and to optimize the noise performance as well as meet the design criteria of strength and

durability. Moreover, the goals of gear designers and NVH engineers are different. The design goal needs to compromise to have a win-win situation on the axle system. Accordingly, an end-to-end solution is also needed to bridge the gap between gear designers and NVH engineers. In this study, a rear axle system modeling methodology is proposed which considers from gear design parameters to vibro-acoustic analysis. The simulation models can be applied to optimize the gear TE and tune the axle system dynamic parameters to make the system less sensitive to the given TE.

Firstly, gear tooth profile modifications (TPM) and machine tool settings are optimized to reduce TE and dynamic responses. The loaded tooth contact analysis (LTCA) is performed with some combinations of TPM and machine tool settings. An artificial neural network model, namely the Feed-Forward Back Propagation (FFBP), combined with improved Particle Swarm Optimization (PSO) algorithm, is constructed to predict the TE. The results of LTCA are used to train the model. With the optimal hypoid gear TPM and machine tool settings, system-level analysis of the vehicle axle system is performed to verify the improvement of dynamic response.

Secondly, an ease-off hypoid tooth surface modification methodology is applied. The ease-off surface is the deviation of the real design pinion surface from the ideal conjugate of its mating gear surface. The ease-off topography can be modified by different TPM parameters and machine tool settings. The highly sensitive parameters for ease-off topography is used to

construct the sensitivity matrix. The optimal design parameters can be calculated with the sensitivity matrix and the variation of ease-off topography between the target surface and the original surface.

Thirdly, a full axle system model is created to include the flexibility of axle shafts and bearings, manufactural and assembly errors, and axle housing geometry. The detailed finite element model and boundary element model of the axle housing is used to simulate the vibration response and noise radiation for the given work condition of the rear axle systems.

Finally, a case study is presented to validate the proposed method with experimental data of a hypoid gear rear axle system with specified design parameters and working conditions. The modal characteristics and dynamic response before and after the TPM are shown. The vibration and sound pressure measurements are compared with simulation results. The results conclude that the minimization of TE, the main excitation of vehicle axle gear whine noise and vibration, with optimal TPM parameters and tuning the system dynamics parameters can improve the overall NVH behavior. The proposed approach provides a better understanding of an optimal design hypoid gear set and axle components to efficiently control the noise and vibration of the automotive rear axle system.

Table of Contents

List of Figures

List of Tables

Chapter 1 Introduction

1.1 Motivation

Hypoid and bevel gear pairs are widely used in the automotive and aerospace industry to transmit torque between two non-parallel and non-intersecting crossed shafts. The most common applications are vehicle rear axle systems of rear-wheel-drive or all-wheel-drive powertrain and helicopter gearboxes. The rear axle system is designed to transfer power from the engine to wheels, allow the wheels to rotate at different speeds through its differential, and act as final gear reduction to increase the torque as Figure 1. However, the axle whine noise, a continuous, steady-state tonal sound, is always the major concern and the quality issue of the noise, vibration, and harshness (NVH) performance of the axle system. Such noise can be as a result of resonant conditions or the torque fluctuations from engine order vibration and gear transmission error excitation. The vibration transmitted through gear shafts and bearings to the axle housing and radiated as noise is the main mechanism of gear whine noise generation. Therefore, systematic research on dynamics and resonance characteristics of axle components and an approach for hypoid gear design aiming to reduce the vibration excitation are needed in order to design a smoother, quieter, more durable axle system application.

The goal of this study is to control the noise and vibration level on the vehicle axle system application by providing a comprehensive approach to analyze the system characteristics and dynamics and the gear design parameters, which have better performance for transmission error excitation and contact pattern. The dynamic response of the axle system, such as bearing reaction forces, housing surface velocity, and radiation noise are investigated and compared.

1.2 Literature Review

The NVH performance of a modern vehicle is an important factor to evaluate the design quality on ride comfort for the passenger. One of the influential sources of discomfort is noise and vibration induced by the powertrain system. Qatu [1, 2] presented an overview of automotive NVH engineering and a summary of recent research in the general area of NVH with an emphasis on the automotive field. The axle gear whine is the main noise source which is excited by the gear transmission error (TE). There are two ways to alleviate this problem, to reduce the TE fluctuation from gear design and manufacture and to tune the axle system parameters to desensitize the excitation. Wang [3-5] investigated the effect of component flexibility on TE and included gear-shaft interaction and gyroscopic effect into axle system dynamics. Tooth profile modification is one of the effective ways to reduce TE fluctuation and tooth contact pressure distribution from the gear design point of view. Hypoid and spiral bevel gears are designed in the rear axle system to transmit torque in the cross axis. Most of the earlier research on tooth profile modification or tooth surface optimization for hypoid and spiral bevel gear set discuss on reducing kinematic loaded TE and the maximum tooth contact pressure without the effect on dynamic behavior or discussing tooth profile modification influence on dynamics for other gear types, such as spur gears or planetary gears. Thus, the goal of this paper is to relate the effect of hypoid and spiral bevel gear tooth profile modification with the dynamic response on the vehicle axle system and provide an approach to optimize the tooth profile modification parameters for reducing the gear whine noise.

There are several types and different shapes of tooth profile modification for the different types of gear. For parallel axis gears with original involute tooth profile, such as spur, helical, and planetary gears, there are linear, parabolic, circular, straight, and quadratic form profile modifications [6]. Linear tip relief is the most popular method. For hypoid and spiral bevel gears, the tooth profile modifications achieved by head cutter variation or machine tool setting on gear generators. Simon [7-13] proposed an optimization methodology to systematically define head-cutter geometry and machine tool settings for face-hobbed hypoid and spiral bevel gears with reduced maximum tooth contact pressure and transmission errors. Shih [14, 15] developed a novel ease-off flank modification methodology for spiral bevel and hypoid gears made by a Cartesian-type gear generator. Fan [16] presented a high-order polynomial representation of the universal motions of machine tool settings on the CNC machine. Mu, et.al. [17] presented a novel tooth surface modification method for designing high contact ratio spiral bevel gears with a higher-order

TE.

The machine tool settings for the hypoid gear tooth generation are key parameters to manufacture desired mating tooth surfaces and have favorable contact patterns on pinion and gear. The methods on the determination of machine tool setting for the generation of hypoid gears by the local synthesis were published by Litvin et al [18]. The modifications of the machine tool settings can modify the micro-geometry of the tooth surface which can directly influence the transmission error (TE) and contact pressure of the gear pair. Minimizing TE and contact pressure of the hypoid gear pair improve not only the dynamic response of the rotor system but also the durability of the structure. Tooth modification induced by machine tool setting is one of the effective ways to reduce TE fluctuation and tooth contact pressure distribution from the gear design point of view. Most of the earlier research on tooth profile modification or tooth surface optimization for hypoid and spiral bevel gears focuses on TE and contact pressure optimization, and the discussion on dynamic behavior is sparse. Thus, the goal of this paper is to relate the effect of hypoid gear modification of machine tool setting with the dynamic response of the geared-rotor system and provide an approach to optimize the machine tool setting parameters for reducing TE.

Different amounts of tooth profile modification will influence the time vary mesh characteristics, including mesh stiffness, static TE, mesh point, and line-of-action (LOA). The hypoid geared rotor system dynamics will have different excitation force and dynamic characteristics due to different mesh stiffness and TE. Most previous studies investigated the impact of tooth profile modification on gear dynamics either for spur gear pairs [19-22] or planetary gear systems [23, 24]. The effects of tooth profile modification on the hypoid geared rotor system have been given less consideration.

The neural network algorithm is suitable for solving the design and optimization problem of hypoid gear pair because of the complex relationships between design parameters and mesh parameters. Hypoid pinion tooth cutter parameters, such as depth and angel of modification, can be used as inputs to get minimize transmission error and maximum contact pressure on the pinion surface. A popular neural network named Back Propagation (BP) algorithm is used to predict the minimum TE with the improved Particle Swarm Optimization (PSO) which is applied to optimize the weights of the BP algorithm. Sun, et.al. [25] studied this combined algorithm for optimization of hypoid gear spiral angle, gear pitch angle, and pinion pitch angle.

In this study, the effect of optimal hypoid gear tooth profile modification which is optimized by the IPSO-BP algorithm on axle dynamics is discussed. The vehicle rear axle system is presented by a 14-DOF lumped parameter hyoid geared rotor system. Finally, a case study is presented and the dynamic responses are calculated and compared between the baseline result and optimal result cases.

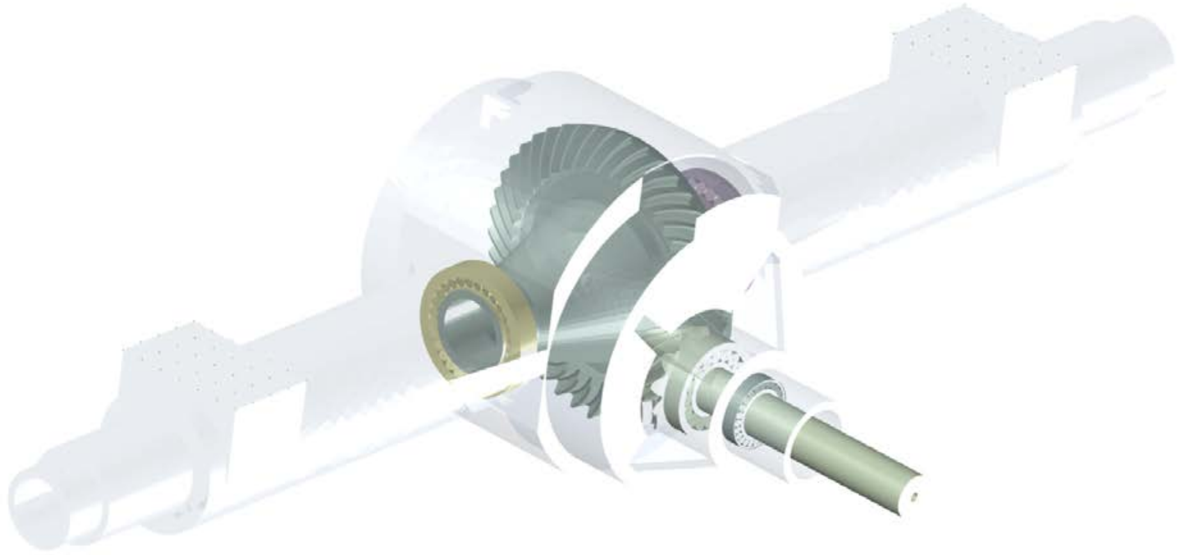

Figure 1 A vehicle rear axle system model. (Transmission 3D)

1.3 Scope and Objectives

From the previous review, the rear axle gear whine noise problem is a comprehensive issue from the gear design, component design and arrangement, and housing structure design to the entire system dynamic characteristic and noise control strategy. However, gear designers and NVH engineers have different design goals when they perform their job duties in an axle design and manufactory company. There is a gap between these two important roles when design a quiet, reliable axle system. Also, gear design optimization normally relied on the design experience of the gear designers or the method of trial-and-error. The design database for the gear design on a company should be put in good use. The design and testing process should be modularized into a standard operation process for sharing the design parameters and testing results.

The focus of this dissertation is to develop a simulation process for controlling the noise and vibration performance for a rear axle system. A comprehensive approach for this purpose is proposed, which provides the methodologies for optimization for the hypoid gear parameters, tuning the axle system dynamics, and evaluation for the response of finite element vibration analysis and boundary element vibro-acoustic analysis.

Through this dissertation, the following tasks are expected to be accomplished.

a) To control the noise and vibration level on the vehicle axle system application by providing an end-to-end solution from the gear design parameters to the vibro-acoustic analysis

b) To propose a robust method to consider all the hypoid gear design parameters of both macro-geometry and micro-geometry, and to optimize the noise performance as well as meet the design criteria of strength and durability

c) To train a neural network model that approximates the calculation of gear mesh characteristics and therefore simplifies the complexity of the analysis process and saves the computation time

d) To perform the ease-off modification on the hypoid gear tooth surface and control the ease-off topography and evaluate their contribution to the dynamic response and NVH performance.

e) To validate the simulation methodology with the experimental data of hypoid gear single flank rolling testing and the axle system NVH test

1.4 Organization

Chapter 1 presents the motivations, objectives, and literature review for this dissertation research. This chapter establishes the purpose of this study and discusses the previous work in hypoid gear geometry, design optimization, gear dynamics, and gear whine noise and NVH research.

Chapter 2 discusses the basis of the modeling of the hypoid gear generation, tooth contact analysis, and gear mesh and dynamic model. The analytic modeling of the hypoid gear tooth surface is generated by the concept of the manufacturing process of the hypoid gear generator. The mesh parameters are synthesized from the results of the loaded tooth contact analysis. The 14 degrees of freedom dynamic model is established for the axle geared-rotor system.

Chapter 3 constructs an artificial neural network model to predict and optimize the design parameters of the gear cutter profile for tooth profile modification. The particle swarm optimization algorithm is used to train and minimize the error of the neural network model. The dynamic analysis is performed to evaluate the improvement of the design modification on the dynamic response.

Chapter 4 constructs another artificial neural network model to predict and optimize the design parameters of the machine tool settings for tooth profile modification. Besides the particle swarm optimization algorithm, the gradient descent algorithm is also used to train and minimize the error of the neural network model. The dynamic analysis is performed to evaluate the improvement of the design modification on the dynamic response. The results of the different training algorithms are compared.

Chapter 5 performs the vibro-acoustic analysis from the dynamic results in Chapter 3 for the cutter profile parameters modification. The model analysis of axle housing is included. The output of the dynamic bearing forces are used as excitation for the steady-state housing vibration analysis and the surface velocity of the housing are interpolated into the boundary surface model as the vibro-acoustic source.

Chapter 6 implements the ease-off surface modification for the hypoid tooth surface. The variation of the ease-off topography between the desired tooth surface and the original surface and the sensitivity matrix which is constructed by the most influenced design parameter is used to solve the modification of these design parameters. The entire simulation process is performed to evaluate the reduction of noise and vibration by controlling the ease-off topography.

Chapter 7 validates the proposed simulation methodology with the experimental data of a real design product of an axle manufacturer. The results of gear single flank testing, the vibration measurement of accelerometers, and the sound pressure measurement of the microphones are compared with the simulation results. The correlation results are shown to validate the effectiveness of the simulation approach.

Chapter 8 gives the general conclusions and summary of the achievements in this dissertation and some recommendations for future work.

Chapter 2 Basis of Modeling of Gear Mesh and Dynamics

2.1 Hypoid Gear Mesh Model

The hypoid gear mesh parameters can be derived from the contact load distribution results which are calculated by a 3-dimensional quasi-static loaded tooth contact analysis program for hypoid and spiral bevel gears [27]. This program combines the semi-analytical theory with the finite element method which can solve the gear tooth contact program efficiently [28]. A hypoid gear pair with multiple contact interfaces are shown in Figure 2(a). The contact cells inside the mesh region are shown in Figure 2(b). The position vector of each contact cells can be defined as $r_i \ (r_{ix}, r_{iy}, r_{iz})$ with respect to the fixed mesh coordinate system. Correspondingly, the normal vector is $n_i \ (n_{ix}, n_{iy}, n_{iz})$ and the contact force is f_i.

The total contact force on all the engaging surfaces is calculated by summing the contact forces on each contact cell. Assuming there are N contact cells.

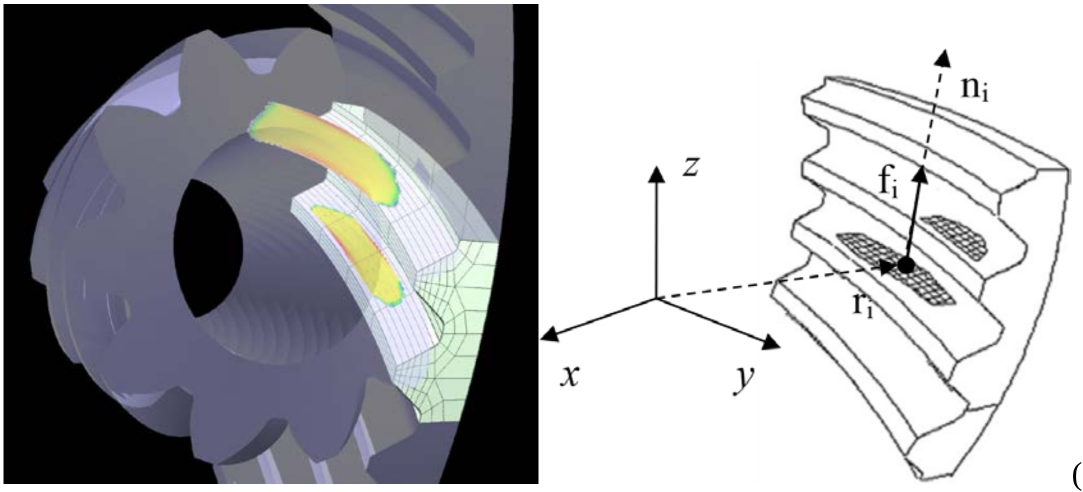

(a)

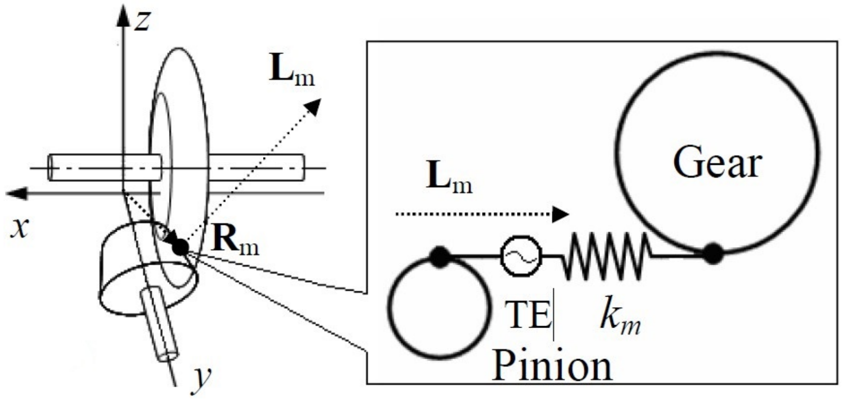

(b)

Figure 2 Illustration of (a) quasi-static loaded tooth contact analysis and Contact cells on the engaging surface (the FE/CM model)

(b) Effective mesh point R_m, LOA L_m, and mesh stiffness k_m [26]

$$F_j = \sum_{i=1}^{N} n_{ij} f_i \quad , F_{total} = \sqrt{\sum_{j=x}^{z} F_j^2}, (j = x, y, z) \tag{2-1}$$

The line-of-action vector L_m (n_x, n_y, n_z) can be obtained from

$$n_j = \frac{F_j}{F_{total}}, (j = x, y, z) \tag{2-2}$$

The total contact moment is given by

$$M_x = \sum_{i=1}^{N} f_i \, [n_{iz} r_{iy} - n_{iy} r_{iz}] \tag{2-3a}$$

$$M_y = \sum_{i=1}^{N} f_i \, [n_{ix} r_{iz} - n_{iz} r_{ix}] \tag{2-3b}$$

$$M_z = \sum_{i=1}^{N} f_i \, [n_{iy} r_{ix} - n_{ix} r_{iy}] \tag{2-3c}$$

The mesh point R_m (x_m, y_m, z_m) can be obtained from

$$y_m = \frac{\sum_{i=1}^{N} r_{iy} f_i}{\sum_{i=1}^{N} f_i} \tag{2-4a}$$

$$x_m = (M_z + F_x y_m)/F_y \tag{2-4b}$$

$$z_m = \left(M_y + F_z x_m\right)/F_x \tag{2-4c}$$

The translational loaded and unloaded transmission errors e_L and ε_0 are the projections of corresponding angular transmission error along the line of action. Finally, the mesh stiffness is defined by

$$k_m = F_{total}/(e_L - \varepsilon_0) \tag{2-5}$$

The above representations are then combined with the geared rotor system dynamic model to enable TE excitation to be applied reasonably well and also to compute meaningful gear mesh response.

2.2 Coupled Multi-body Dynamic Model

The vehicle axle system dynamics can be simulated as the 14 degrees of freedom lumped parameter model of the hypoid geared rotor system which is similar to the model used in Tao's study [26] in Figure 3. The equations of the motion of the geared rotor system in matrix form can be written as

$$[M]\{\ddot{x}\} + [C]\{\dot{x}\} + [K]\{x\} = \{F\} \tag{2-6}$$

where

$$\{x\} = \left\{\theta_D, x_p, y_p, z_p, \theta_{px}, \theta_{py}, \theta_{pz}, x_g, y_g, z_g, \theta_{gx}, \theta_{gy}, \theta_{gz}, \theta_L\right\}^T \tag{2-7}$$

$$[M] = diag\{I_D, M_p, M_p, M_p, I_{px}, I_{py}, I_{pz}, M_g, M_g, M_g, I_{gx}, I_{gy}, I_{gz}, I_L\} \tag{2-8}$$

The stiffness matrix $[K]$ is the lumped shaft-bearing assembly support stiffness and also the function of mesh stiffness and static TE. The damping matrix $[C]$ is assumed to be the viscous type and derived from the damping ratio and mode shape matrix.

The force vector can be written as

$$\{F\} = \{T_D, h_p F_m, -h_g F_m, -T_L\} \tag{2-9}$$

The dynamic mesh force F_m and directional transformation vectors h_l are defined as

$$F_m = \begin{cases} k_m(\delta_d - \varepsilon_0 - b_c) + c_m(\dot{\delta_d} - \dot{\varepsilon_0}) & if \ \ \delta_d - \varepsilon_0 \geq b_c \\ 0 & if \ \ 0 < \delta_d - \varepsilon_0 \leq b_c \\ k_m(\delta_d - \varepsilon_0) + c_m(\dot{\delta_d} - \dot{\varepsilon_0}) & if \ \ \delta_d - \varepsilon_0 \leq 0 \end{cases}$$

(2-10)

$$h_l = \{n_{lx}, n_{ly}, n_{lz}, \lambda_{lx}, \lambda_{ly}, \lambda_{lz}\}, l = p, g \tag{2-11}$$

where δ_d is dynamic TE excitation and ε_0 is unloaded TE. The gear backlash is represented by b_c. The directional rotation radius λ_l are defined as

$$\lambda_{lx} = \ L_l \cdot (X_l \times R_l) = y_l n_z - z_l n_y$$

$$\lambda_{ly} = \ L_l \cdot (X_l \times R_l) = z_l n_x - x_l n_z$$

$$\lambda_{lz} = \ L_l \cdot (Z_l \times R_l) = x_l n_y - y_l n_x \tag{2-12}$$

where L_l and R_l is the line of action and mesh point in the pinion coordinate system ($l = p$) or gear coordinate system ($l = g$), and X_l, Y_l, Z_l are the unit vectors in the pinion or gear coordinate system. The dynamic TE on the pinion and gear side can be given by

$$\delta_d = h_p^T\{x_p, y_p, z_p, \theta_{px}, \theta_{py} - \theta_{gy} * R, \theta_{pz}\} - h_g^T\{x_g, y_g, z_g, \theta_{gx}, 0, \theta_{gz}\} \tag{2-13}$$

$$\delta_d = h_p^T\{x_p, y_p, z_p, \theta_{px}, 0, \theta_{pz}\} - h_g^T\{x_g, y_g, z_g, \theta_{gx}, \theta_{gy} - \theta_{py}/R, \theta_{gz}\} \tag{2-14}$$

These account for the system dynamic response in addition to the kinematic effect of TE. R is the nominal gear ratio.

$$R = \lambda_{gy}/\lambda_{py} \tag{2-15}$$

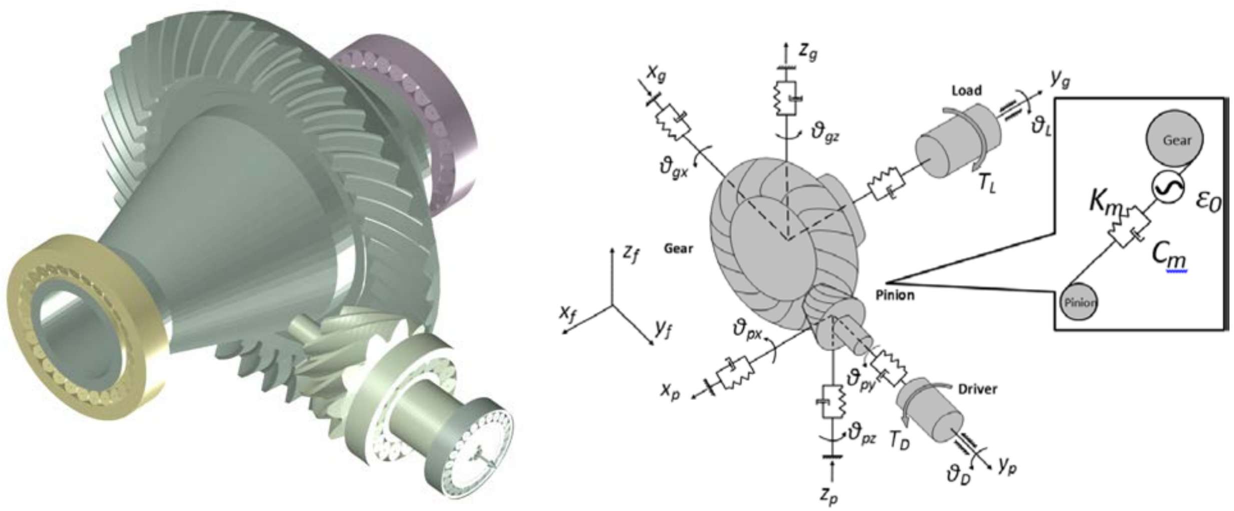

Figure 3 A lumped parameter model of the hypoid geared rotor system [4] (Transmission 3D)

2.3 Shaft-bearing Stiffness Model

The effective lumped parameter shaft-bearing support stiffness matrix is synthesized from the shaft-bearing stiffness model. A static beam FE model is applied for the calculation of effective shaft-bearing lumped stiffness matrix, and the static stiffness of the shaft and bearings under mean mesh load is used. The pinion overhung and gear straddled mounting is assumed as shown in Figure 4. Each bearing is represented as a stiffness matrix that is applied as a spring-type element between the node at the actual bearing center location and a node for the rigid housing. The bearing stiffness matrix is computed based on a set of nonlinear bearing load-displacement equations. It is assumed that the operating load variation does not have a significant influence on the bearing stiffness.

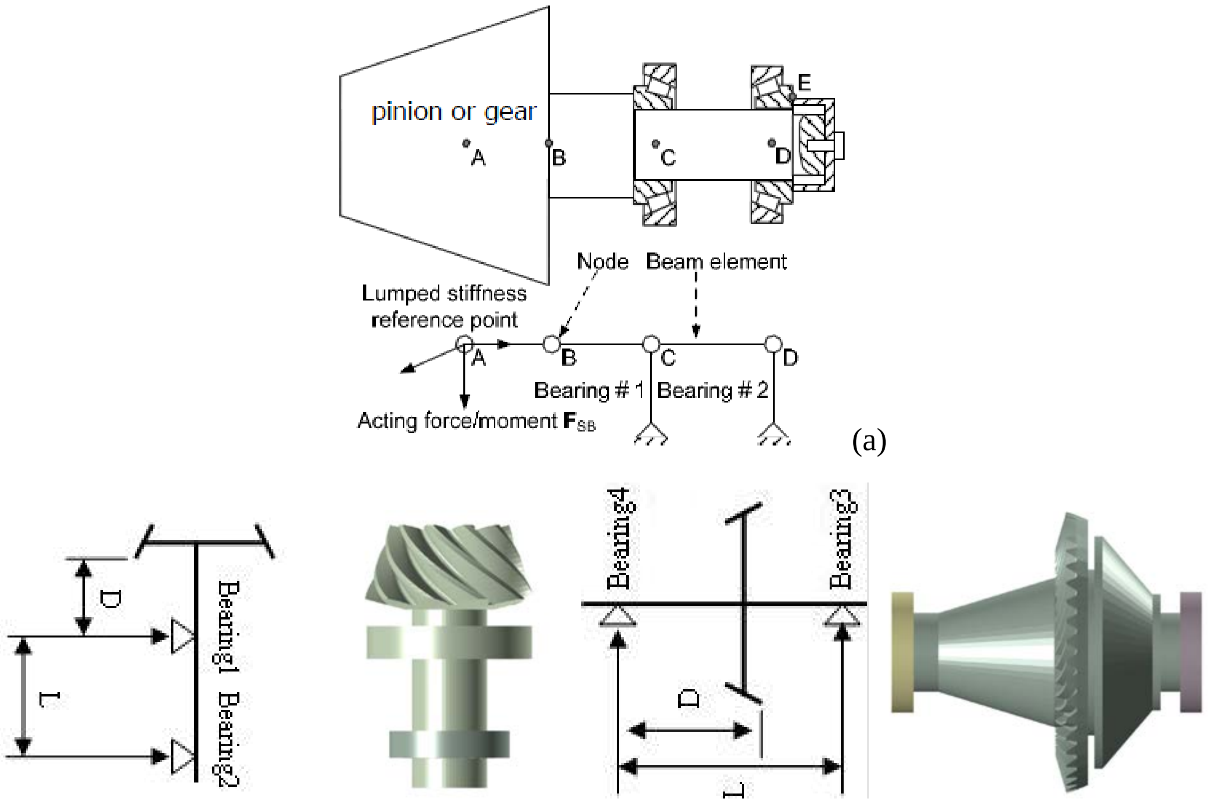

(a)

(b)

Figure 4 Illustrations of a) shaft-bearing lumped model; b) shaft-bearing layout [4]

The load-displacement relation at the effective lumped support point can be derived by

$$\begin{Bmatrix} [\Delta_{SB}]_{5x5} \\ [\Delta_{other}] \end{Bmatrix}_{5xn} = [K_{FE}]^{-1}_{nxn} \begin{Bmatrix} [\mathrm{F}_{SB}]_{5x5} \\ 0 \end{Bmatrix}_{5xn} \quad (2\text{-}16)$$

where $[\Delta_{SB}]$ is the displacement in the five degrees of freedom (DOF) of the node at the lumped stiffness point, $[\Delta_{other}]$ is the other DOF displacement, $[K_{FE}]$ is the assembly stiffness matrix of the beam finite element mode, $[\mathrm{F}_{SB}]$ is a matrix formed by five sets of forcing vectors acting on the reference node. The effective lumped stiffness matrix can be determined by

$$[\mathrm{K}_{SB}]_{5x5} = [\mathrm{F}_{SB}][\Delta_{SB}]^{-1} \quad (2\text{-}17)$$

The full lumped stiffness matrix in Eq. (1) can be assembled by

$$[K] = Diag[\ldots[\mathrm{K}_{SB}]\ldots] + Diag[\ldots[\mathrm{K}_m]\ldots] + Diag\left[[\mathrm{K}_{tp}]\ldots[\mathrm{K}_{tg}]\right] \quad (2\text{-}18)$$

where $[\mathrm{K}_m]$ is the gear mesh coupling stiffness matrix, $[\mathrm{K}_{tp}]$ is the coupling stiffness matrix of the torsional spring that connects the pinon and the engine, and $[\mathrm{K}_{tg}]$ is the coupling stiffness matrix of the torsional spring that connects the gear and the load.

Chapter 3 Optimization of Hypoid Gear Tooth Profile Modifications on Vehicle Axle System Dynamics

3.1 Introduction

The NVH performance of a modern vehicle is an important factor to evaluate the design quality on ride comfort for the passenger. One of the influences sources of discomfort is noise and vibration induced by the powertrain system. Qatu [1, 2] presented an overview of automotive NVH engineering and a summary of recent research in the general area of NVH with an emphasis on the automotive field. The axle gear whine is the main noise source which is excited by the gear transmission error (TE). There are two ways to alleviate this problem, to reduce the TE fluctuation from gear design and manufacture and to tune the axle system parameters to desensitize the excitation. Wang [3, 4, 5] investigated the effect of component flexibility on TE and included gear-shaft interaction and gyroscopic effect into axle system dynamics. Tooth profile modification is one of the effective ways to reduce TE fluctuation and tooth contact pressure distribution from the gear design point of view. Hypoid and spiral bevel gears are designed in the rear axle system to transmit torque in the cross axis. Most of the earlier research on tooth profile modification or tooth surface optimization for hypoid and spiral bevel gear set discuss on reducing kinematic loaded TE and the maximum tooth contact pressure without the effect on dynamic behavior or discussing tooth profile modification influence on dynamics for other gear types, such as spur gears or planetary gears. Thus, the goal of this chapter is to relate the effect of hypoid and spiral bevel gear tooth profile modification with the dynamic response on the vehicle axle system and provide an approach to optimize the tooth profile modification parameters for reducing the gear whine noise. There are several types and different shapes of tooth profile modification for the different types of gear. For parallel axis gears with original involute tooth profile, such as spur, helical, and planetary gears, there are linear, parabolic, circular, straight, and quadratic form profile modifications [6]. Linear tip relief is the most popular method. For hypoid and spiral bevel gears, the tooth profile modifications achieved by head cutter variation or machine tool setting on gear generators. Simon [7, 8, 9, 10, 11, 12, 13] proposed an optimization methodology to systematically define head-cutter geometry and machine tool settings for face-hobbed hypoid and spiral bevel gears with reduced maximum tooth contact pressure and transmission errors. Shih [14, 15] developed a novel ease-off flank modification methodology for spiral bevel and hypoid gears made by a Cartesian-type gear generator. Fan [16] presented a high-order polynomial representation of the universal motions of machine tool settings on the CNC machine. Mu, et.al. [17] presented a novel tooth surface modification method for designing high contact ratio spiral bevel gears with a higher-order TE. Hypoid gear tooth cutter profile variation is adopted in this study.

Different amounts of tooth profile modification will influence the time vary mesh characteristics, including mesh stiffness, static TE, mesh point, and line-of-action (LOA). The hypoid geared rotor system dynamics will have different excitation force and dynamic characteristics due to different mesh stiffness and TE. Most previous studies investigated the impact of tooth profile modification on gear dynamics either for spur gear pairs [19, 20, 21,22] or planetary gear systems [23, 24]. The effects of tooth profile modification on the hypoid geared rotor system have been given less consideration.

The neural network algorithm is suitable for solving the design and optimization problem of hypoid gear pair because of the complex relationships between design parameters and mesh parameters. Hypoid pinion tooth cutter parameters, such as depth and angel of modification, can be used as inputs to get minimize transmission error and maximum contact pressure on the pinion surface. A popular neural network named Back Propagation (BP) algorithm is used to predict the minimum TE with the improved Particle Swarm Optimization (PSO) which is applied to optimize the weights of the BP algorithm. Sun, et.al. [25] studied this combined algorithm for optimization of hypoid gear spiral angle, gear pitch angle, and pinion pitch angle.

In this chapter, the effect of optimal hypoid gear tooth profile modification which is optimized by the IPSO-BP algorithm on axle dynamics is discussed. The vehicle rear axle system is presented by a 14-DOF lumped parameter hyoid geared rotor system. Finally, a case study is presented and the dynamic responses are calculated and compared between the baseline result and optimal result cases.

3.2 Hypoid Gear Tooth Contact Analysis

The hypoid gear mesh parameters can be derived from the contact load distribution results which are calculated by a 3-dimensional quasi-static loaded tooth contact analysis program for hypoid and spiral bevel gears [27]. This program combines the semi-analytical theory with the finite element method which can solve the gear tooth contact program efficiently [28].

A hypoid gear pair with multiple contact interfaces are shown in Figure 5(a). The contact cells inside the mesh region are shown in Figure 5(b). The position vector of each contact cells can be defined as $r_i \ (r_{ix}, r_{iy}, r_{iz})$ with respect to the fixed mesh coordinate system. Correspondingly, the normal vector is $n_i \ (n_{ix}, n_{iy}, n_{iz})$ and the contact force is f_i.

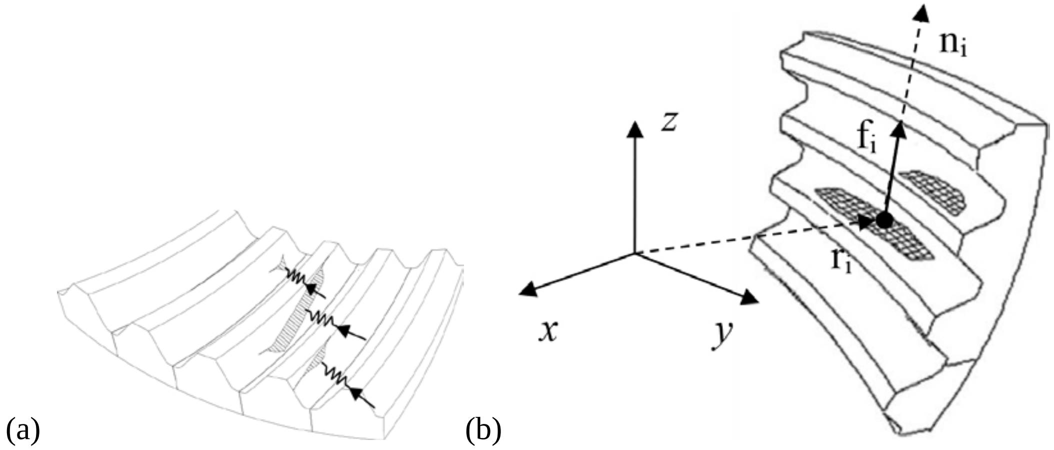

Figure 5 Illustration of (a) multi-point coupling of hypoid gear pair, and (b) contact cells on the engaging surface.

The total contact force on all the engaging surfaces is calculated by summing the contact forces on each contact cell. Assuming there are N contact cells.

$$F_j = \sum_{i=1}^{N} n_{ij} f_i \quad , F = \sqrt{\sum_{j=x}^{z} F_j^2}, (j = x, y, z) \tag{3-1}$$

The line-of-action vector L_m (n_x, n_y, n_z) can be obtained from

$$n_j = \frac{F_j}{F}, (j = x, y, z) \tag{3-2}$$

The total contact moment is given by

$$M_x = \sum_{i=1}^{N} f_i \left[n_{iz} r_{iy} - n_{iy} r_{iz}\right] \tag{3-3a}$$

$$M_y = \sum_{i=1}^{N} f_i \left[n_{ix} r_{iz} - n_{iz} r_{ix}\right] \tag{3-3b}$$

$$M_z = \sum_{i=1}^{N} f_i \left[n_{iy} r_{ix} - n_{ix} r_{iy}\right] \tag{3-3c}$$

The mesh point R_m (x_m, y_m, z_m) can be obtained from

$$y_m = \frac{\sum_{i=1}^{N} r_{iy} f_i}{\sum_{i=1}^{N} f_i} \tag{3-4a}$$

$$x_m = (M_z + F_x y_m)/F_y \tag{3-4b}$$

$$z_m = \left(M_y + F_z x_m\right)/F_x \tag{3-4c}$$

The translational loaded and unloaded transmission errors $e_L$and ε_0 are the projections of corresponding angular transmission error along the line of action. Finally, the mesh stiffness is defined by

$$k_m = F/(e_L - \varepsilon_0) \tag{3-5}$$

The above representations are then combined with the geared rotor system dynamic model to enable TE excitation to be applied reasonably well and also to compute meaningful gear mesh response.

3.2 Hypoid Gear Tooth Profile Modification by Cutter Variation

Hypoid gear tooth geometry modification can be achieved by modifying machine tool setting parameters and the profile of tool cutters. A Gleason type hypoid gear set is used with the generated pinion and FORMATE (non-generated) gear. The pinion is the driving member and the concave side of the pinion tooth is the drive side. The concave side of the pinion tooth is chosen as the modified target by defining two modification variables on the pinion cutter blade surface. The modification depth is measured from the cutter tip or the tooth root to the tip relief start point as shown in Figure 6. The modification angle is the angle between the original tooth surface and the modified surface. By varying these two variables into tooth contact analysis, the minimized TE can be searched by the following optimization process.

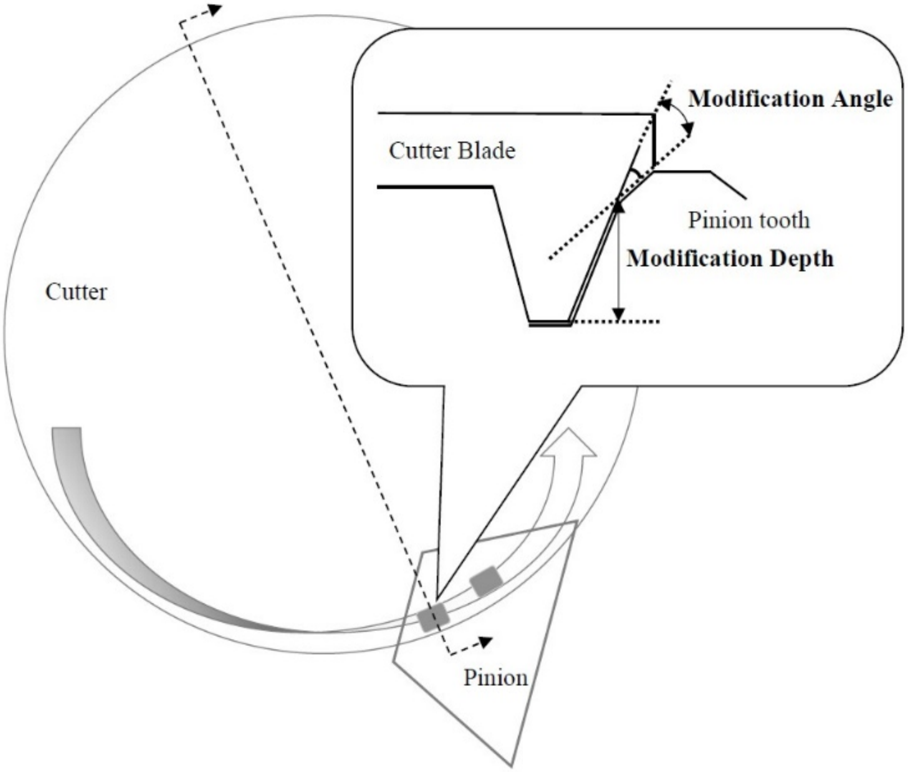

Figure 6 Schematics of pinion cutter profile and modification variables.

3.3 Artificial Neural network Optimization Approach

The feed-forward neural network type is used to connect cutter variations and machine tool setting parameters with zero to peak TE and maximum contact pressure. In this type of network, the data moves only forward from the input layer, through the hidden layers and to the output layer, which can be shown in Figure 7. No cycles or loops are in the network structure. Each node in one layer connects with all nodes in the next layer with a different weight value on each connection, such as input weights (IWs) and layer weights (LWs). Each layer has its own bias (B) to be added to the value that comes from the previous layer. The difference between the net output value and the real target value is the error of this network. The network should be trained to minimize this error, which is defined as the cost function.

Particle Swarm Optimization (PSO) and Gradient Descent (GD) algorithms are two of the training algorithms to minimize the cost function and calculate all best weights and biases. PSO uses a population of candidate solutions or particles to move around the searching space. Each particle’s position and velocity are influenced by its local best value and the group's best value in the next iteration. After several iterations, the algorithm is expected to move the swarm toward the best solutions. The PSO algorithm is a global optimization algorithm that is initially used to simulate a bird’s foraging behavior. The PSO structure is shown in Figure 8. The inertia weight of the PSO algorithm is used to control the global search and the local optimization ability. The improved PSO algorithm has a higher inertia weight at the beginning iterations to obtain a stronger global searching ability. As the iteration goes on, the inertia weight becomes lower to obtain stronger local optimization ability for faster convergence performance. GD is another optimization algorithm to find a minimum of the cost function by taking steps proportional to the negative of the gradient of the function at the current iteration.

The cutter variations and machine tool setting parameters are the input nodes to the network, as the zero to peak TE and maximum contact pressure the real target values. With training the network with PSO and GD algorithm to an acceptable cost function, mean square error (MSE), the optimal machine tool settings can be predicted by using the trained neural network model.

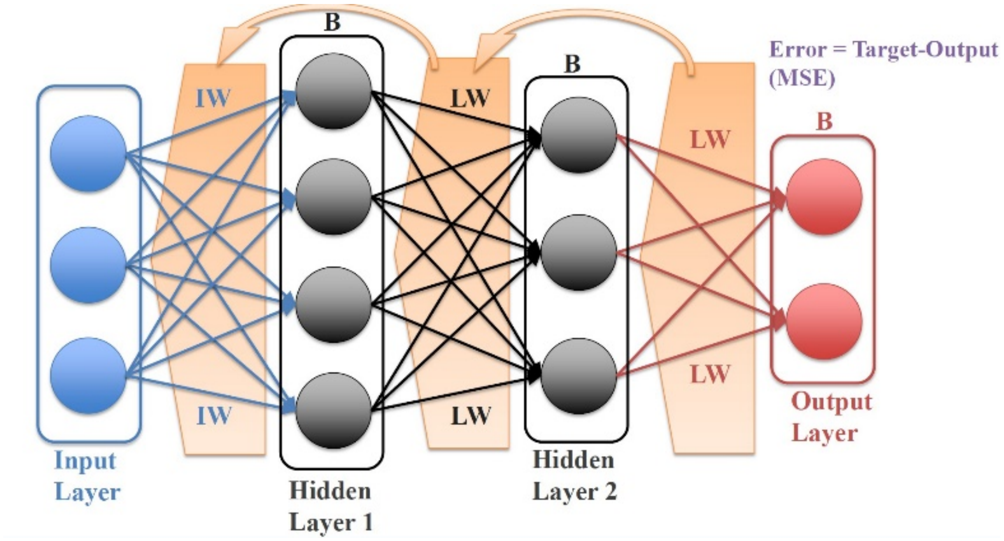

Figure 7 The feed-forward backpropagation neural network model structure

The optimization steps are as follows:

1. Execute 3-dimensional quasi-static loaded tooth contact analysis program with varying modification variables as model inputs. The results of static TE fluctuation amplitude defined as zero-to-peak TE are model outputs.
2. The inputs and outputs are collected to train the IPSO-BP model with some test cases to evaluate the accuracy of the predictive model by the Root Mean Square Error (RMSE) equation.

$$RMSE = \sqrt{\frac{\sum_{n=1}^{k}(1-\frac{Q_p}{Q_c})^2}{k}} \qquad (3\text{-}6)$$

3. Optimize the modification variable with the predicted model to obtain the minimum TE.

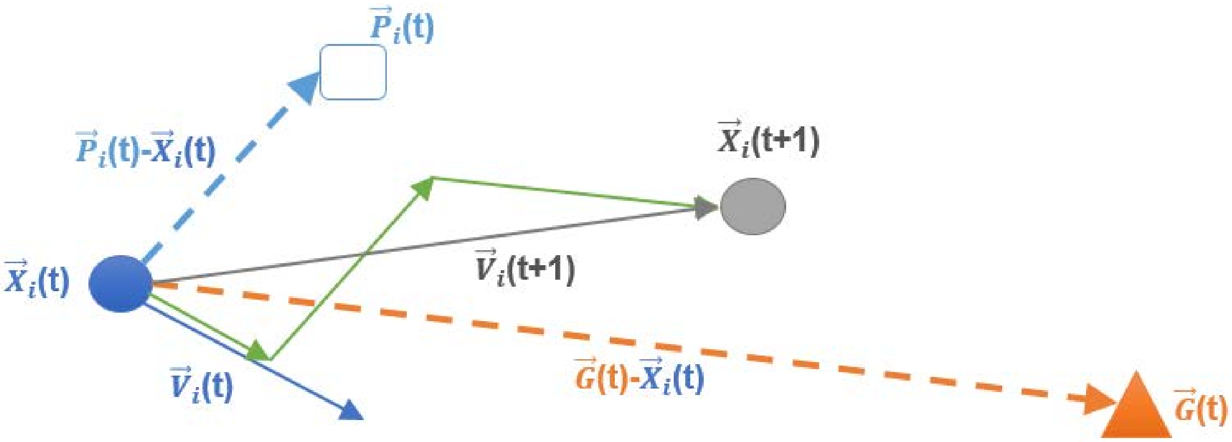

Figure 8 The PSO network structure.

3.4 Dynamic Analysis

The 14 degrees of freedom lumped parameter model of the hypoid geared rotor system is similar to the model used in Tao's study [27] in Figure 9. The equations of the motion of the geared rotor system in matrix form can be written as

$$[M]\{\ddot{x}\} + [C]\{\dot{x}\} + [K]\{x\} = \{F\} \tag{3-7}$$

where

$$\{x\} = \left\{\theta_D, x_p, y_p, z_p, \theta_{px}, \theta_{py}, \theta_{pz}, x_g, y_g, z_g, \theta_{gx}, \theta_{gy}, \theta_{gz}, \theta_L\right\}^T \tag{3-8}$$

$$[M] = diag\left\{I_D, M_p, M_p, M_p, I_{px}, I_{py}, I_{pz}, M_g, M_g, M_g, I_{gx}, I_{gy}, I_{gz}, I_L\right\} \tag{3-9}$$

The stiffness matrix $[K]$ is the lumped shaft-bearing assembly support stiffness and also the function of mesh stiffness and static TE. The damping matrix $[C]$ is assumed to be the viscous type and derived from the damping ratio and mode shape matrix.

The force vector can be written as

$$\{F\} = \{T_D, h_p F_m, -h_g F_m, -T_L\} \tag{3-10}$$

The dynamic mesh force F_m and directional transformation vectors h_l are defined as

$$F_m = k_m(\delta_d - \varepsilon_0) + c_m(\dot{\delta_d} - \dot{\varepsilon_0}) \tag{3-11}$$

$$h_l = \{n_{lx}, n_{ly}, n_{lz}, \lambda_{lx}, \lambda_{ly}, \lambda_{lz}\}, l = p, g \tag{3-12}$$

where δ_d is dynamic TE excitation and ε_0 is unloaded TE. Rotational radius λ_l are defined as

$$\begin{aligned} \lambda_{lx} &= L_l(X_l \times R_l) \\ \lambda_{ly} &= L_l(Y_l \times R_l) \\ \lambda_{lz} &= L_l(Z_l \times R_l) \end{aligned} \tag{3-13}$$

where L_l and R_l is the line of action and mesh point in the pinion coordinate system ($l = p$) or gear coordinate system ($l = g$), and X_l, Y_l, Z_l are the unit vectors in the pinion or gear coordinate system. The dynamic TE is given by

$$\delta_d = h_p^T\{x_p, y_p, z_p, \theta_{px}, \theta_{py}, \theta_{pz}\} - h_g^T\{x_g, y_g, z_g, \theta_{gx}, \theta_{gy}, \theta_{gz}\} \tag{3-14}$$

which accounts for the system dynamic response in addition to the kinematic effect of TE.

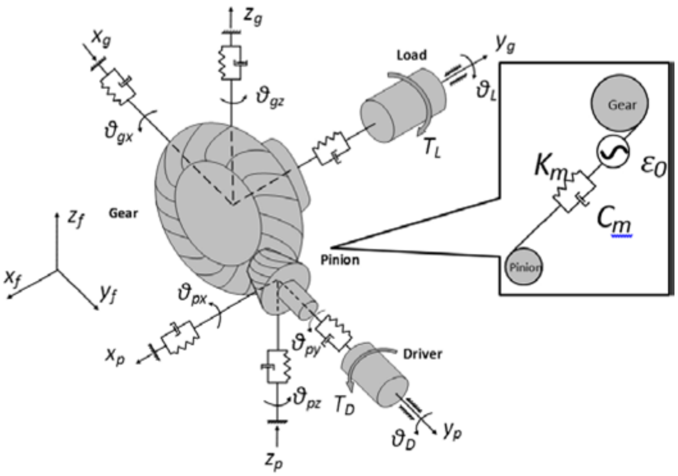

Figure 9 A lumped parameter model of the hypoid geared rotor system.

3.5 Simulation Results

In this section, the practical design of a hypoid gear pair is taken as an example for numerical simulation. The main design parameters of the gear pair and the working condition are shown in Table 1. The results of contact and dynamic analysis are defined as baseline cases.

Table 1 Design Parameters of the hypoid gear rotor system.

	Pinion	Gear
Number of teeth	10	43
Spiral Angle [degree]	45.997	33.8608
Pitch Angle [degree]	16.9192	72.717
Pitch Radius [mm]	48	168
Face Width [mm]	52.2474	47.752

Mean Cone Distance [mm]	138.775	152.147
Pitch Apex beyond cross point [mm]	-9.538	4.89447
Type	Left hand	Right hand
Loaded Side	Concave	Convex
Offset [mm]	31.75	
Shaft Angle [degree]	90	
Torque Load [Nm]	320	
Rotational Speed [rpm]	3000	

The datasets of the neural network model are comprised of the following: the input data is the different combinations of modification variables, while the output data is the zero-to-peak TE and max contact pressure obtained from the tooth contact analysis.

The training set of the neural network model is as illustrated in Figure 10. After the model is trained, 12 testing cases are tested using the network. The RMSEs between the actual values and the predicted values of zero-to-peak TE and maximum contact pressure are 1.88 % and 1.64 % respectively as presented in Figure 11.

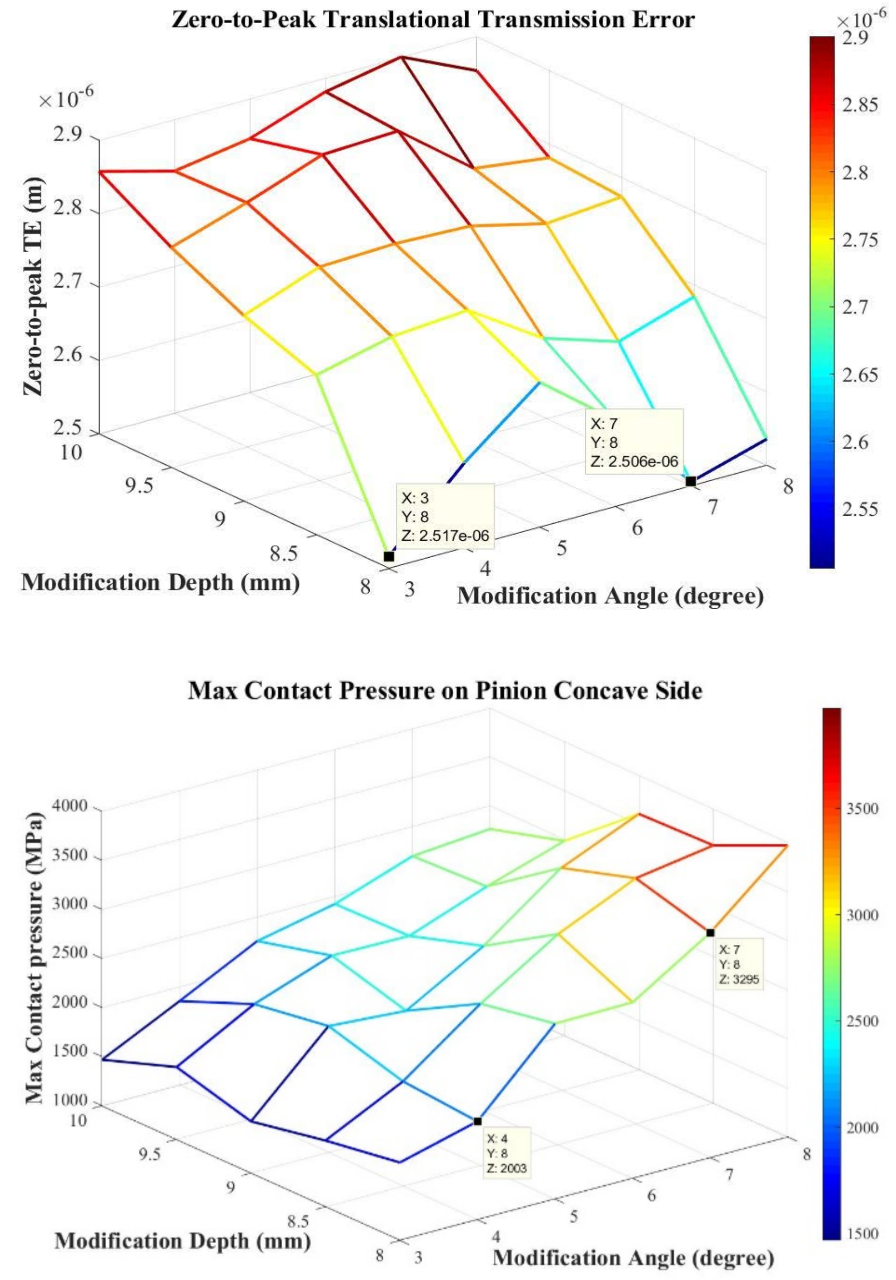

Figure 10 Input and output data for training the neural network model.

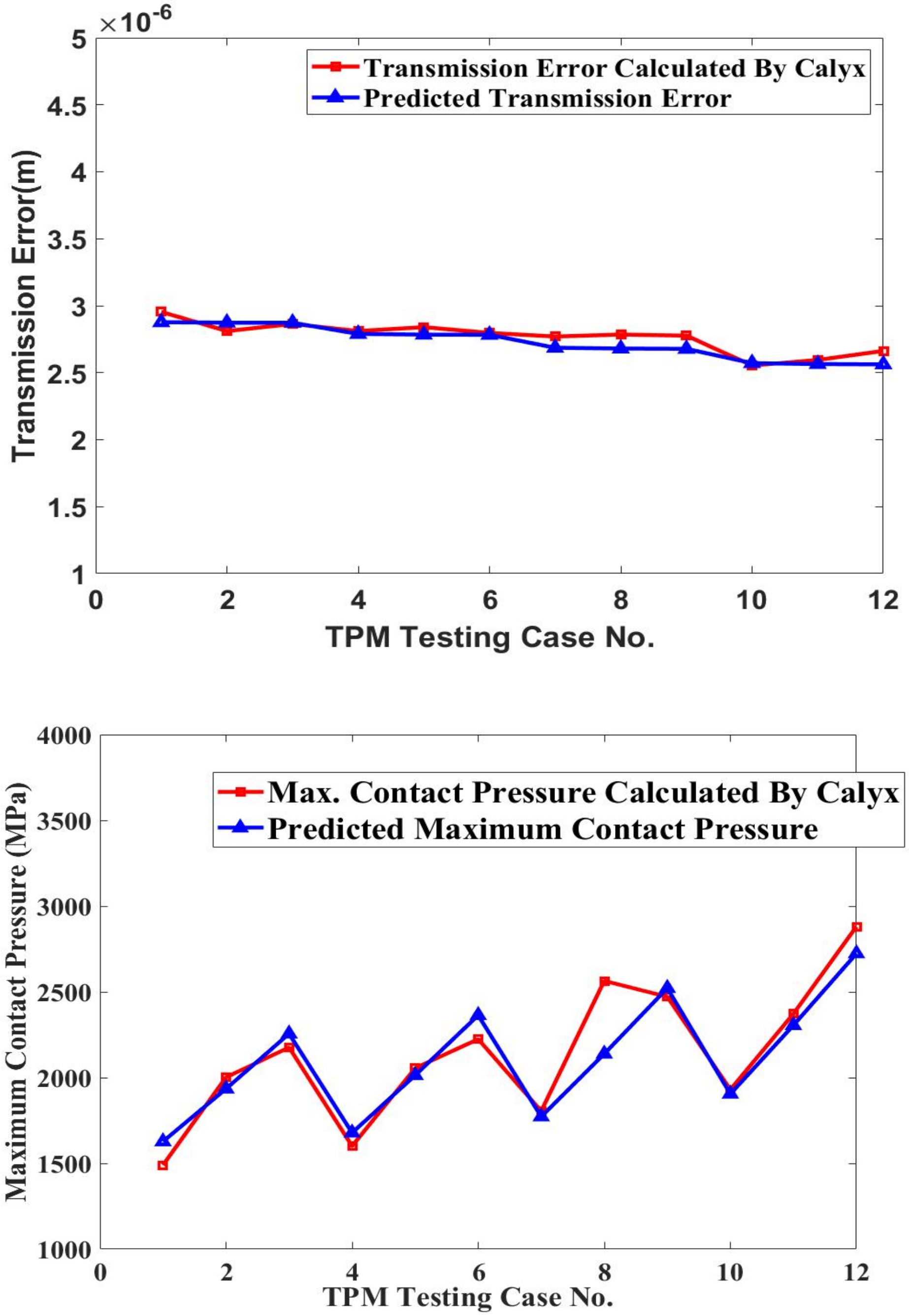

Figure 11 Testing cases for the neural network model.

The efficiency of the trained model at predicting the tooth contact properties is much higher than that of the original contact analysis method. This allows the prediction of a large amount of input data in a significantly shorter time. 16,281 combinations of tooth contact modification parameters were used as input to the trained network model to predict the output values in approximately 4 minutes, as illustrated in Figure 12.

According to the figure, in order to achieve the minimum zero-to-peak TE, the modified depth of 8 mm is preferred. For the modified angle, however, the maximum contact pressure increases as the angle increases. By using the maximum contact pressure of the baseline case, which is 2696 MPa, as the upper limit, data points with the lowest zero-to-peak TE are chosen. Two sets of modification variables, depth 8 mm with 3 degrees angle (TPM D8A3) and depth 8 mm with 5 degrees angle (TPM D8A5), are selected to proceed to the dynamic analysis to be compared with the baseline case in terms of dynamic performance.

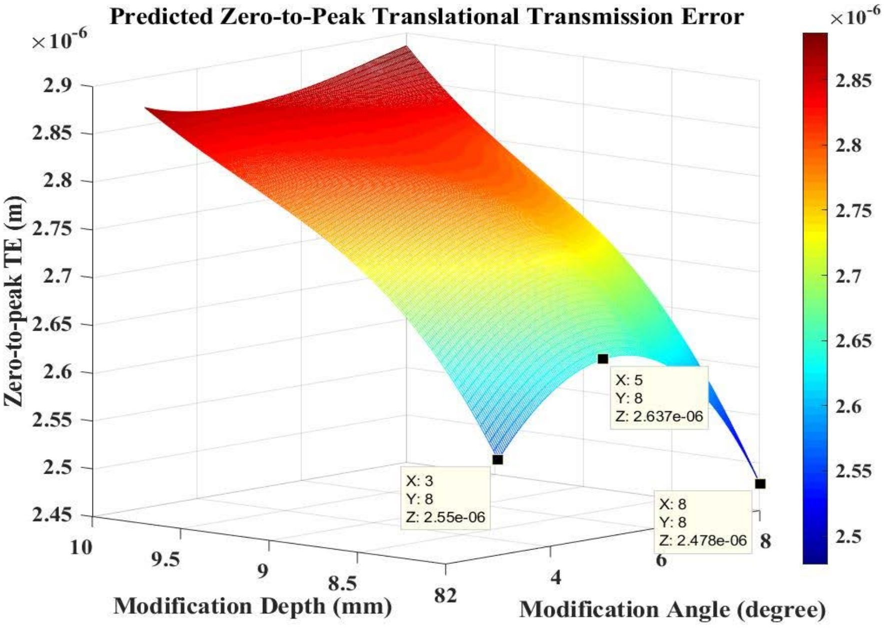

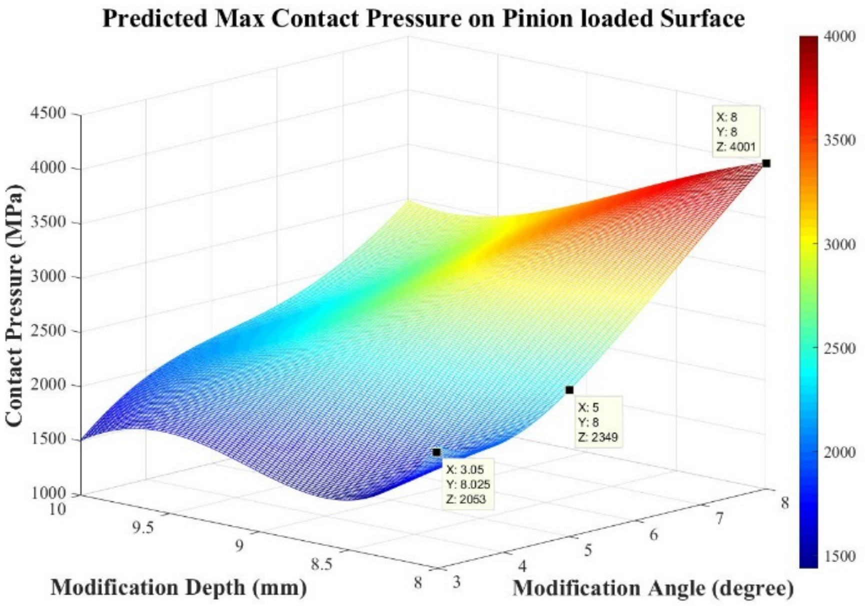

Figure 12 Zero-to-peak transmission error and maximum contact pressure predicted results.

Before dynamic analysis, the pinion tooth contact pressure patterns of the three cases which are the baseline, TPM D8A3, and TPM D8A5 are verified first. The results are shown in Figure 13. It can be found that with tooth tip profile modification the edge contact effect can be alleviated. The maximum value of contact pressure of TPM D8A3 is lowest than baseline and TPM D8A5. From the gear design point of view, TPM D8A3 is a better option for design criteria for strength and durability.

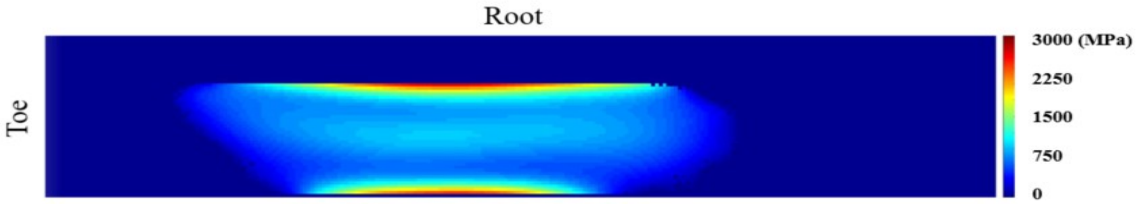

(a) Baseline Case

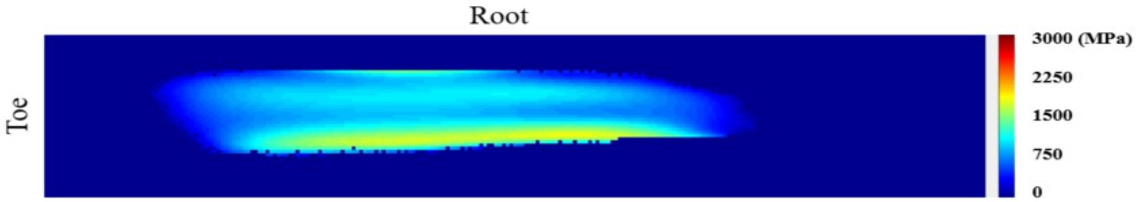

(b) Depth 8 Angle 3 Case

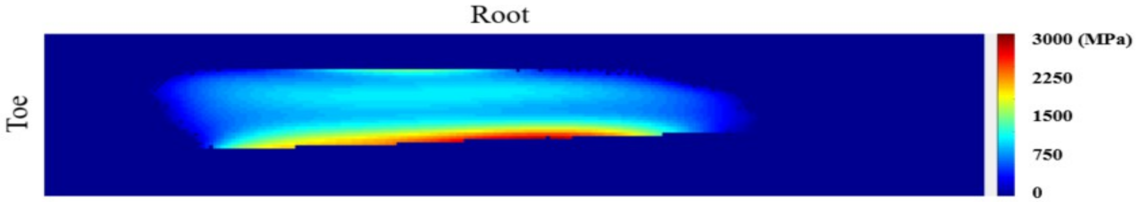

(c) Depth 8 Angle 5 Case

Figure 13 Comparison of pinion tooth contact pressure pattern.

Time-varying mesh parameters, such as translational TE and mesh stiffness, varying with pinion roll angle are calculated and compared among the three cases in Figure 14 and Figure 15. As shown in Figure 14, the translational TE with tooth profile modification may increase in quantity but decrease in vibrating amplitude which is defined as the zero-to-peak TE. The fluctuation of static translational TE is the excitation input into the geared rotor system. It can be seen in Figure 15 that the mesh stiffness decreased with TPM applied. It will slightly change the natural frequency of the entire geared rotor system.

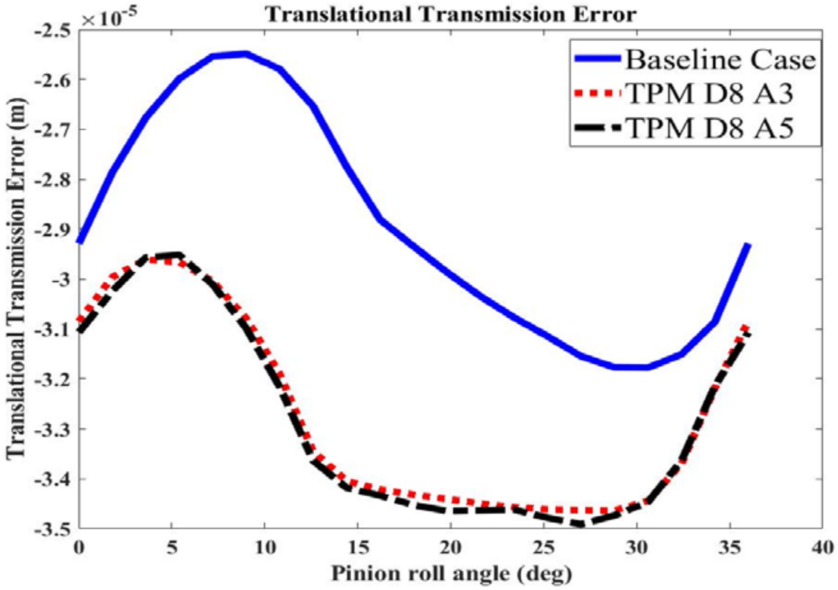

Figure 14 Time-varying translational transmission error (mm).

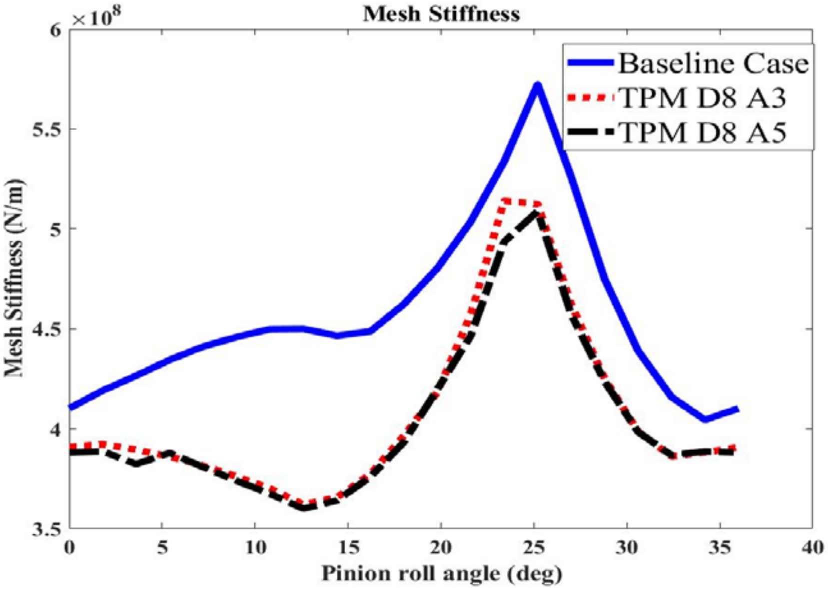

Figure 15 Time-varying mesh stiffness (N/mm).

Time-average mesh force and zero-to-peak translational TE are applied to the linear time-invariant (LTI) analysis. The dynamic response of dynamic TE, dynamic mesh force, and dynamic bearing resultant force are calculated among the three cases separately, and the comparison results are presented in Figure 16 to Figure 18. Dynamic TE and dynamic mesh force spectrum are used to evaluate the vibration of the geared rotor system. Moreover, the dynamic bearing resultant force is the direct input excitation to the gearbox housing. From each spectrum comparisons, it can be observed that the natural frequency is shifted down with TPM applied due to small average mesh stiffness. The magnitude of each spectrum is decreasing with TPM because of lower TE fluctuation input, where TPM D8A3 has slightly better performance than TPM D8A5 not only the magnitude but also the contact pressure distribution.

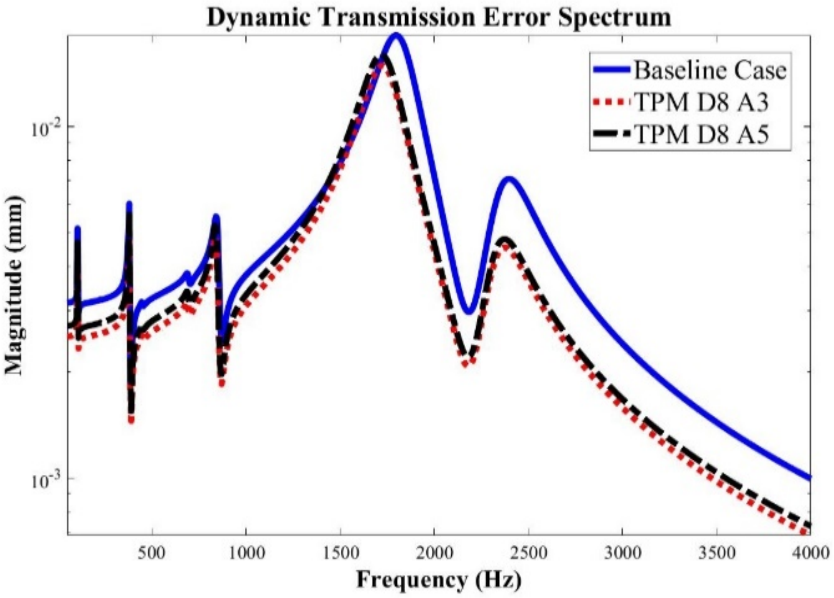

Figure 16 Dynamic transmission error spectrum.

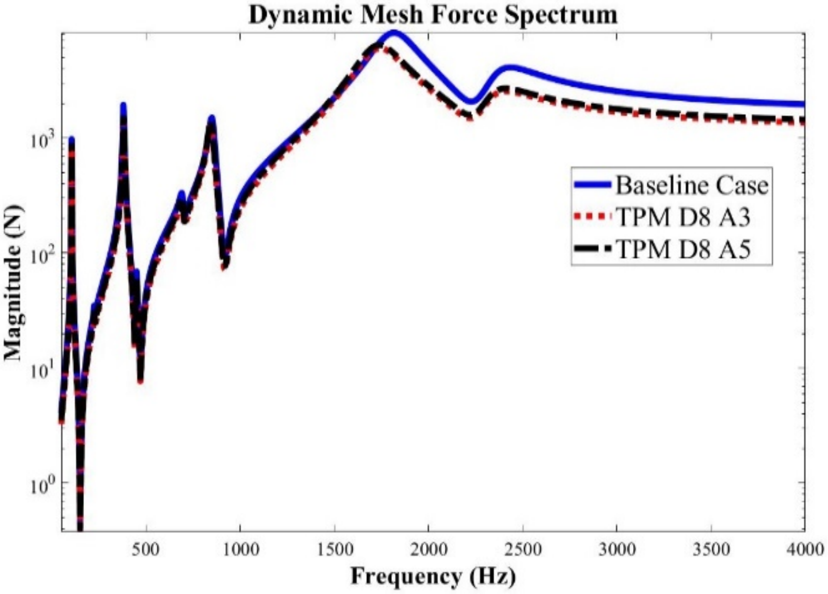

Figure 17 Dynamic mesh force spectrum.

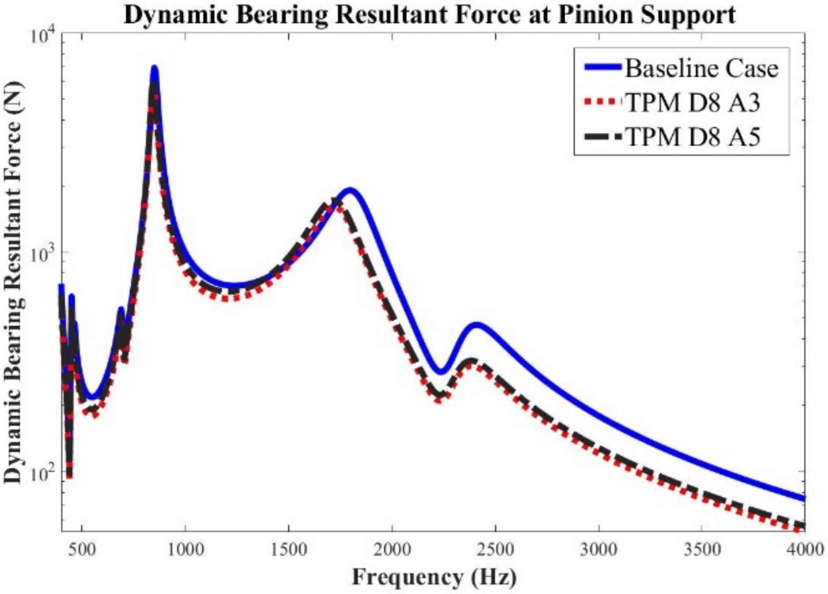

Figure 18 Dynamic bearing resultant force spectrum at pinion support.

3.6 Conclusion

In this chapter, the effect of optimal tooth profile modification on the vehicle axle system is discussed. An approach with IPSO-BP neural network algorithm to obtain minimum transmission error and improved dynamic response with optimal tooth profile modification parameters is presented. A case study of a hypoid gear pair with specified design parameters and working condition is calculated and compared with optimized TPM cases. The results revealed that by using tooth profile modifications obtained through the proposed method, the following improvements can be identified when compared to the baseline case:

1. Lower maximum contact pressure contributed by the prevention of edge contact situations, which is the main cause of stress concentration.
2. Reduction of the variance of zero-to-peak transmission error, which is the source of vibration in the axle system.
3. An overall decrement in the magnitude of dynamic responses, including dynamic transmission error, dynamic mesh force, and dynamic bearing resultant force, that are commonly used to evaluate the vibration response in system dynamics.

The results conclude that optimal tooth profile modification parameters acquired by minimizing TE can improve the overall NVH behavior. The proposed approach provides a better understanding of the effects of optimal tooth profile modification on vehicle axle system dynamics.

Chapter 4 Optimization of Machine Tool Settings on Hypoid Gear Dynamics

4.1 Introduction

The machine tool settings for the hypoid gear tooth generation are key parameters to manufacture desired mating tooth surfaces and have favorable contact patterns on pinion and gear. The methods on the determination of machine tool setting for the generation of hypoid gears by the local synthesis were published by Litvin et al [18]. The modifications of the machine tool settings can modify the micro-geometry of the tooth surface which can directly influence the transmission error (TE) and contact pressure of the gear pair. Minimizing TE and contact pressure of the hypoid gear pair improve not only the dynamic response of the rotor system but also the durability of the structure. Tooth modification induced by machine tool setting is one of the effective ways to reduce TE fluctuation and tooth contact pressure distribution from the gear design point of view. Most of the earlier research on tooth profile modification or tooth surface optimization for hypoid and spiral bevel gears focuses on TE and contact pressure optimization, and the discussion on dynamic behavior is sparse. Thus, the goal of this paper is to relate the effect of hypoid gear modification of machine tool setting with the dynamic response of the geared-rotor system and provide an approach to optimize the machine tool setting parameters for reducing TE.

There are several types of tooth profile modification for hypoid and spiral bevel gears, which can be achieved by head cutter variation or machine tool setting on gear generators. Simon [7-13] proposed an optimization methodology to systematically define head-cutter geometry and machine tool settings for face-hobbed hypoid and spiral bevel gears with reduced maximum tooth contact pressure and transmission errors. Shih and Fong [14, 15] developed a novel ease-off flank modification methodology for spiral bevel and hypoid gears made by a Cartesian-type gear generator. Fan [16] presented a high-order polynomial representation of the universal motions of machine tool settings on the CNC machine. Mu, et.al. [17] presented a novel tooth surface modification method for designing high contact ratio spiral bevel gears with a higher-order TE. The accurate mesh model considering the work holding equipment errors based on the generated process was proposed by Liu et.al [31]. The influence of errors on mesh behavior and gear flank geometry has been investigated. Hypoid gear machine tool setting variation on the pinion is adopted in this study.

A different set of machine tool setting will influence the time vary mesh characteristics, including mesh stiffness, static TE, mesh point, and line-of-action (LOA). The hypoid geared rotor system dynamics will have different excitation force and dynamic characteristics due to different mesh stiffness and TE. Most previous studies investigated the impact of tooth profile modification on gear dynamics either for spur gear pairs or planetary gear system. The effects of tooth modification by machine tool setting on hypoid geared rotor system have been given less consideration.

The neural network is suitable for solving the design and optimization problem of hypoid gear pair because of the complex relationships between design parameters and mesh parameters. Hypoid pinion machine tool setting parameters, such as machine center to back distance and sliding base distance, can be used as inputs to get minimized transmission error and contact pressure on the pinion surface. A popular neural network type named Feed-Forward Back Propagation (FFBP) is used to predict the minimum TE. The Particle Swarm Optimization (PSO) and Gradient Descent (GD) training algorithms are applied to optimize the weights and biases of the neural network performance. Sun, et.al. [25] studied this combined algorithm for optimization of hypoid gear spiral angle, gear pitch angle, and pinion pitch angle.

In this chapter, the optimization of hypoid gear machine tool settings by neural network algorithms on gear dynamics is discussed. The dynamic response is calculated from a lumped parameter hyoid geared rotor system model. Finally, a case study is presented and the dynamic responses are compared between the baseline result and optimal result cases.

4.2 Simulation Methods

4.2.1 Hypoid Gear Tooth Contact and Mesh Analysis

The hypoid gear mesh parameters, which are mesh points, line of action, loaded transmission error, and mesh stiffness, can be derived from the contact load distribution results which are calculated by a 3-dimensional quasi-static loaded tooth contact analysis program for hypoid and spiral bevel gears [27]. This program combines the semi-analytical theory with the finite element method which can solve the gear tooth contact program efficiently [28].

The machine tool settings normally including machine center to back setting, cutter radial setting, sliding base, blank offset, root angle, tilt angle, swivel angle, and cradle angle. The modification of machine tool settings will have different mesh parameters which are time-varying with the pinion roll angle. The different micro-geometry of the tooth surface which defined by different machine tool settings ends up inducing different TE excitation for gear dynamics. TE fluctuation is the main source of gear dynamic response. Zero to peak TE is defined to represent the magnitude of TE fluctuation which is half of the difference between peak to peak values. The maximum contact pressure of the tooth surface is also calculated from tooth contact analysis to evaluate the effect of variation by machine tool settings during the entire mesh cycle.

4.2.2 Neural Network Model with PSO and GD Algorithm

The feed-forward neural network type is used to connect machine tool setting parameters with zero to peak TE and maximum contact pressure. In this type of network, the data moves only forward from the input layer, through the hidden layers and to the output layer, which can be shown in FIGURE 1. No cycles or loops are in the network structure. Each node in one layer connects with all nodes in the next layer with a different weight value on each connection, such as input weights (IWs) and layer weights (LWs). Each layer has its own bias (B) to be added to the value that comes from the previous layer. The difference between the net output value and the real target value is the error of this network. The network should be trained to minimize this error, which is defined as the cost function.

Particle Swarm Optimization (PSO) and Gradient Descent (GD) algorithms are two of the training algorithms to minimize the cost function and calculate all best weights and biases. PSO uses a population of candidate solutions or particles to move around the searching space. Each particle’s position and velocity are influenced by its local best value and the group's best value in the next iteration. After several iterations, the algorithm is expected to move the swarm toward the best solutions. GD is another optimization algorithm to find a minimum of the cost function by taking steps proportional to the negative of the gradient of the function at the current iteration.

The machine tool setting parameters are the input nodes to the network, as the zero to peak TE and maximum contact pressure the real target values. With training the network with PSO and GD algorithm to an acceptable cost function, mean square error (MSE), the optimal machine tool settings can be predicted by using the trained neural network model.

4.2.3 Dynamic Analysis

With optimal machine tool settings, the dynamic analysis of the 14 degrees of freedom lumped parameter model of the hypoid geared rotor system, which is similar to the model used in Tao's study [26] is performed. The equations of the motion of the geared rotor system in matrix form can be written as

$$[M]\{\ddot{x}\} + [C]\{\dot{x}\} + [K]\{x\} = \{F\} \tag{4-1}$$

where

$$\{x\} = \left\{\theta_D, x_p, y_p, z_p, \theta_{px}, \theta_{py}, \theta_{pz}, x_g, y_g, z_g, \theta_{gx}, \theta_{gy}, \theta_{gz}, \theta_L\right\}^T$$

$$[M] = diag\left\{I_D, M_p, M_p, M_p, I_{px}, I_{py}, I_{pz}, M_g, M_g, M_g, I_{gx}, I_{gy}, I_{gz}, I_L\right\}$$

The stiffness matrix [K] is the lumped shaft-bearing assembly support stiffness and also the function of mesh stiffness and static TE. The damping matrix [C] is assumed to be the viscous type and derived from the damping ratio and mode shape matrix.

The force vector can be written as

$$\{F\} = \left\{T_D, h_p F_m, -h_g F_m, -T_L\right\} \tag{4-2}$$

The dynamic mesh force F_m and directional transformation vectors $h_l$are defined as

$$F_m = k_m(\delta_d - \varepsilon_0) + c_m(\dot{\delta_d} - \dot{\varepsilon_0}) \quad (4\text{-}3)$$

$$h_l = \{n_{lx}, n_{ly}, n_{lz}, \lambda_{lx}, \lambda_{ly}, \lambda_{lz}\}, l = p, g \quad (4\text{-}4)$$

where δ_d is dynamic TE excitation and ε_0 is unloaded TE. Rotational radius λ_l are defined as

$$\lambda_{lx} = \ L_l(X_l \times R_l)$$

$$\lambda_{ly} = \ L_l(Y_l \times R_l)$$

$$\lambda_{lz} = \ L_l(Z_l \times R_l) \quad (4\text{-}5)$$

where $L_l$and R_l is the line of action and mesh point in the pinion coordinate system($l = p$) or gear coordinate system ($l = g$), and X_l, Y_l, Z_l are the unit vectors in the pinion or gear coordinate system. The dynamic TE is given by

$$\delta_d = h_p^T\{x_p, y_p, z_p, \theta_{px}, \theta_{py}, \theta_{pz}\} - h_g^T\{x_g, y_g, z_g, \theta_{gx}, \theta_{gy}, \theta_{gz}\} \quad (4\text{-}6)$$

which accounts for the system dynamic response in addition to the kinematic effect of TE.

4.3 Hypoid Gear TPM by Machine Tool Settings

The machine tool settings normally including machine center to back setting, cutter radial setting, sliding base, blank offset, root angle, tilt angle, swivel angle, and cradle angle as Figure 19. The modification of machine tool settings will have different mesh parameters which are time-varying with the pinion roll angle. The different micro-geometry of the tooth surface which defined by different machine tool settings ends up inducing different TE excitation for gear dynamics. TE fluctuation is the main source of gear dynamic response. Zero to peak TE is defined to represent the magnitude of TE fluctuation which is half of the difference between peak to peak values. The maximum contact pressure of the tooth surface is also calculated from tooth contact analysis to evaluate the effect of variation by machine tool settings during the entire mesh cycle.

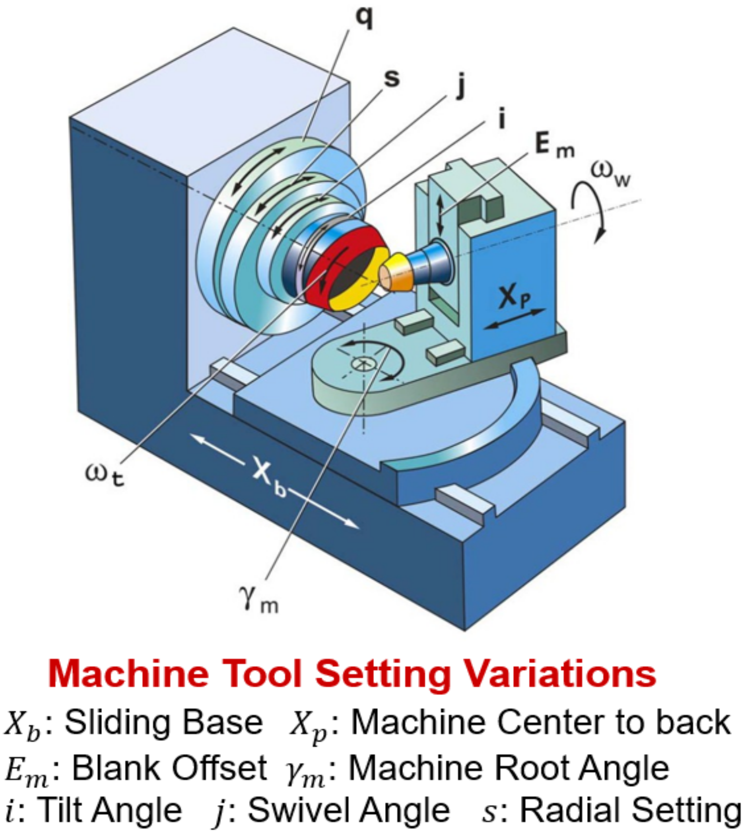

Figure 19 Schematics of machine tool setting parameters. (Fan 2008 [16])

4.4 Simulation Results and Discussion

In this section, the practical design of a hypoid gear pair is taken as an example for numerical simulation. The main design parameters of the gear pair and the working condition are shown in Table 2. The results of contact and dynamic analysis are defined as a baseline case. Based on the methods of local synthesis from Litvin et al [18], generated pinion machine tool settings are calculated for the desired meshing condition. The variation of pinion machine tool settings on the loaded side (concave side) is considered into the simulation, where the FORMATE gear machine tool settings are unchanged. The pinion and gear machine tool settings are shown in Table 3 and Table 4.

Table 2 Design parameters and working conditions of the hypoid gear rotor system.

	Pinion	Gear
Number of teeth	10	43
Spiral Angle [deg]	45.997	33.8608
Pitch Angle [deg]	16.9192	72.717
Pitch Radius [mm]	48	168
Face Width [mm]	52.2474	47.752
Mean Cone Distance [mm]	138.775	152.147
Pitch Apex beyond cross point	-9.538	4.89447
Type	Left hand	Right hand
Loaded Side	Concave	Convex
Offset [mm]	31.75	
Shaft Angle [deg]	90	
Torque Load [Nm]	320	
Rotational Speed [rpm]	3000	

Table 3 Pinion Machine Tool Settings.

	Concave	Convex
Point radius of the cutter [mm]	108.458	120.015
Cutter blade angle [deg]	20	25
Machine root angle [deg]	**16.11248**	16.11248
Basic tilt angle [deg]	**0**	0
Basic swivel angle [deg]	**11.3066**	14.46
Basic cradle angle [deg]	58.122	59.69
Machine back to center [mm]	**2.5439**	-0.16557
Sliding base setting [mm]	**-5.995**	-5.244
Cutter radial setting [mm]	**124.87**	135.5245
Blank offset setting [mm]	**26.67**	38.10
Ratio of roll	4.4295	4.6022

Table 4 Gear Machine Tool Settings.

Cutter radius [mm]	114.3
Cutter blade angle [deg]	22.5
Basic machine root angle [deg]	70.403
Point width [mm]	3.81
Basic machine center to back [mm]	1.2897
Basic horizontal [mm]	85.7
Basic vertical [mm]	96.18

4.4.1 Define the Range of Each Machine Tool Settings

First, the tooth contact and mesh analysis are performed with variations on only one of the generated pinion machine tool settings. The variation of this machine tool setting can be located at the best value of zero to peak TE and maximum contact stress. Then the analysis is performed on another parameter variation one by one. From Figure 20 to Figure 23, the variation of machine center to back, sliding base, radial setting, and blank offset with respect to zero to peak TE and maximum contact stress are shown. By setting an upper limit of maximum contact stress for 4000 Mpa, the minimum value of zero to peak TE can be located on each machine tool setting variation calculation for machine center to back + 0.4 mm, sliding base - 2.75 mm, radial setting - 0.6 mm, and blank offset + 0.6 mm separately.

From Figure 24 to Figure 26, the variation of tilt angle, swivel angle, and root angle with respect to zero to peak TE and maximum contact stress are shown. By setting the same upper limit of maximum contact stress, the minimum value of zero to peak TE can be located on each machine tool setting variation for tilt angle + 0 degree, swivel angle + 0 degree, and root angle + 0.3 degrees. These machine tool settings are categorized as Case 1 one by one which each machine tool settings are chosen independently for comparison purpose with optimization cases from the neural network model. The calculation range of each machine tool settings for the neural network model can be defined by the tendency of these curves.

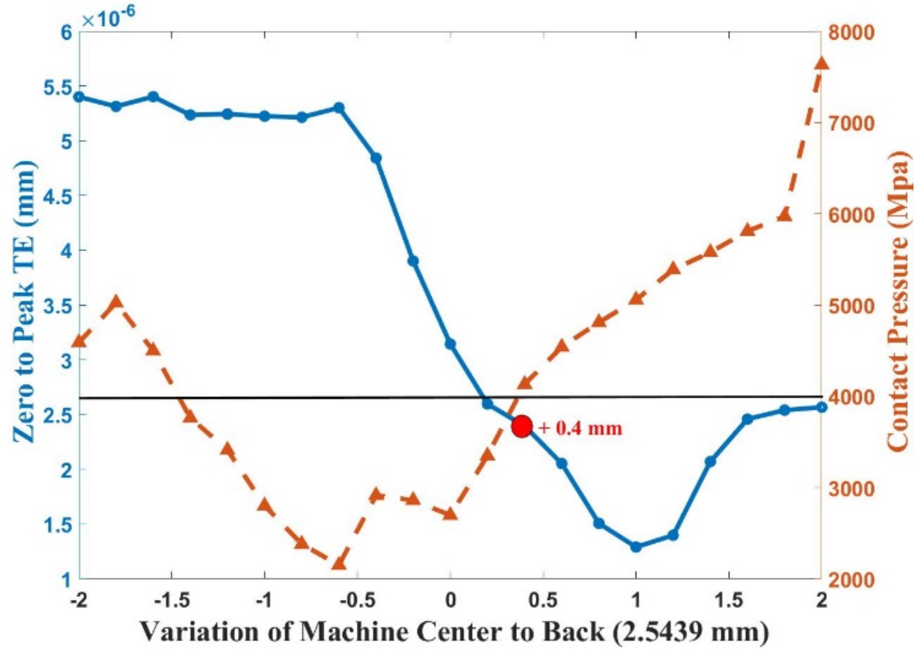

Figure 20 Variation of machine center to back with respect to zero to peak TE and maximum contact pressure (Baseline value 2.5439 mm)

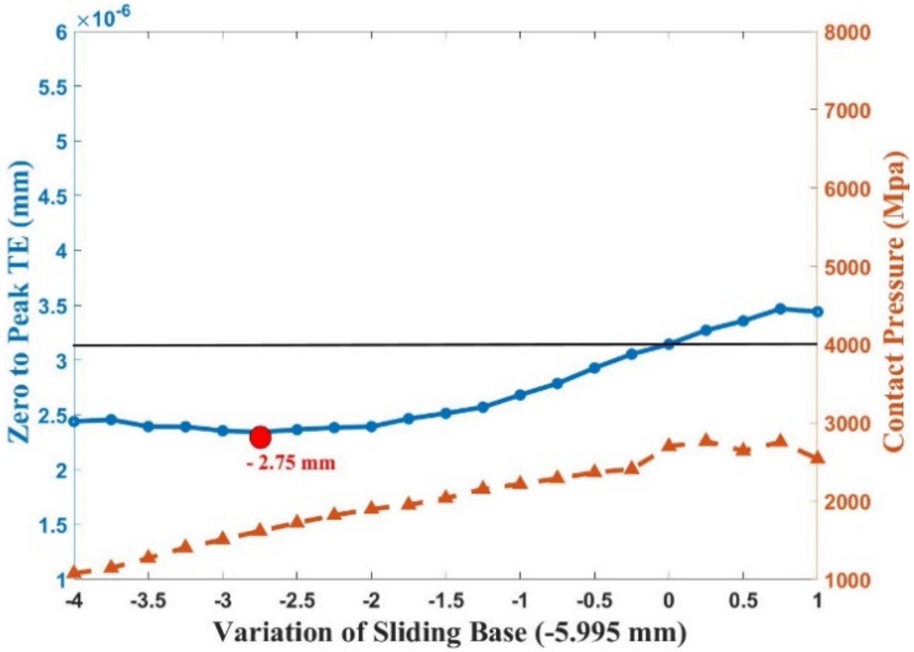

Figure 21 Variation of sliding base with respect to zero to peak TE and maximum contact pressure

(Baseline value -5.995 mm)

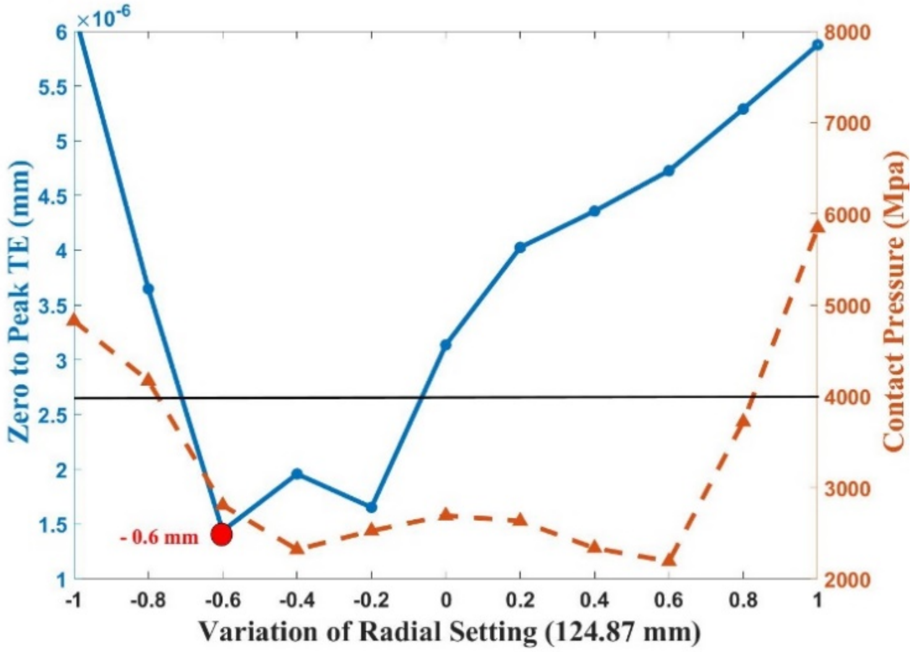

Figure 22 Variation of radial setting with respect to zero to peak TE and maximum contact pressure

(Baseline value 124.87 mm)

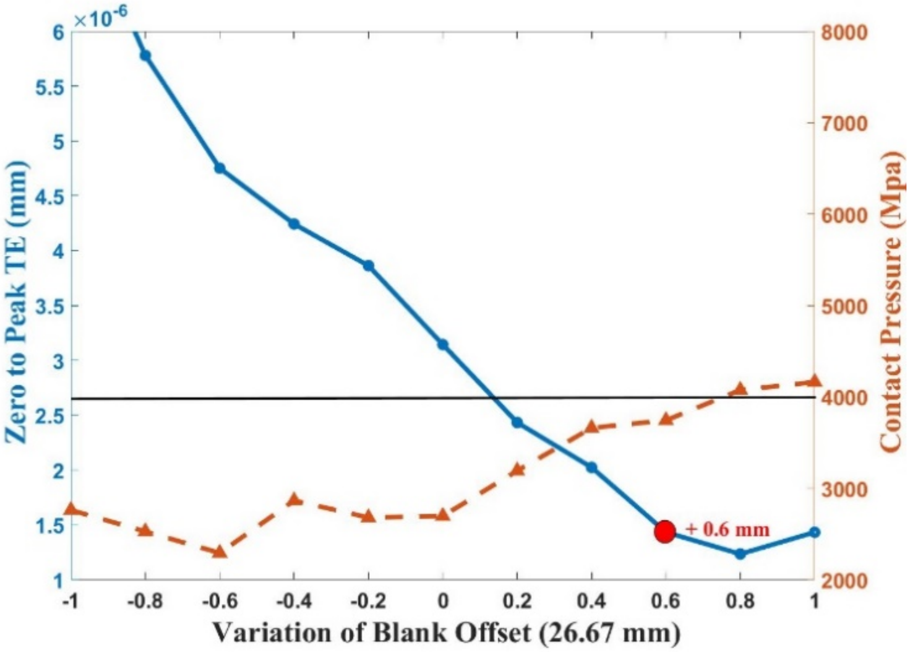

Figure 23 Variation of blank offset with respect to zero to peak TE and maximum contact pressure (Baseline value 26.67 mm)

Base on the tendency of each machine tool setting, the variation of tilt angle, swivel angle, and root angle either have less influence on zero to peak TE or are already the best value with no variation. For saving the computational cost, only four machine tool settings, which are machine center to back, sliding base, radial setting, and blank offset, are defined to perform tooth contact and mesh analysis. The variations of these four selected parameters at the same time are the neural network inputs and zero to peak TE and maximum contact pressure are network targets. With inputs and targets as training data, the neural network can be trained by the optimization algorithms.

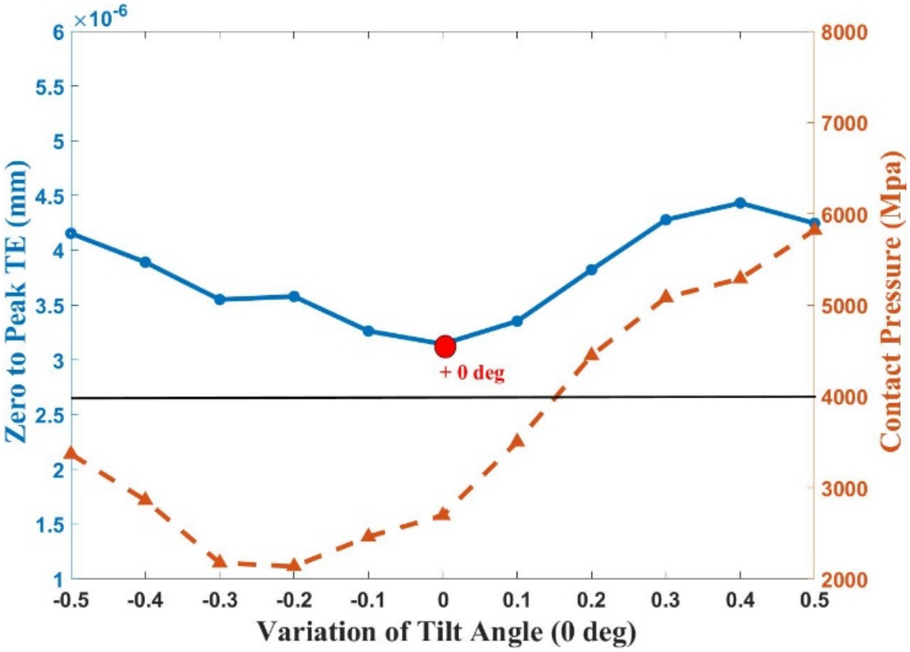

Figure 24 Variation of tilt angle with respect to zero to peak TE and maximum contact pressure

(Baseline value 0 degrees)

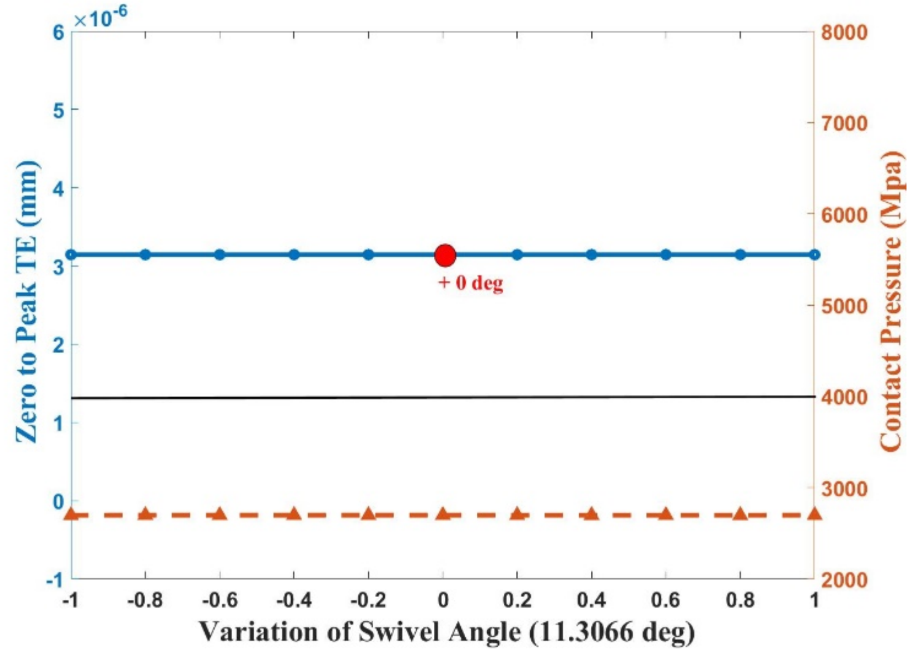

Figure 25 Variation of swivel angle with respect to zero to peak TE and maximum contact

pressure (Baseline value 11.3066 degrees)

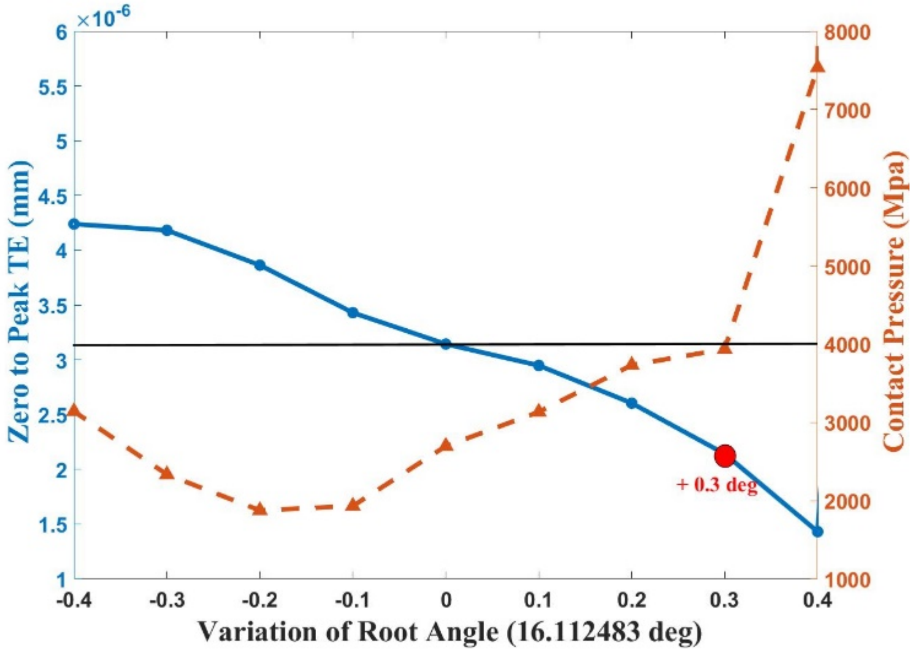

Figure 26 Variation of root angle with respect to zero to peak TE and maximum contact pressure (Baseline value 16.112483 degrees)

4.4.2 Training Neural Network Model with PSO and GD

With the training data from the previous step, the neural network can be trained with two optimization algorithms, PSO and GD. After obtaining the minimum cost function (mean square error), the predicted machine tool settings for PSO and GD are categorized as Case 2 and Case 3 for the dynamic analysis of the lumped parameter model of the hypoid geared rotor system. The structure of the neural network model in MATLAB can be shown in Figure 27. The different machine tool settings for baseline case, Case 1 optimized parameters one by one, Case 2 optimized by neural network PSO optimization algorithm, and Case 3 optimized by neural network GD optimization algorithm can be shown in Table 5.

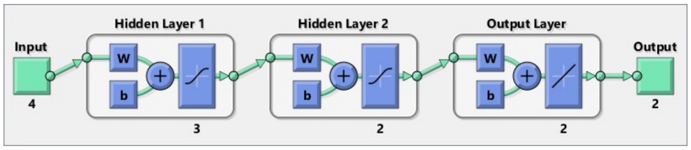

Figure 27 The structure of neural network model in MATLAB

Table 5 Machine Tool Settings of different optimization cases.

	Baseline Case	Case 1 1 by 1	Case 2 NN PSO	Case 3 NN GD
Machine back to center [mm]	2.5439	2.9439 (+ 0.4)	4.0439 (+ 1.5)	3.5439 (+ 1.0)
Sliding base setting [mm]	-5.995	-8.745 (- 2.75)	-5.495 (+ 0.5)	-5.995 (+0)
Cutter radial setting [mm]	124.87	124.27 (- 0.6)	124.76 (-0.11)	125.17 (+0.3)
Blank offset setting [mm]	26.67	27.27 (+ 0.8)	26.59 (-0.08)	26.97 (+0)
Basic tilt angle [deg]	0	0 (+ 0)	0	0
Basic swivel angle [deg]	11.3066	11.3066 (+ 0)	11.3066	11.3066
Machine root angle [deg]	16.11248	16.41248 (+ 0.3)	16.11248	16.11248

4.4.3 Mesh and Dynamic results

Time-varying mesh parameters, such as translational TE and mesh stiffness, varying with pinion roll angle are calculated and compared among all the cases in Figure 28 and Figure 29. As shown in Figure 28, although the average translational TE of Case 1 decreases, the amplitude of Case 1 increases significantly which means the zero-to-peak TE increases and has a worse dynamic response. Case 2 NN PSO may increase in quantity but a decreasing vibration amplitude compared with the Baseline Case. Case 3 NN GD also has a smaller amplitude than the Baseline Case. The fluctuation of static translational TE is the excitation input into the geared rotor system. So, Case 2 NN PSO and Case 3 NN GD have an improvement in dynamic response.

It can be seen in Figure 29 that the mesh stiffness decreased for all machine tool setting variation cases with Baseline Case. It will slightly change the natural frequency of the entire geared rotor system.

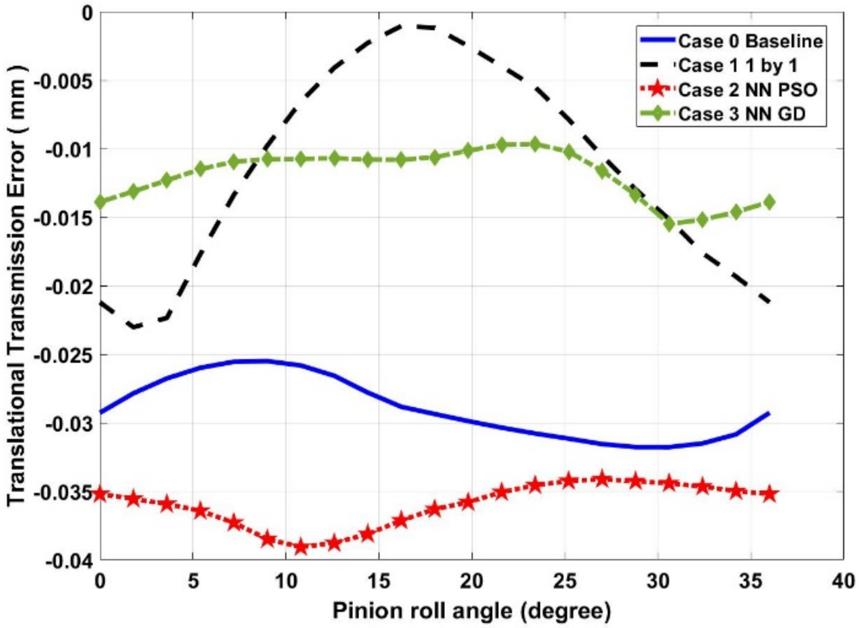

Figure 28 Time-varying translational TE

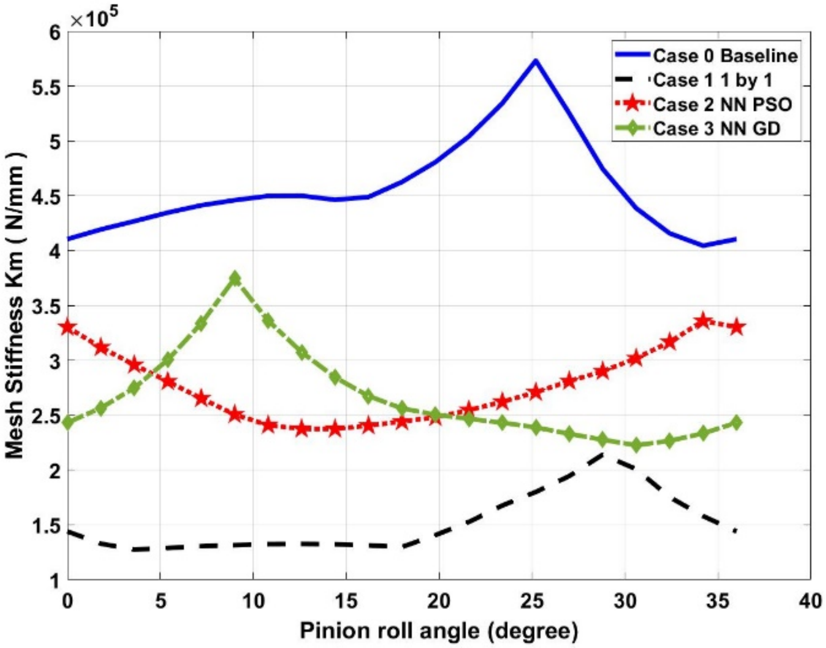

Figure 29 Time-varying mesh stiffness

Time-average mesh force and zero-to-peak translational TE are applied to the linear time-invariant (LTI) analysis in the lumped parameter model of the hypoid geared rotor system. The dynamic response of dynamic TE, dynamic mesh force are calculated among all the cases separately, and the comparison results are presented in Figure 30 and Figure 31. Dynamic TE and dynamic mesh force spectrum are used to evaluate the vibration of the geared rotor system. For Case 1, the magnitude of the spectrum is larger than the baseline case because of the larger TE fluctuation. A combination of every single parameter optimal value may not be the optimal case for all machine tool settings considered together. Because machine tool settings are related to each other dependently. From the dynamic response of Case 1, the variation of all machine tool settings should be considered together.

For machine tool settings optimized by the neural network model, Case 2 and Case 3 have improved dynamic response nearly all frequency domain. Case 2 NN PSO has the best result among all cases because the PSO optimization algorithm has a higher inertia weight at the beginning iterations to obtain a stronger global search ability and as the iteration goes on, the inertia weight becomes lower to obtain stronger local optimization ability for faster convergence performance.

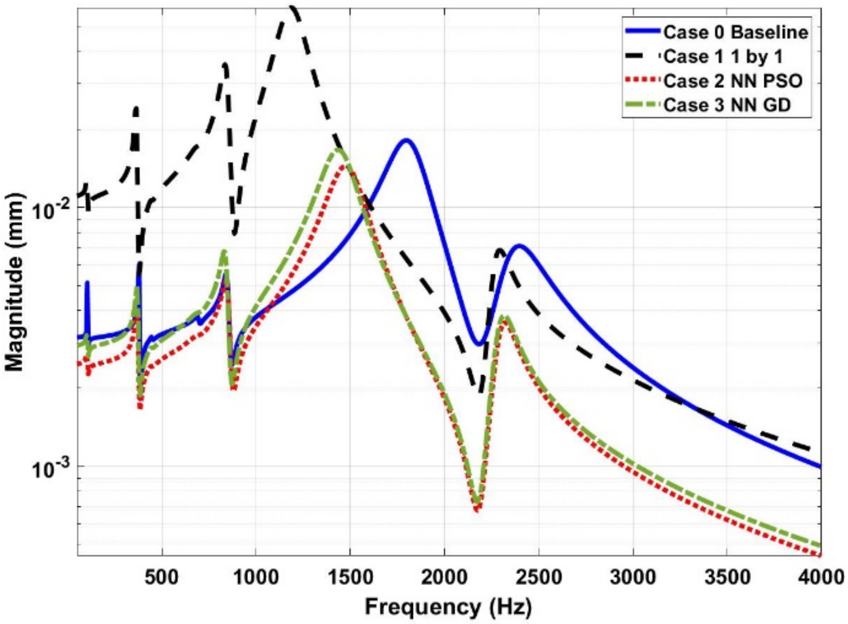

Figure 30 Dynamic transmission error spectrum

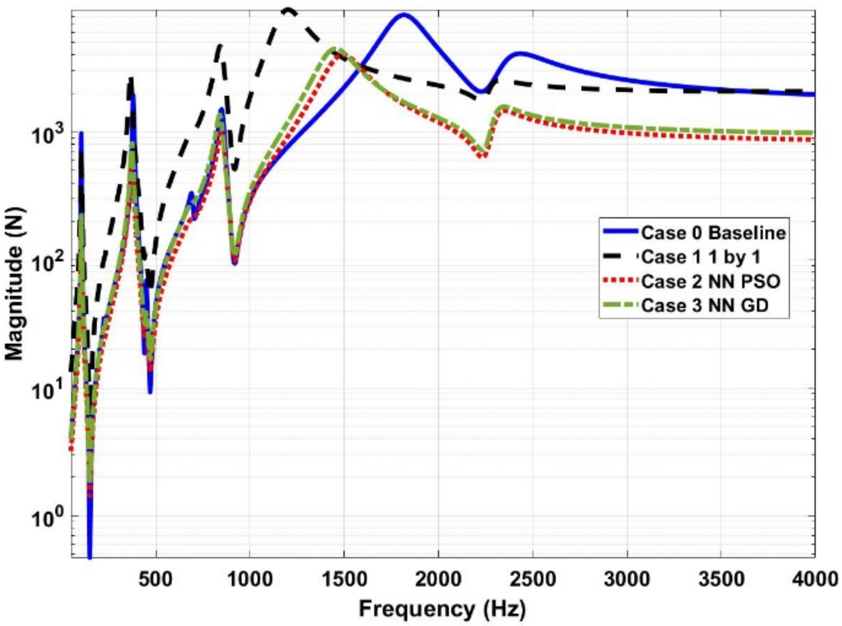

Figure 31 Dynamic mesh force spectrum

4.5 Conclusion

In this chapter, the optimization of machine tool settings on hypoid gear dynamics is discussed. An approach with feed-forward backpropagation neural network algorithm to obtain minimum zero-to-peak transmission error and improved dynamic response with machine tool setting parameters is presented. A case study of a hypoid gear pair with specified design parameters and working condition is calculated and compared with optimized cases. The results revealed that by using optimal machine tool settings obtained through the proposed method the zero-to-peak transmission error decrease, which is the source of vibration in the hypoid geared rotor system. The magnitude of dynamic responses, including dynamic transmission error and dynamic mesh force are decreased too, which are commonly used to evaluate the vibration response in gear dynamics. The results conclude that optimal machine tool settings acquired by minimizing zero-to-peak TE can improve the overall NVH behavior.

Chapter 5 Axle Housing Vibro-acoustic Analysis

5.1 Introduction

The forced vibration and acoustic analysis of the axle housing are presented in this section. The finite element (FE) model is used for the forced vibration analysis. The FE model of an axle housing for a typical vehicle axle application is shown in Figure 32 (a). The bearing loads calculated from previous dynamic analyses are applied at the center point of the bearing circles and rigid couplings are assumed between the center point and bearing outer race sleeves.

The frequency response functions (FRFs) are calculated for the frequency up to 4 kHz. The housing FRFs will be used as input to a boundary element (BE) model to further evaluate the sound radiation from the gearbox housing. The boundary element model of gearbox housing is shown in Figure 32 (b). Fast multi-pole BE method is applied to calculate the gearbox sound radiation, which accelerates the computation with a realistic system modeling [29-30]. To obtain an accurate estimate of sound power, 20 numerical microphones are mounted on a sphere surface enveloping the gearbox according to the international standard ISO 3745. The sound power is computed by integrating the sound pressure at these locations in the sphere.

The sound power level is calculated as

$$L_w = L_p + 10log_{10}\left(\frac{s}{s_0}\right) + c_1 + c_2 \tag{5-1}$$

$$c_1 = -10log_{10}\left[\frac{B}{B_0}\left(\frac{313.14}{273.15+T}\right)^{0.5}\right] \quad (5\text{-}2)$$

$$c_2 = -15log_{10}\left[\frac{B}{B_0}\left(\frac{296.15}{273.15+T}\right)^{0.5}\right] \quad (5\text{-}3)$$

where s is the area of the measurement surface and s_0 = 1 m^2; the symbol B is the barometric air pressure during measurements, in Pascal; the symbol B_0 is the reference barometric pressure; the symbol T is the air temperature during measurement; and L_p is the weighed surface sound pressure level over the measurement surface in decibels:

$$L_p = 10log_{10}\left\{\left(\frac{1}{N}\left[\Sigma_i 10^{0.1\left(L_{p,i}+W\right)}\right]\right)\right\} \quad (5\text{-}4)$$

$$L_{p,i} = 20log_{10}\left[\frac{p_i}{p_0}\right] \quad (5\text{-}5)$$

where N is the number of microphone positions and W is the weighting function applied by the filter at the frequency of analysis. Also, p_i is the root mean square pressure in Pascal and p_0 = $2x10^{-5}$.

(a)

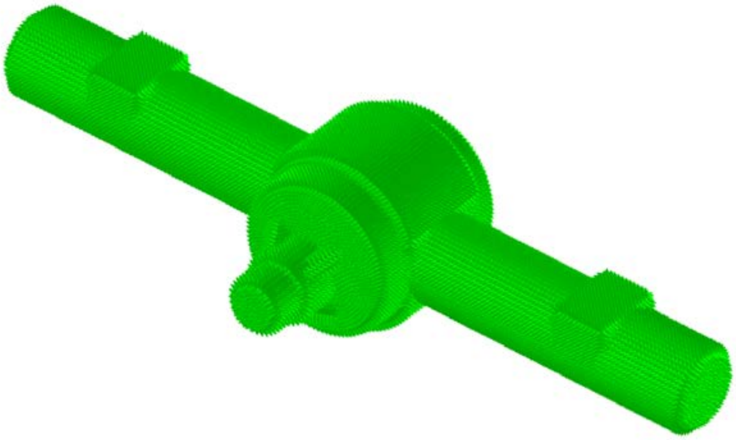
(b)

Figure 32 Axle housing structure a) finite element model b) boundary element model.

5.2 Modal analysis

The axle NVH performance is an important topic for the vehicle manufacturer to design an axle system which has meeting the international standard for noise radiation and maintain the structural durability. The hypoid gear dynamic transmission error and dynamic mesh force are the primary excitations for the axle housing noise and vibration. The vibratory energy of the gear pair caused by transmission error is transmitted structurally through shaft-bearing-housing assembly and radiates off from exterior housing. In this chapter, the axle housing vibro-acoustic analysis is performed and compares the results between the baseline case and optimized case from the neural network model.

The mode shapes and natural frequencies of 14 degrees of freedoms hypoid geared-rotor system with baseline gear shape and the optimized case can be compared in Figure 33. The hypoid gear pair out-of-phase torsional modes are the main excitation modes to the axle noise problem. For the 14 degrees of freedoms hypoid geared-rotor system model, θ_{py} (the 6th DOF) and θ_{gy}(the 12th DOF) should have the same sign convention which can be identified as mode 3, mode 7, and mode 8 with frequency 569.4 Hz, 1551.7 Hz, and 3193.6 Hz respectively for baseline case. The same trend is for the optimized case with the smaller frequencies of 569.1 Hz, 1538.5 Hz, and 3175.4 Hz because of the decreasing mesh stiffness and the zero-to-peak transmission error.

5.3 Dynamic Analysis

The dynamic bearing force on the actual pinion and gear bearing positions are calculated and transformed back from shaft-bearing relation for the four bearing positions of the axle system. The pinion head and the gear head dynamic bearing forces are plotted as Figure 34 and Figure 35 on the horizontal, axial, and vertical direction. On the pinion bearing force, there are three peaks excitation with around 600, 1500, and 3000 Hz. On the gear bearing force, there are two peaks excitation with around 600 and 1500 Hz.

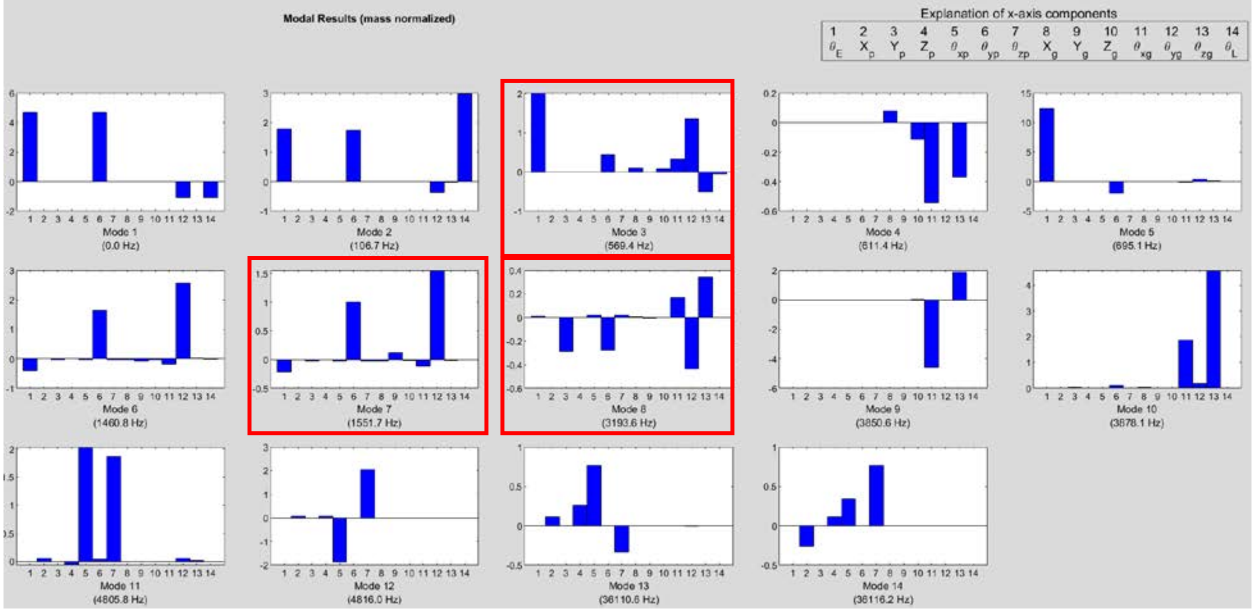

(a) Baseline Case

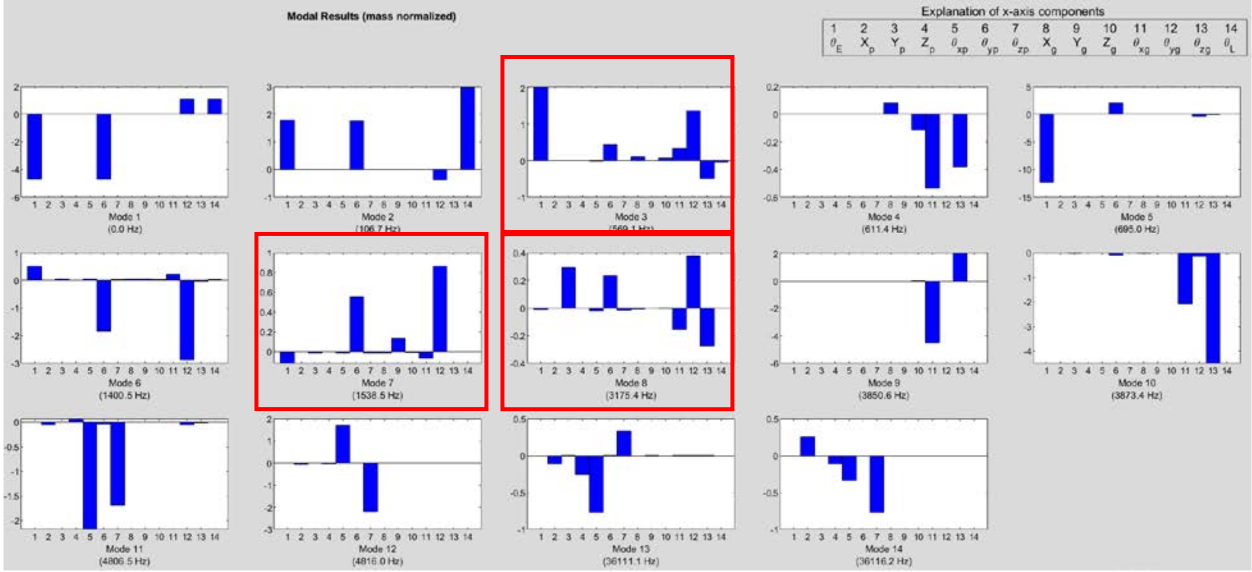

(b) The optimized case from neural network model - D8A3 Case

Figure 33 14 DOF gear-rotor system mode shape and natural frequencies comparison

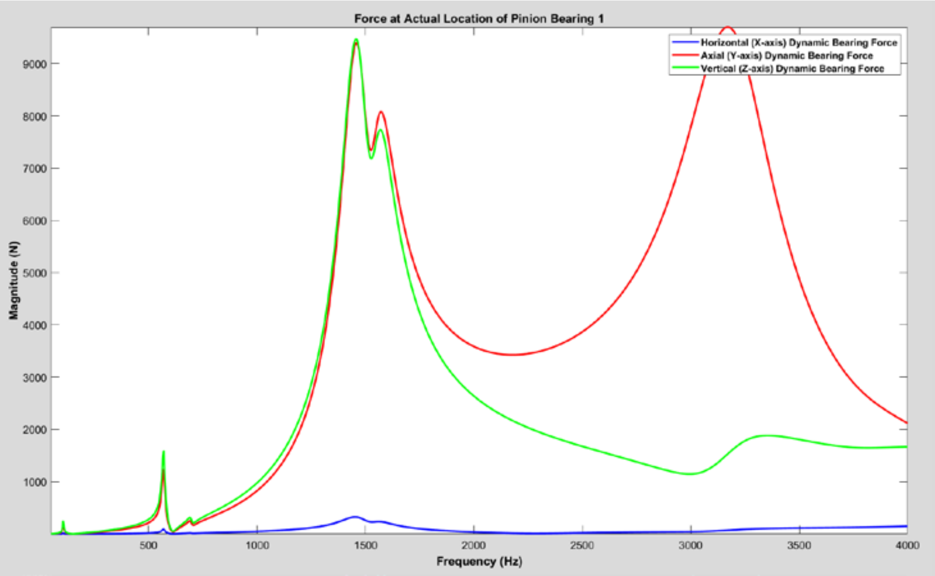

(a) Baseline

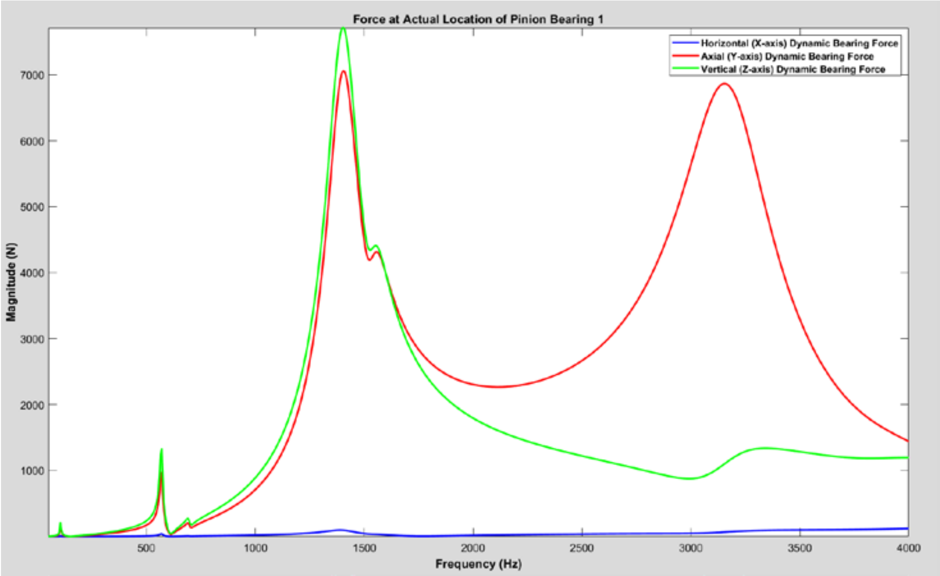

(b) The optimized case from neural network model - D8A3 Case

Figure 34 Dynamic bearing force spectrum of pinion head bearing

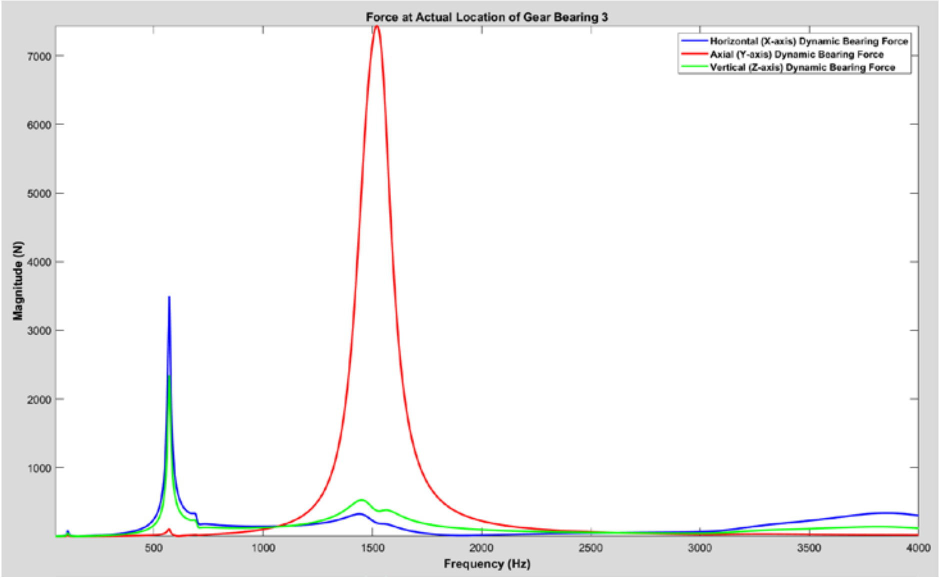

(a) Baseline

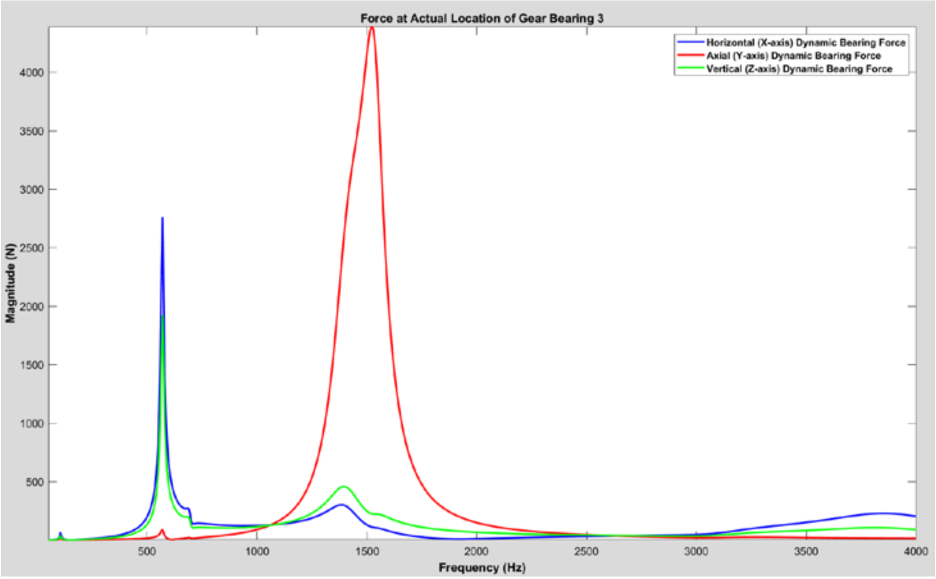

(b) The optimized case from neural network model - D8A3 Case

Figure 35 Dynamic bearing force spectrum of gear head bearing

Both pinion and gear dynamic bearing force have significant magnitude reduction on the peak mode for the optimized case compared with baseline. Using these dynamic bearing force as input excitation for the housing dynamic steady-state analysis with the modal superposition method through Abaqus CAE. The peak mode of 1500 Hz housing surface velocity is calculated and plotted as Figure 36. The dynamic response and surface velocity distribution can be observed. The hot point for frequency 1500 Hz is near the top of the pinion head bearing housing surface.

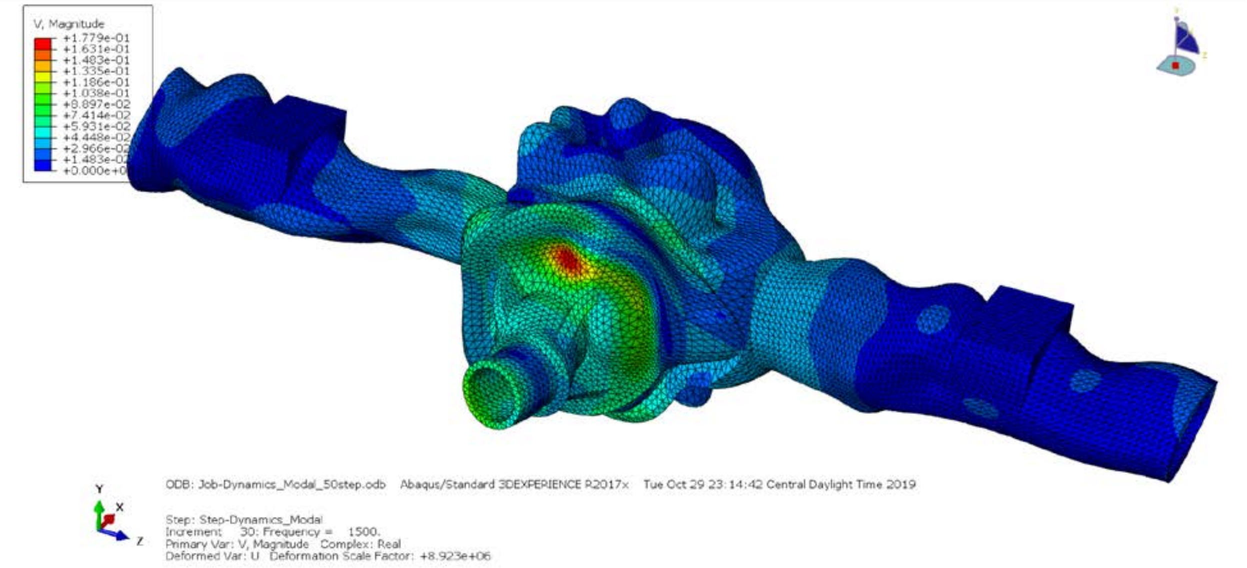

```
ODB: Job-Dynamics_Modal_50step.odb    Abaqus/Standard 3DEXPERIENCE R2017x    Tue Oct 29 23:14:42 Central Daylight Time 2019

Step: Step-Dynamics_Modal
Increment     30: Frequency =    1500.
Primary Var: V, Magnitude   Complex: Real
Deformed Var: U   Deformation Scale Factor: +8.923e+06
```

(a) Baseline

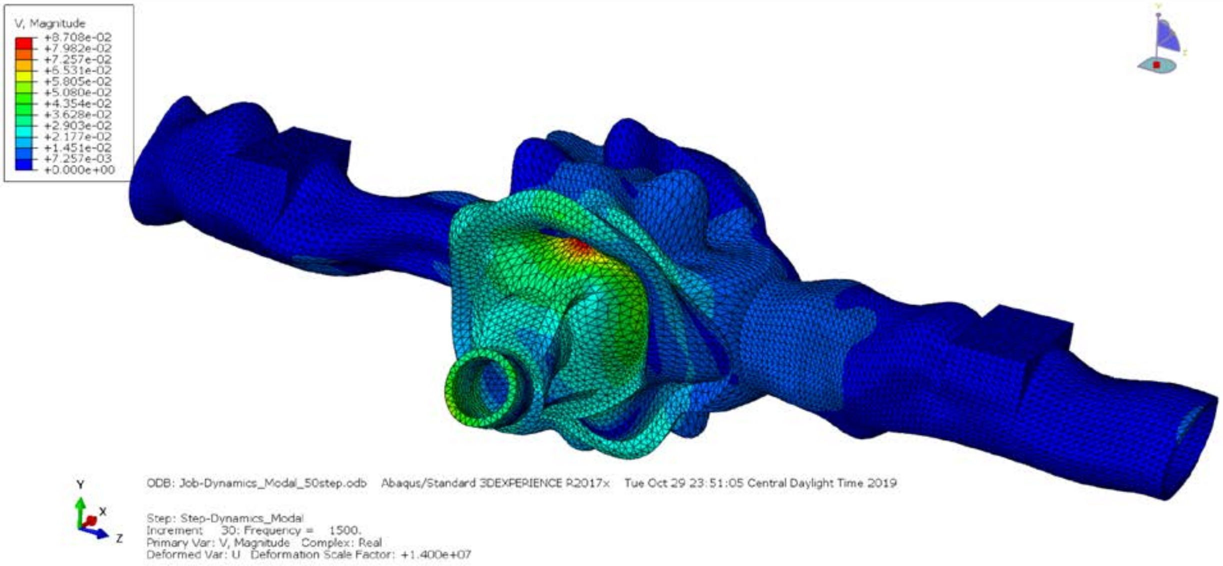

(b) The optimized case from neural network model - D8A3 Case

Figure 36 Axle housing surface velocity at frequency 1500 Hz

The reduction of the surface velocity can be seen from both the housing surface distribution at 1500Hz and the nodal velocity response on the pinion nose position through all frequency range as Figure 37.

5.4 Vibro-acoustic Analysis

The surface velocity of the axle housing calculated from the dynamic analysis is the input for the noise radiation analysis using the boundary element method. The sound pressure distributions for both cases on the housing surface at frequency 1500 Hz are plotted as Figure 38. The sound pressure near the pinion head bearing position is alleviated for the optimized case compared with the baseline case. The sound pressure distributions for both cases on the far-field sphere with radius 1 meter at frequency 1500 Hz are plotted as Figure 39. The sensors for sound pressure level with 1-meter distance from the axle housing origin are plotted as Figure 40 for all frequency range. The reduction of 5 dBA at the frequency of 1500 Hz.

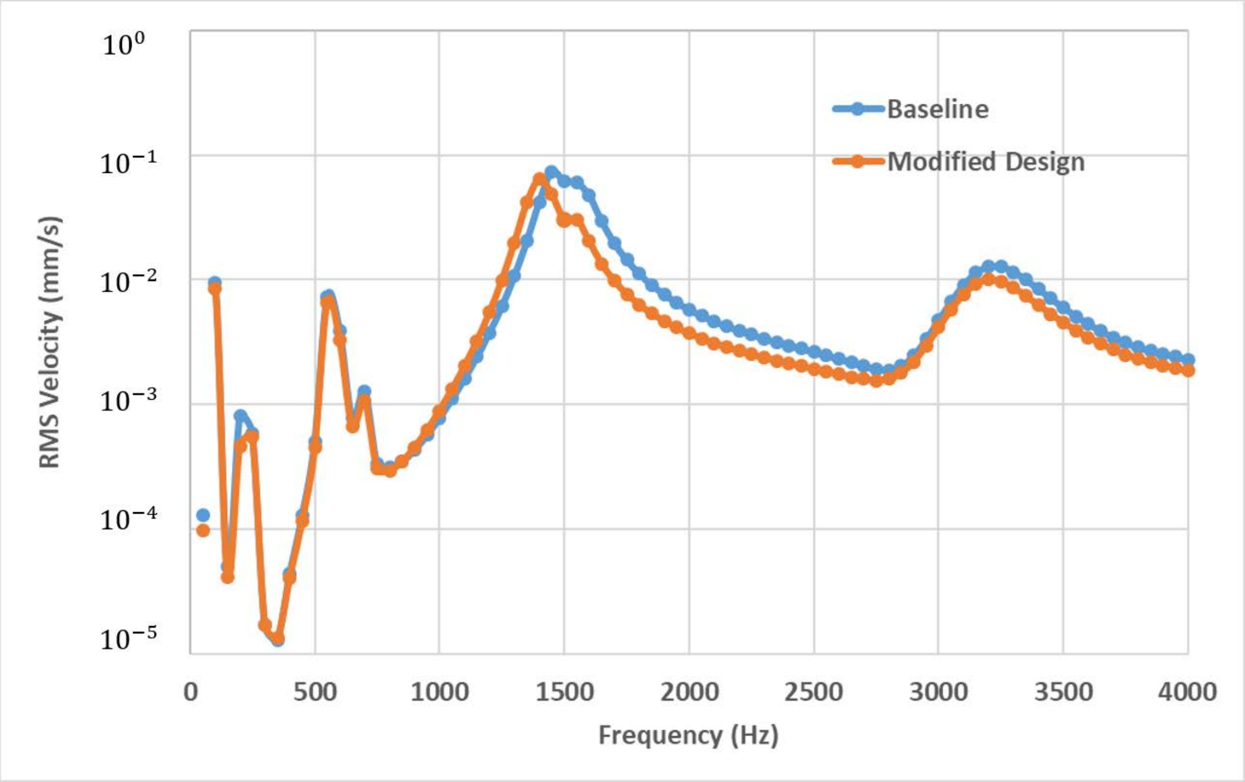

Figure 37 Housing nodal surface velocity on the pinion nose position

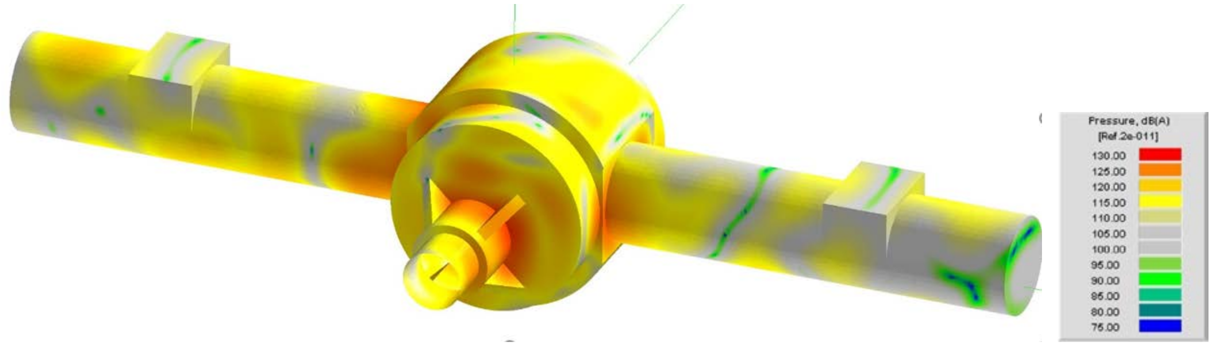

(a) Baseline

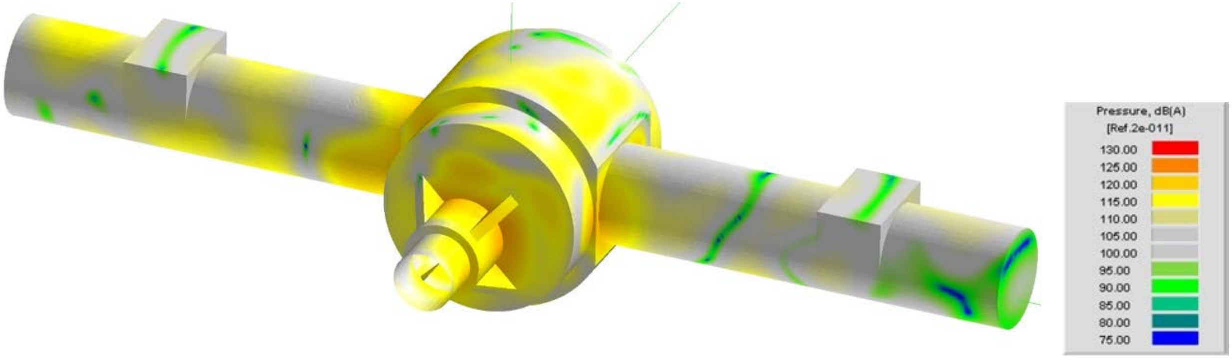

(b) Modified Design

(c) The optimized case from neural network model - D8A3 Case

Figure 38 Sound pressure distribution on the axle housing surface

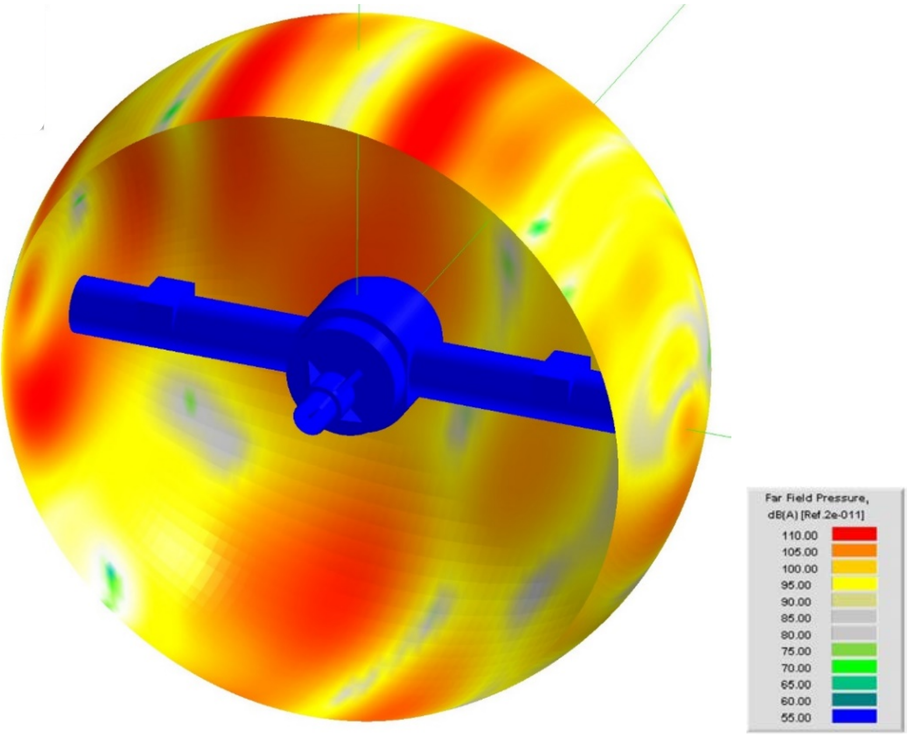

(a) Baseline

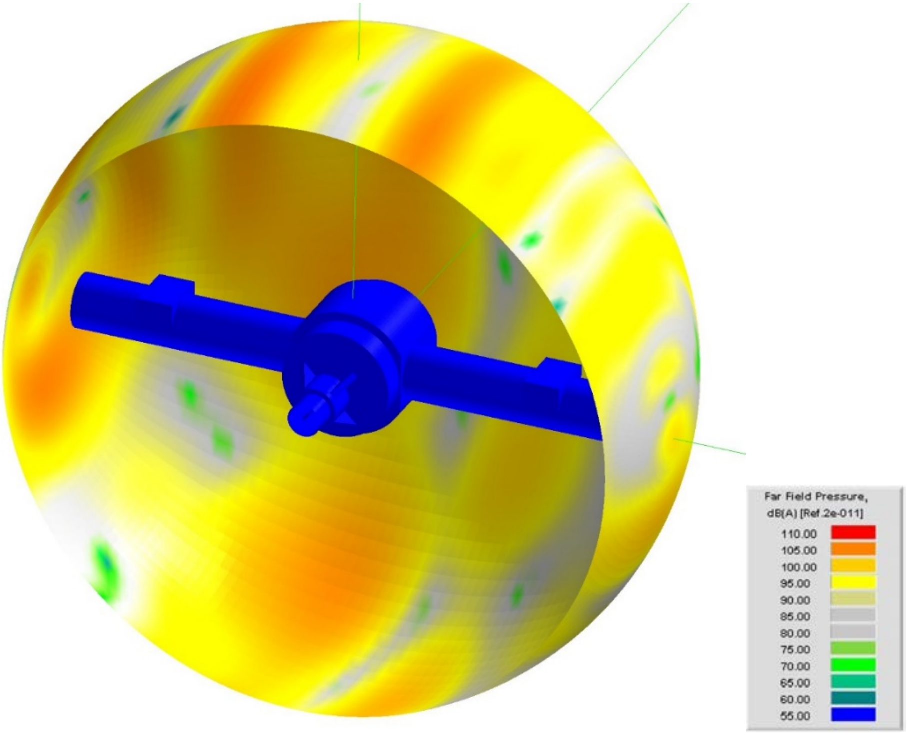

(b) Modified Design

Figure 39 Far-field sound pressure on the sphere with radius 1 meter

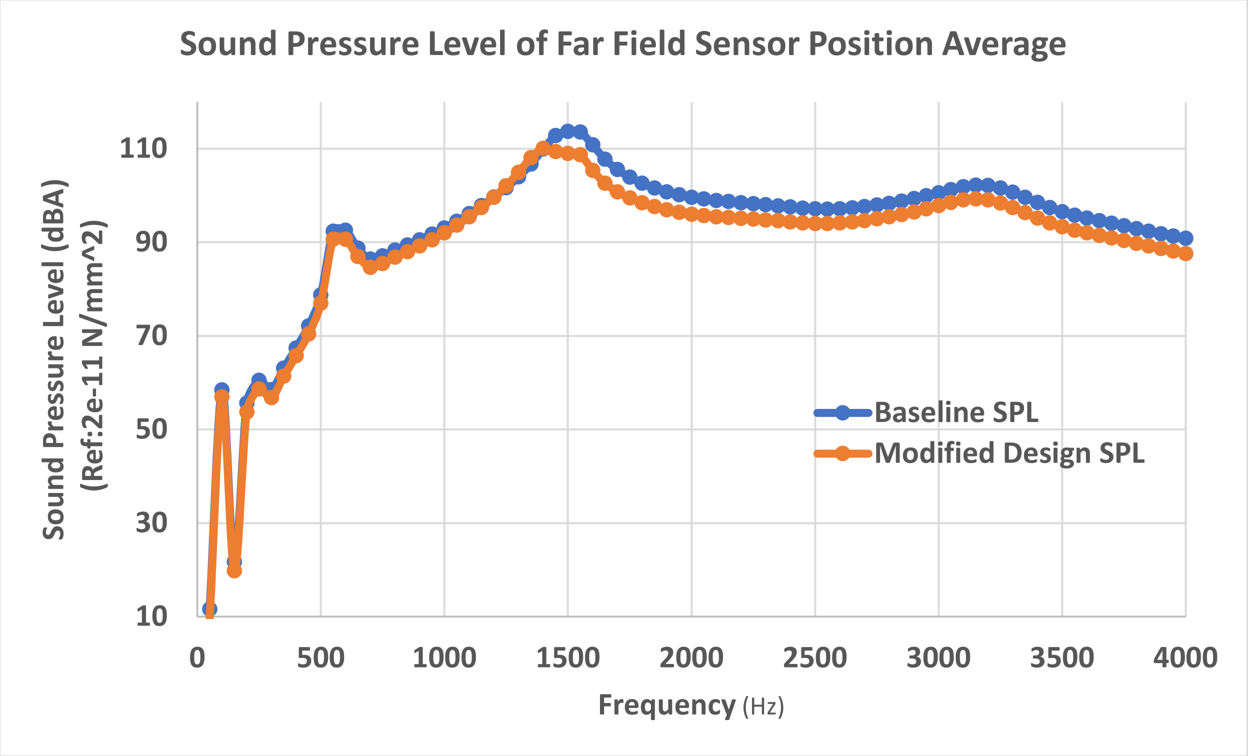

Figure 40 Sound pressure level average on far-field sensors with distance 1 meter

5.5 Conclusion

In this chapter, the forced vibration and acoustic analysis of the axle housing are performed with the comparisons of the results between the baseline case and optimized case from the neural network model. The detailed finite element model and boundary element model of the axle housing is used to simulate the vibration response and noise radiation for the given work condition of the rear axle systems. The optimized case for the tooth profile modification can be concluded having better performance on the reduction of the axle housing surface vibration response and velocity for all the frequency range. Moreover, the vibro-acoustic response for the sound pressure level of the housing surface and the far-field sphere has reduced after modified. The reduction of SPL has up to 5 dB for the modified case at the frequency of 1500 Hz.

Chapter 6 Ease-off Modification on Hypoid Gear Tooth Surface

6.1 Introduction

Tooth profile modification on the flank has a significant influence on minimizing the transmission error variation and reducing the noise and vibration level in the hypoid gear design process. Ease-off topography modification is an effective approach to optimize tooth flank. Shih [15] proposed a flank modification methodology for face-hobbing spiral bevel and hypoid gears based on the ease-off topography of the gear drive. Kolivand [32-33] proposed a methodology based on the ease-off topography which is used to determine the unloaded contact patterns and find the instantaneous contact curve through surface roll angles. Fan [16] described a method of tooth flank form error correction utilizing the universal motions for spiral bevel and hypoid gears produced by the face-milling process. The sensitivity of the changes of the tooth flank form geometry to the changes of the universal motion coefficients is investigated.

The ease-off topography shows the deviations of a pinion's tooth flanks with respect to the fully conjugated tooth flank derived from the mating gear as Figure 41. The real pinion tooth surface is not perfect because of the manufacture and assembly errors and the deflection after applying load. Therefore, the design of the pinion surface has a pre-design transmission error on the outside portion of the contact area to reduce assembly sensitivity and avoid edge contact.

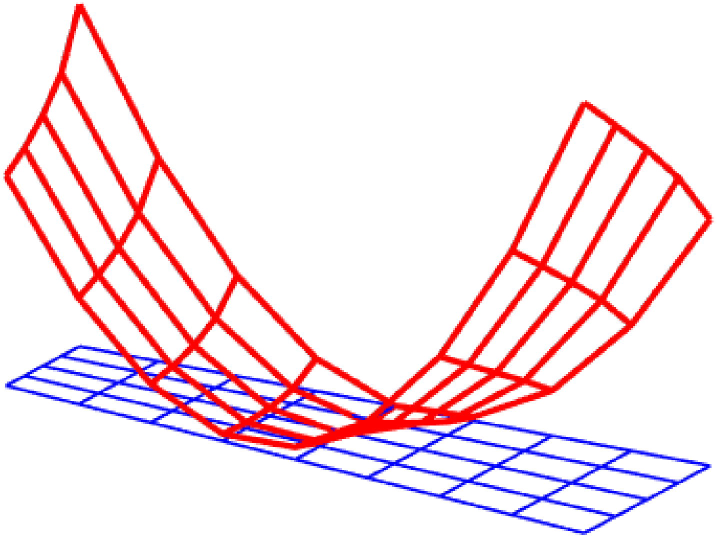

Figure 41 The ease-off topography

The ease-off flank modification is implemented in this chapter to modify the tooth profile. The different topographies of contact characteristics are evaluated with the comprehensive simulation process to validate the noise and vibration performance. The entire simulation flow chart is shown in Figure 42. The basic gear design is modified to the desire tooth surface by the method of ease-off modification. The loaded tooth contact analysis is performed on the gear pair and axle system model. The geared-rotor system model is developed to calculate the dynamic mesh force. The dynamic bearing force is used as an excitation force on the finite element axle housing for the further steady-state vibration analysis. The housing surface velocity is calculated for vibro-acoustic analysis.

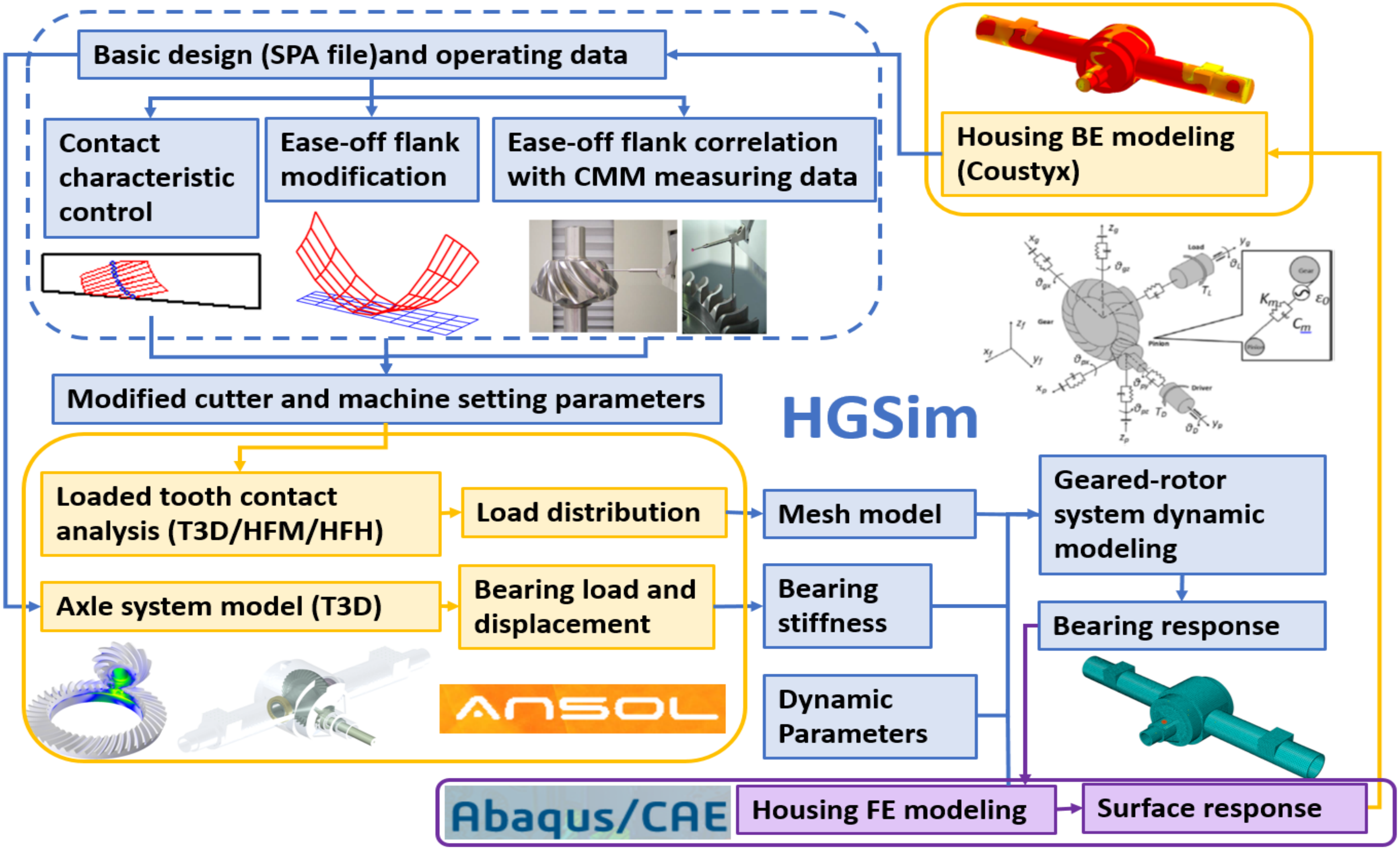

Figure 42 Simulation flow chart of the ease-off flank modification

6.2 Ease-off Topography Modification

The tooth surface modification can be achieved by the modification of the design parameters including gear cutter parameters, machine tool settings, and the high-order coefficients of the universal motion. The universal motions are described as the higher-order polynomial representation of machine settings, which can be used to correct the higher-order components of tooth flank form errors.

$$X_p = X_{e0} + X_{e1}q + X_{e2}q^2 + X_{e3}q^3 + X_{e4}q^4$$

$$X_b = X_{b0} + X_{b1}q + X_{b2}q^2 + X_{b3}q^3 + X_{b4}q^4$$

$$X_e = X_{e0} + X_{e1}q + X_{e2}q^2 + X_{e3}q^3 + X_{e4}q^4$$

$$S_r = S_{r0} + S_{r0}q + S_{r1}q^2 + S_{r2}q^3 + S_{r3}q^4$$

$$j_r = j_{r0} + j_{r1}q + j_{r2}q^2 + j_{r3}q^3 + j_{r4}q^4$$

$$i_r = i_{r0} + i_{r1}q + i_{r2}q^2 + i_{r3}q^3 + i_{r4}q^4$$

$$\gamma_m = \gamma_{m0} + \gamma_{m1}q + \gamma_{m2}q^2 + \gamma_{m3}q^3 + \gamma_{m4}q^4$$

$$R_a = R_{a0} + R_{a1}q + R_{a2}q^2 + R_{a3}q^3 + R_{a4}q^4 \tag{6-1}$$

The algorithm used for flank modification based on ease-off topography is similar to Shih [15]. For the desired product with quieter running characteristic and NVH performance, the gear surface can be reconstructed from CMM data for each surface grid points of the ease-off topography. The ease-off topography of baseline design can be established by the mathematical model or CMM data. The normal variation of the difference vector at topographical grid points can be written in the matrix form

$$\begin{Bmatrix} \delta D_1 \\ \vdots \\ \vdots \\ \delta D_p \end{Bmatrix} = \begin{bmatrix} \delta D_1/\delta\zeta_1 & \cdots & \cdots & \delta D_1/\delta\zeta_q \\ \vdots & \ddots & & \vdots \\ \vdots & & \ddots & \vdots \\ \delta D_p/\delta\zeta_1 & \dots & \dots & \delta D_p/\delta\zeta_q \end{bmatrix} \begin{Bmatrix} \delta\zeta_1 \\ \vdots \\ \vdots \\ \delta\zeta_q \end{Bmatrix} \tag{6-2}$$

$$\{\delta D_i\} = [S_{ij}]\{\delta\zeta_j\} \quad (i = 1, \cdots, p; j = 1, \cdots, q)$$

$\{\delta D_i\}$ - Ease-off variations of the grid points

$[S_{ij}]$ - Sensitivity matrix with respect to the selected design parameters

$\{\delta\zeta_j\}$ - Modifications of selected design parameters

Since the sensitivity matrix is usually ill-conditioned or even nearly singular, singular value decomposition (SVD) is used to avoid numerical divergence.

6.3 Numerical Example

6.3.1 Ease-off Topography Modification

A numerical example of a face-milling gear pair with an 11 to 41 gear ratio is presented to calculate the modification of the selected design parameters including cutter parameters, machine tool settings, and polynomial coefficients of the universal motion. The original design parameters and machine tool settings are shown in Table 6 and Table 7.

Table 6 Design Parameters of Example Gear Pair

Design Parameters		**Pinion**	**Gear**
Number of teeth	–	11	41
Modulus	(mm)	4.024	
Face width	(mm)	29.78	26.00
Shaft angle	(mm)	90	
Offset	(mm)	23.00	
Pressure angle	(deg)	19.00	
Spiral angle	(deg)	50.47	32.55
Hand of spiral	–	Left	Right

Table 7 Machine Tool Settings of Example Gear Pair

Machine Settings		**Pinion Concave**	**Gear Convex**
Machine root angle	(deg)	-6	64.1833
Machine center to cross point	(mm)	0.3283	2.7499
Blank offset	(mm)	24.2703	0
Sliding base	(mm)	16.7557	0
Radial setting	(mm)	66.5199	
Horizontal setting	(mm)		38.0375
Vertical setting	(mm)		55.7178
Tilt angle	(deg)	22.45	0
Swivel angle	(deg)	327.11	0
Ratio of roll	–	3.725713	0
Point radius of blade	(mm)	64.1985	63.5
Pressure angle of blade	(deg)	10	19

The modification is performed on the pinion concave surface and the gear convex remains unchanged. The original unloaded transmission error and contact pattern for pinion and gear from TCA are shown in Figure 43. The sensitivity matrix is calculated from the most influential design parameters and the ease-off sensitivity topography can be obtained by changing the selected parameters as shown in Figure 44 to Figure 56.

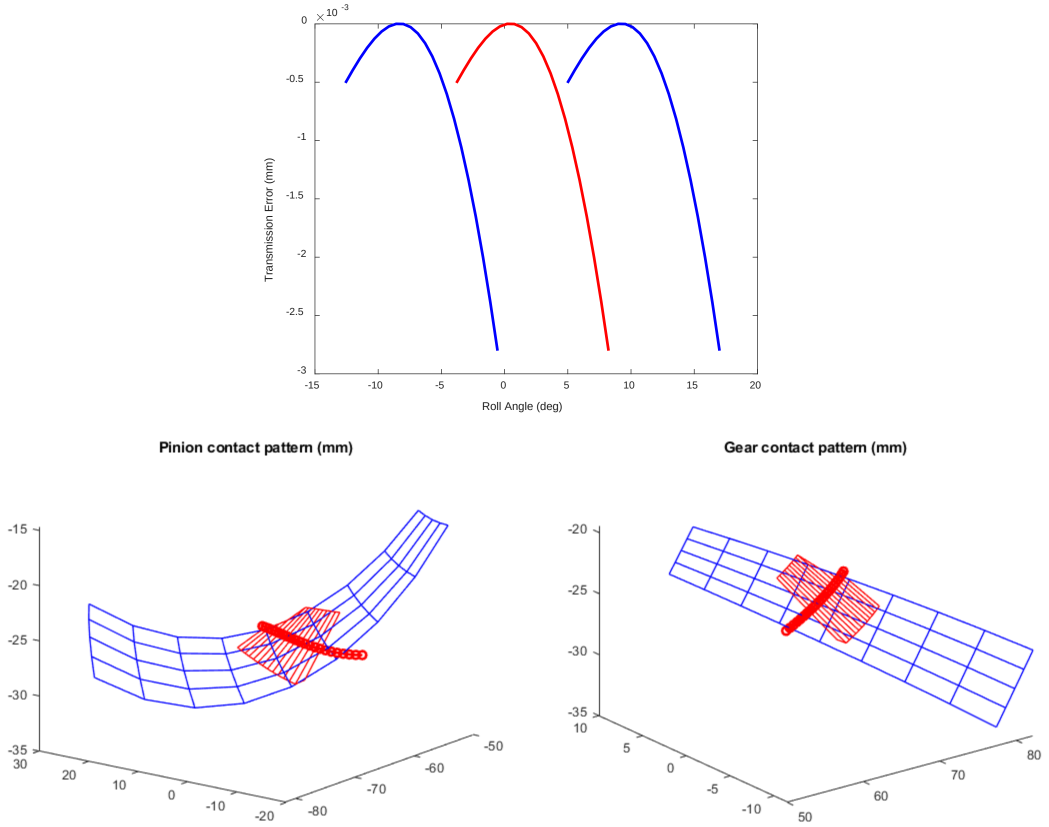

Figure 43 TE and contact pattern on original pinion concave and gear convex surface

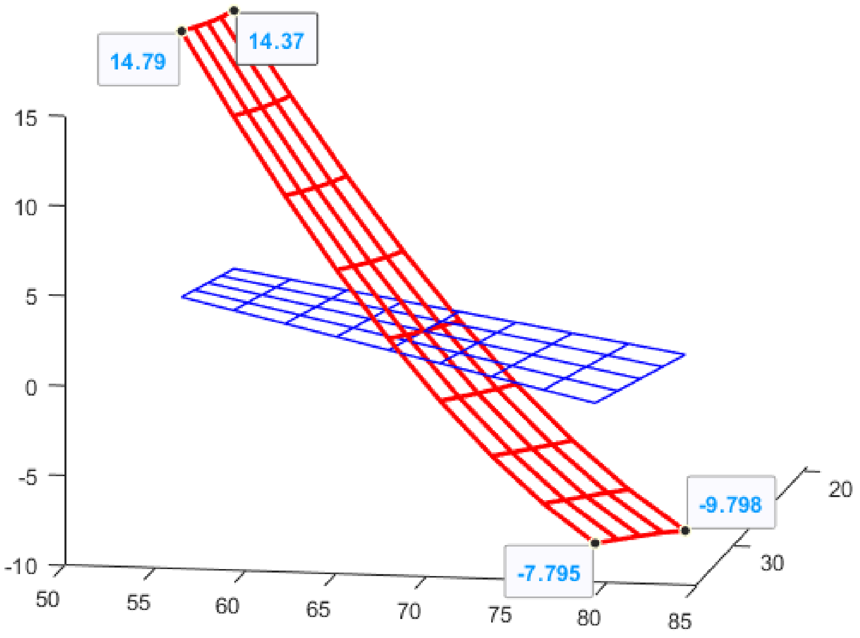

Figure 44 Ease-off Sensitivity Topography of Cutter Point Radius

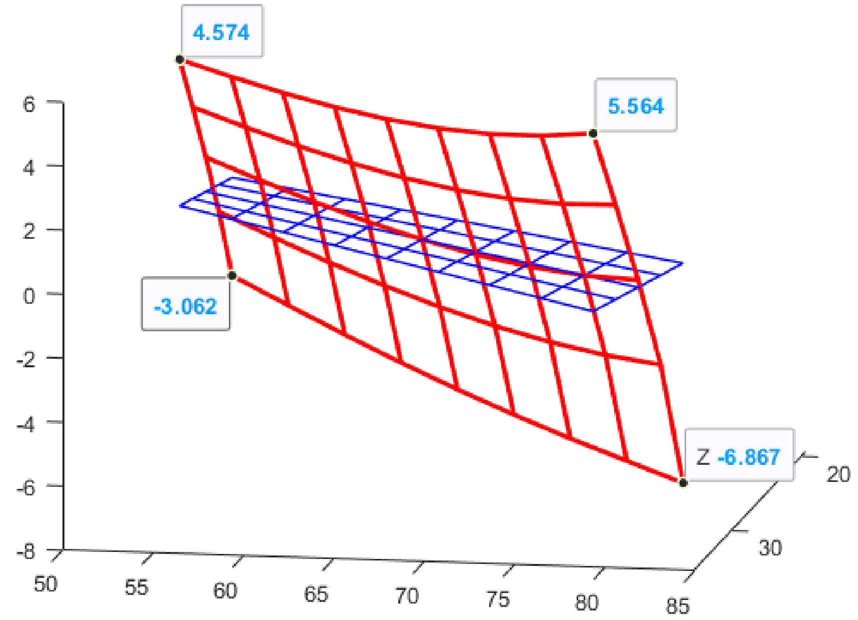

Figure 45 Ease-off Sensitivity Topography of Blade Angle

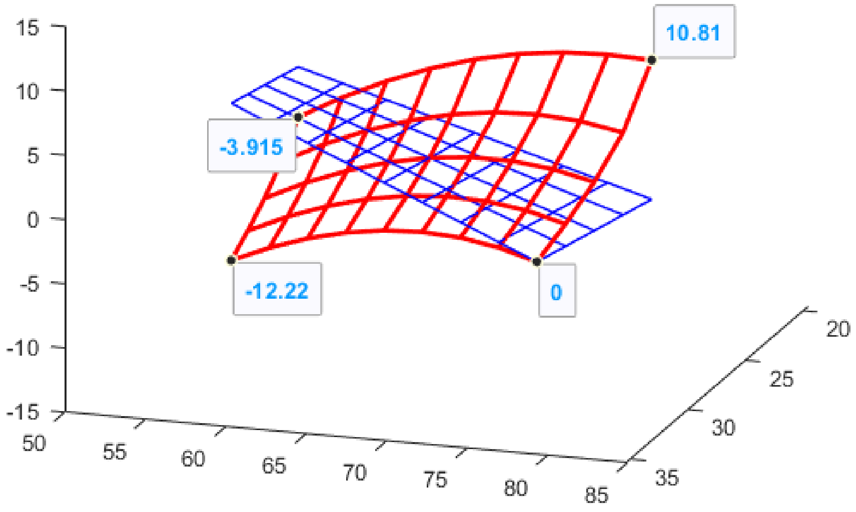

Figure 46 Ease-off Sensitivity Topography of Machine Center to Back

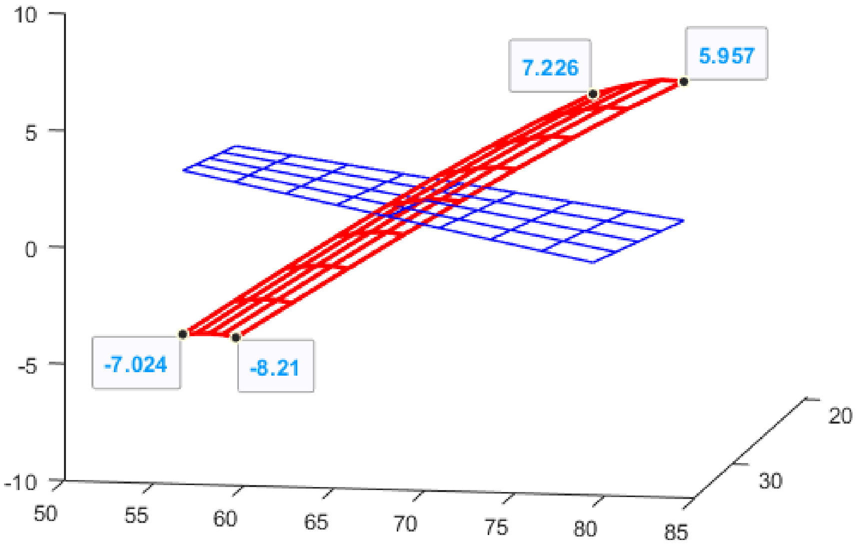

Figure 47 Ease-off Sensitivity Topography of Sliding Base

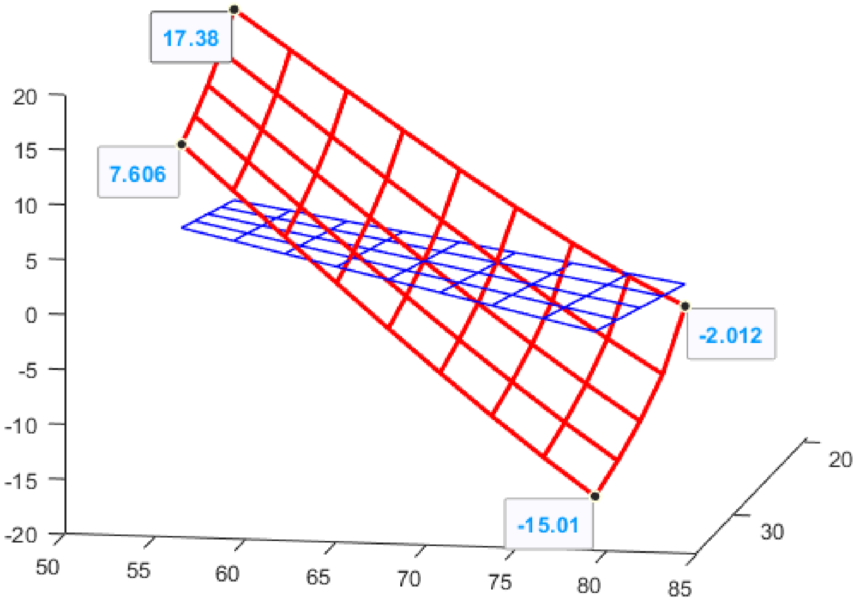

Figure 48 Ease-off Sensitivity Topography of Blank Offset

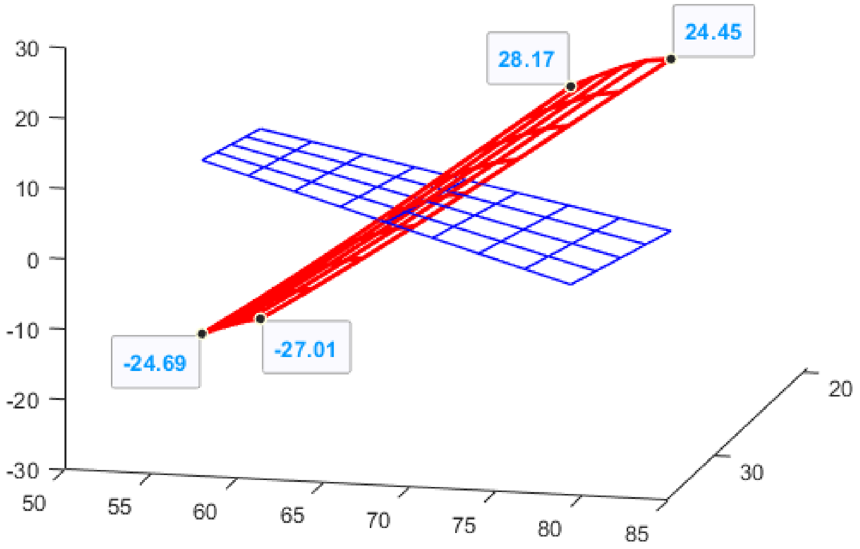

Figure 49 Ease-off Sensitivity Topography of Radial Setting

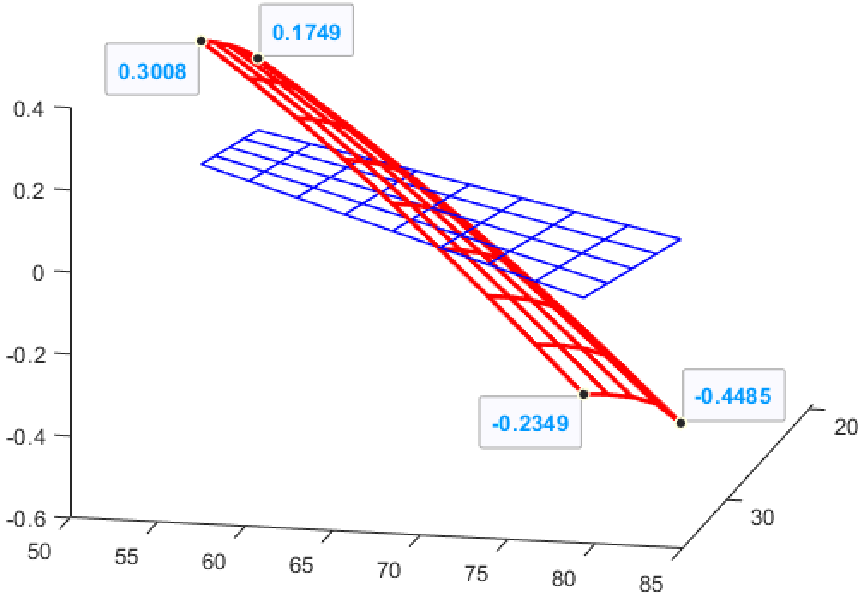

Figure 50 Ease-off Sensitivity Topography of Ratio of Roll

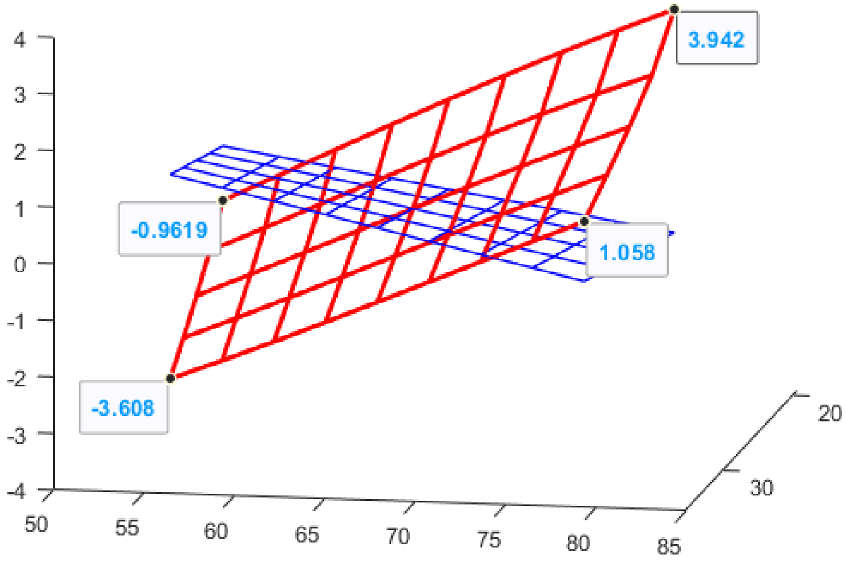

Figure 51 Ease-off Sensitivity Topography of Swivel Angle

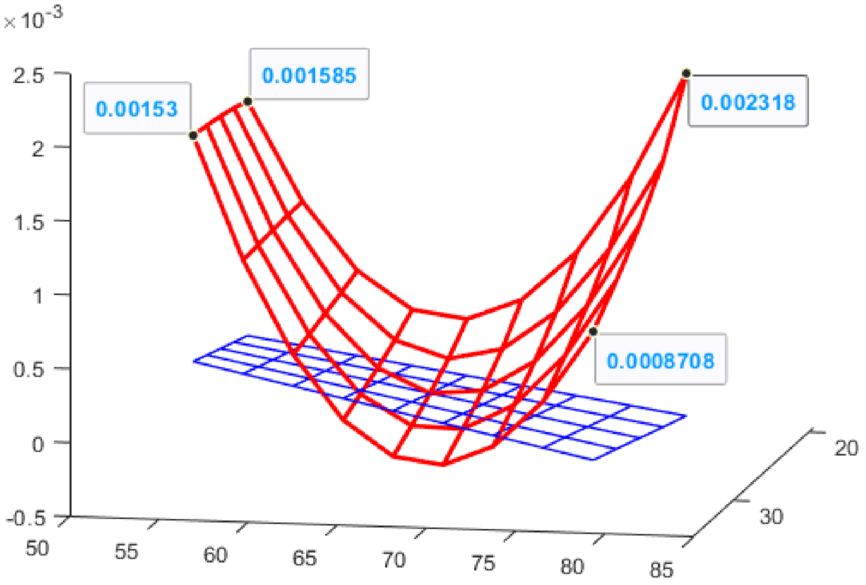

Figure 52 Ease-off Sensitivity Topography of Helical motion 1st order

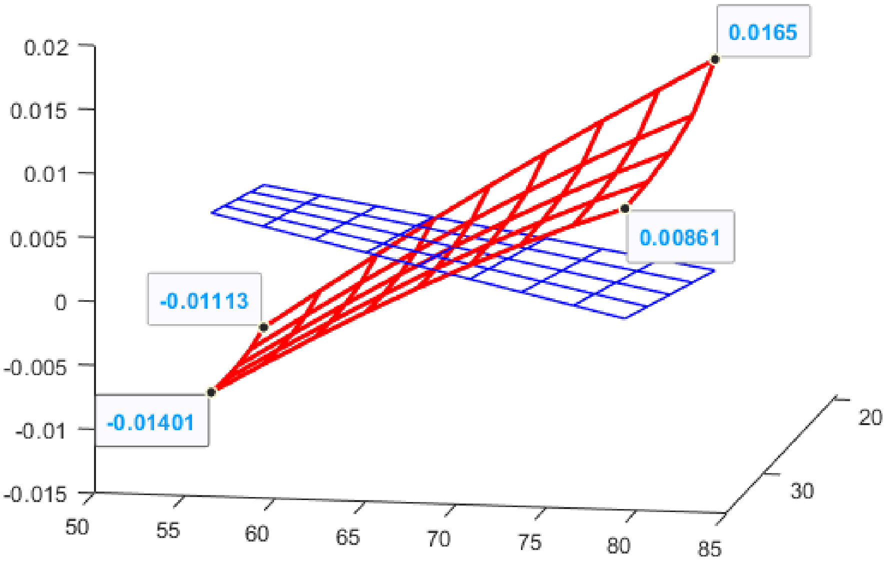

Figure 53 Ease-off Sensitivity Topography of Vertical motion 1st order

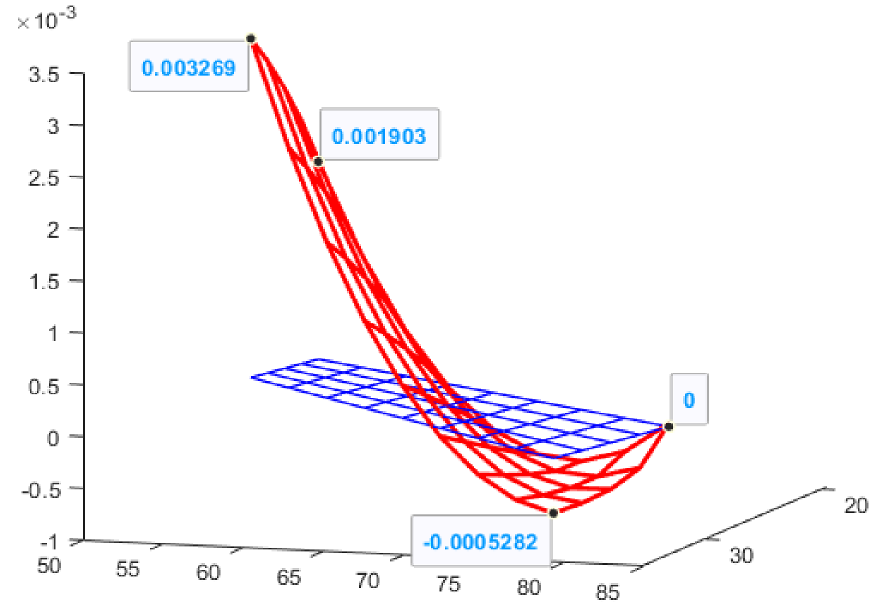

Figure 54 Ease-off Sensitivity Topography of Vertical motion 2nd order

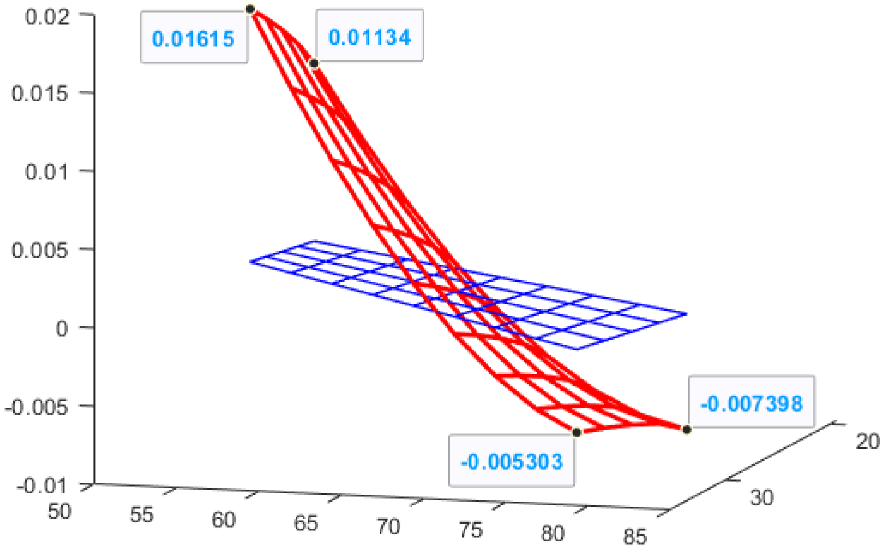

Figure 55 Ease-off Sensitivity Topography of Radial motion 1st order

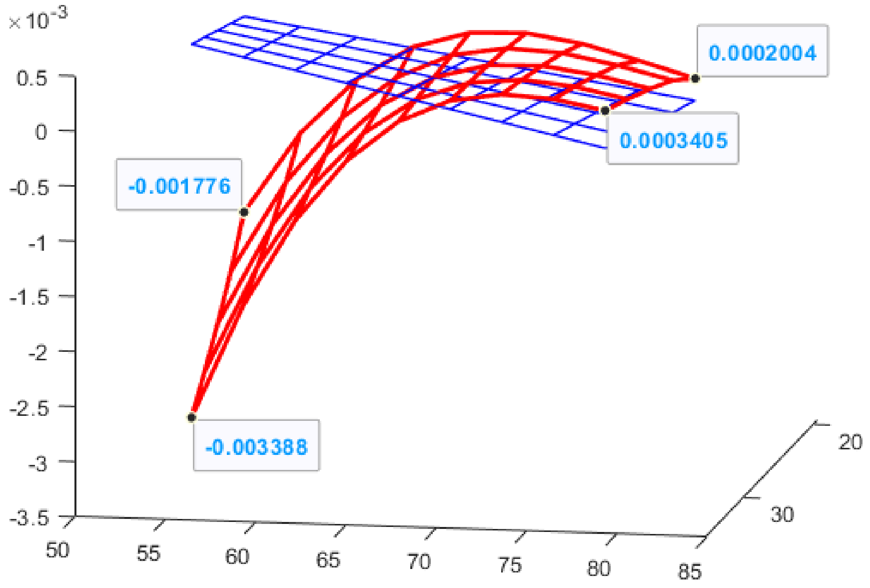

Figure 56 Ease-off Sensitivity Topography of Radial motion 2nd order

The modified pinion design parameters of the cutter, machine tool settings, and polynomial are listed in Table 8. The ease-off topography of the target gear pair and the modified gear pair are shown in Figure 57 and Figure 58. The grid values on the four corners are close between the target and modified topography. The contact pattern of pinion and gear modified tooth surface are validated with the FE/CM model in Calyx with the modified design parameters. The results are close for the contact area and direction for contact trace as shown in Figure 59.

Table 8 Modifications of pinion design parameters

Design Parameters			**Value**
Pinion Cutter Point Radius	R_c	mm	-2.0936
Blade angle	ϕ_b	rad	0.0047
Machine root angle	λ_m	rad	0.0422
Machine center to back	X_p	mm	0.8357
Sliding base	X_b	mm	0.4198
Machine offset	X_e	mm	-0.6480
Radial setting	S	mm	-1.1826
Ratio of roll	R_{aq}	-	0.0558
Tilt angle	i_0	rad	-0.0074
Swivel angle	j_0	rad	-0.1067
Cradle angle	q_0	rad	0
Modified roll motion 1st order	$2C$	-	0
Modified roll motion 2nd order	$6D$	-	0
Helical motion 1st order	H_1	-	-0.0389
Helical motion 2nd order	H_2	-	0
Helical motion 3rd order	H_3	-	0
Helical motion 4th order	H_4	-	0
Vertical motion 1st order	V_1	-	0.0092
Vertical motion 2nd order	V_2	-	0.0032
Vertical motion 3rd order	V_3	-	0
Vertical motion 4th order	V_4	-	0
Radial motion 1st order	R_1	-	-0.0125
Radial motion 2nd order	R_2	-	-0.0320
Radial motion 3rd order	R_3	-	0
Radial motion 4th order	R_4	-	0

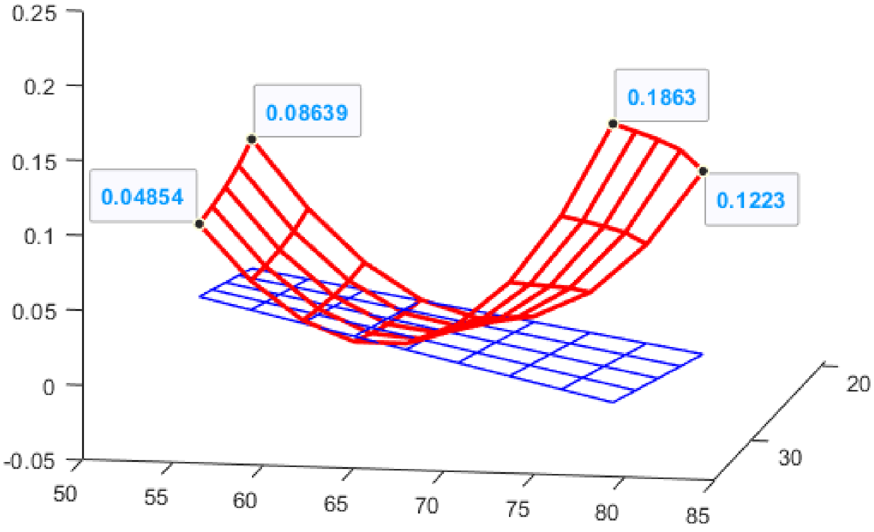

Figure 57 The ease-off target topography (mm)

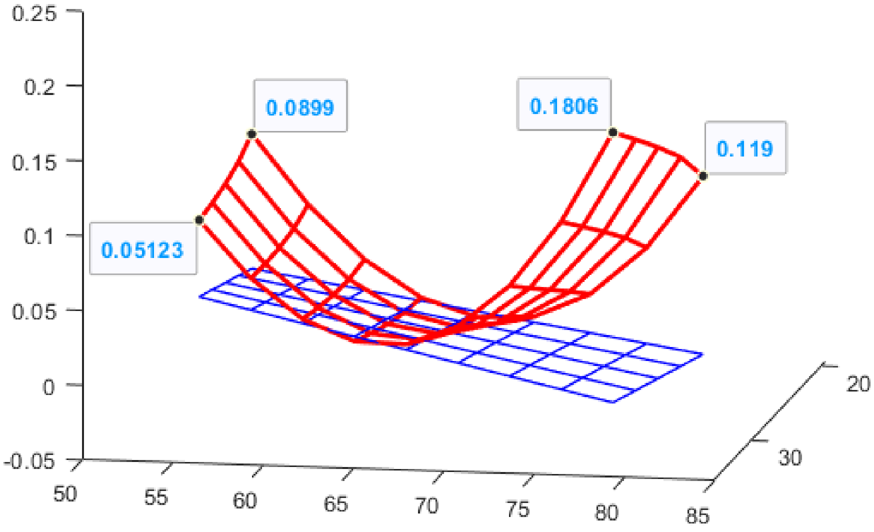

Figure 58 The ease-off topography after modification (mm)

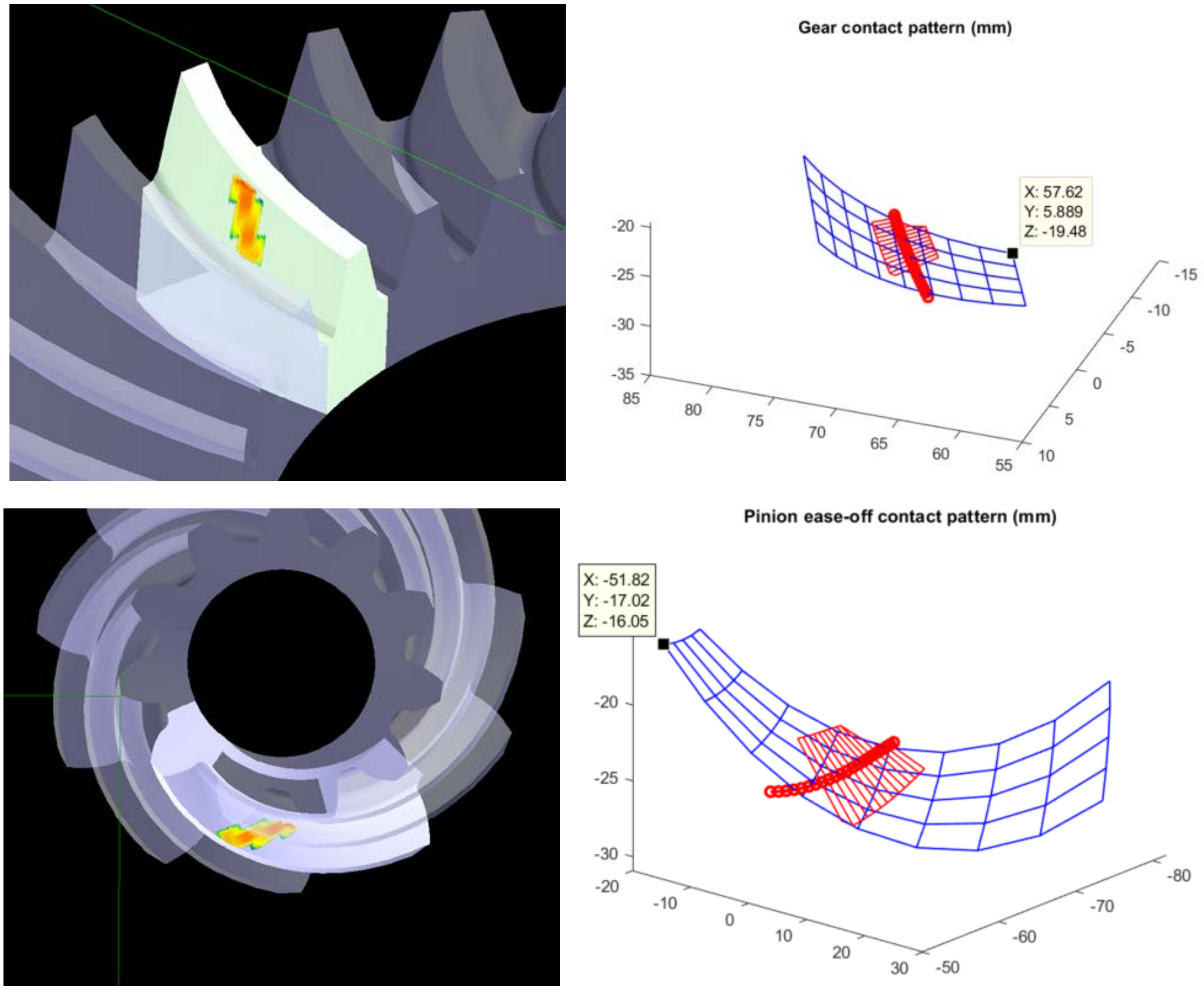

Figure 59 The modified contact pattern of pinion and gear validation with FE/CM model

6.3.2 Noise and Vibration Performance Evaluation

The other numerical case is performed to verify the influence of the modification of the ease-off topography. The contact characteristics can be controlled by the method proposed by Zhang [34] and ease-off flank modification. The three cases are chosen as contact pattern near the toe side, in the middle, and near the heel side with different contact trace inclination angle and length of contact ellipse. The contact patterns and control parameters are shown in Figure 60. The basic design parameters of the example gear are list on Table 9 Basic design parameters. The machine tool settings of the pinion concave side for the three different contact patterns are list in Table 10. The ease-off topographies of three cases are checked first. The ease-off topographies and unloaded transmission errors are plotted as Figure 61. The results are close to our control goals. The toe case has the lowest peak to peak unloaded transmission error among the three cases. The contact patterns on pinion and gear tooth surface are plotted as Figure 62.

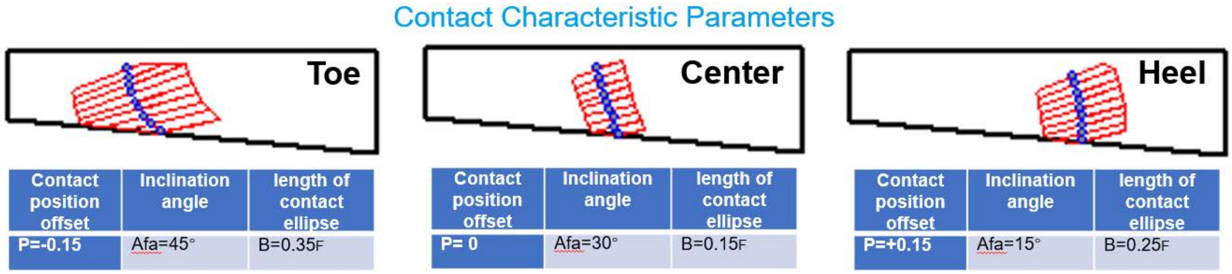

Contact position offset	Inclination angle	length of contact ellipse
P=-0.15	Afa=45°	B=0.35F

Contact position offset	Inclination angle	length of contact ellipse
P= 0	Afa=30°	B=0.15F

Contact position offset	Inclination angle	length of contact ellipse
P=+0.15	Afa=15°	B=0.25F

Figure 60 Contact patterns and control parameters for three numerical cases

Table 9 Basic design parameters

Item	Pinion	Gear
Number of Teeth	11	41
Modulus/mm	4.024	
Face Width of Tooth/mm	29.78	26.00
Shaft Angle/°	90	
Offset /mm	23.00	
Average Pressure Angle/°	19.00	
Spiral Angle/°	50.47	32.62
Hand of Spiral	Left	Right

Table 10 Machine tool settings for three cases

	Case Toe	Case Center	Case Heel	
Item	Pinion Concave	Pinion Concave	Pinion Concave	Gear Convex
Machine root angle	-2.00°	-2.00°	-2.00°	64.1833°
Machine Center to Cross point (mm)	-1.32	0.93	-2.42	2.66
Work offset(mm)	19.03	21.64	21.69	
Sliding base (mm)	7.87	5.86	8.88	
Radial distance(mm)	66.86312	77.26521	69.84586	
Horizontal(mm)				30.39
Vertical(mm)				65.62
Tilt angle	21.26707°	21.4849°	21.69494°	
Swivel angle	339.87585°	344.14035°	337.75531°	
Ratio of roll	3.4744	3.66907	3.51903	
Point radius of blade (mm)	74.105	87.895	76.275	74.17
Pressure angle of blade	14°	14°	14°	19°

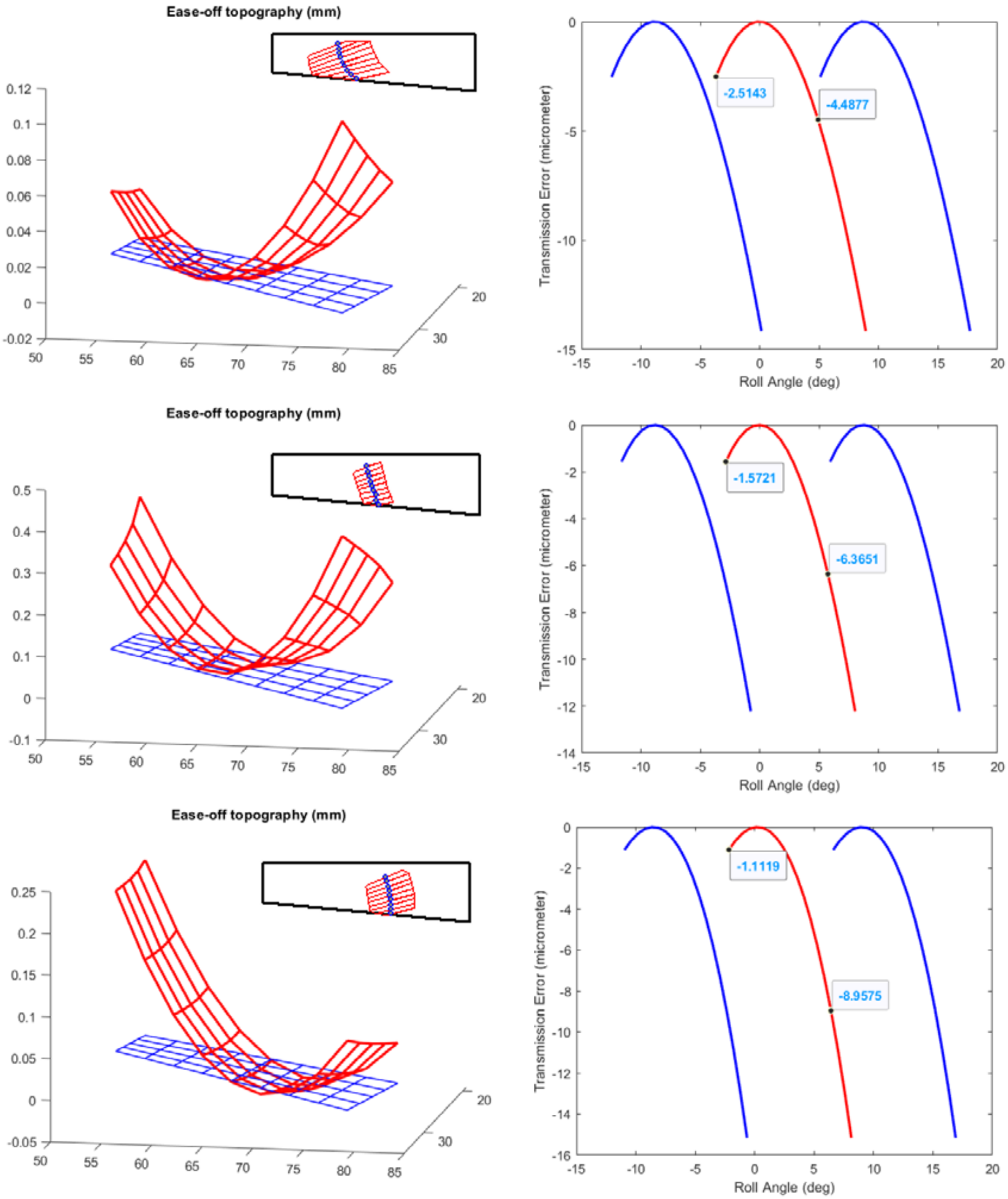

Figure 61 Ease-off topography and unloaded transmission errors of the three example cases

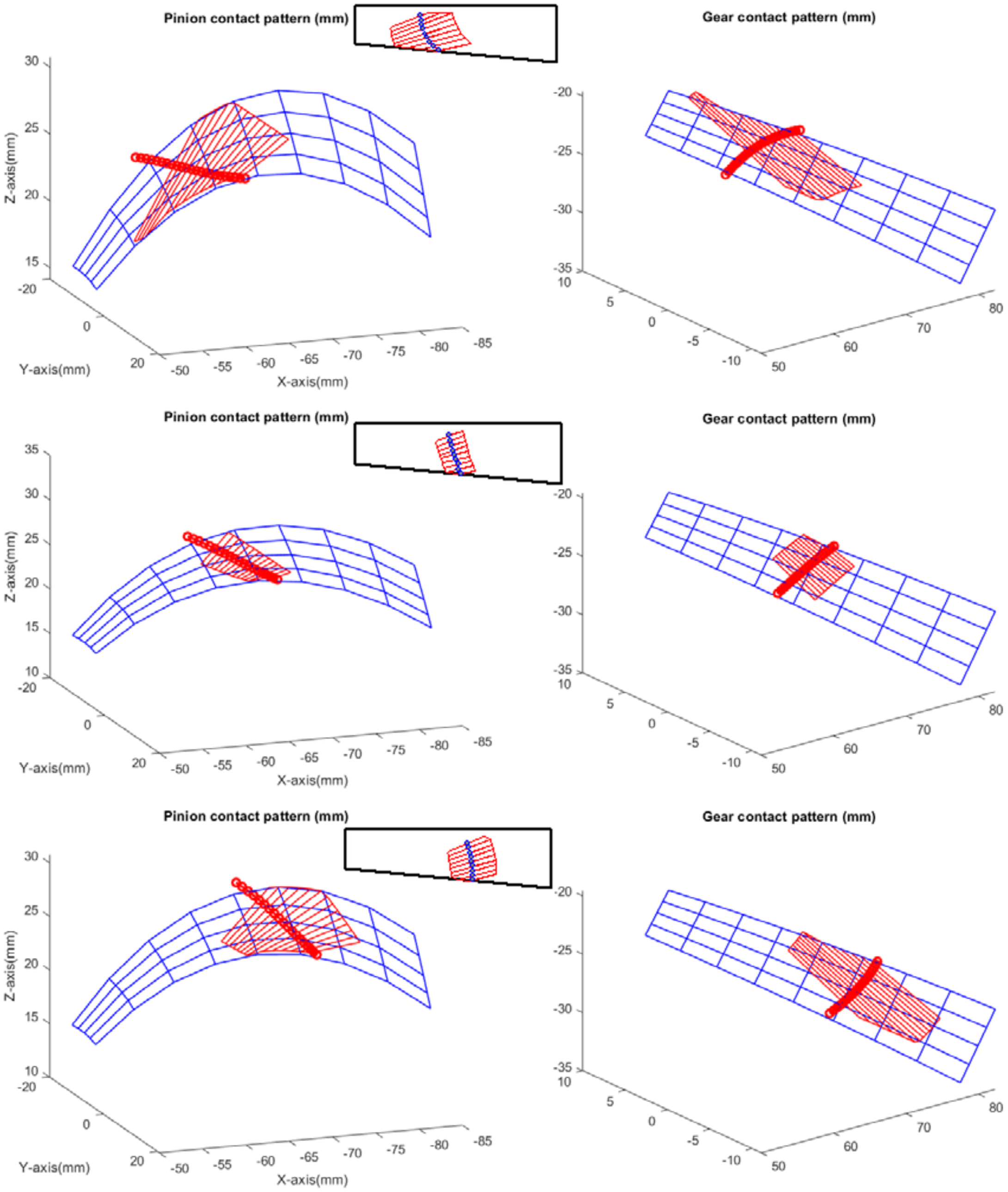

Figure 62 The contact patterns of pinion and gear tooth surface for the three cases

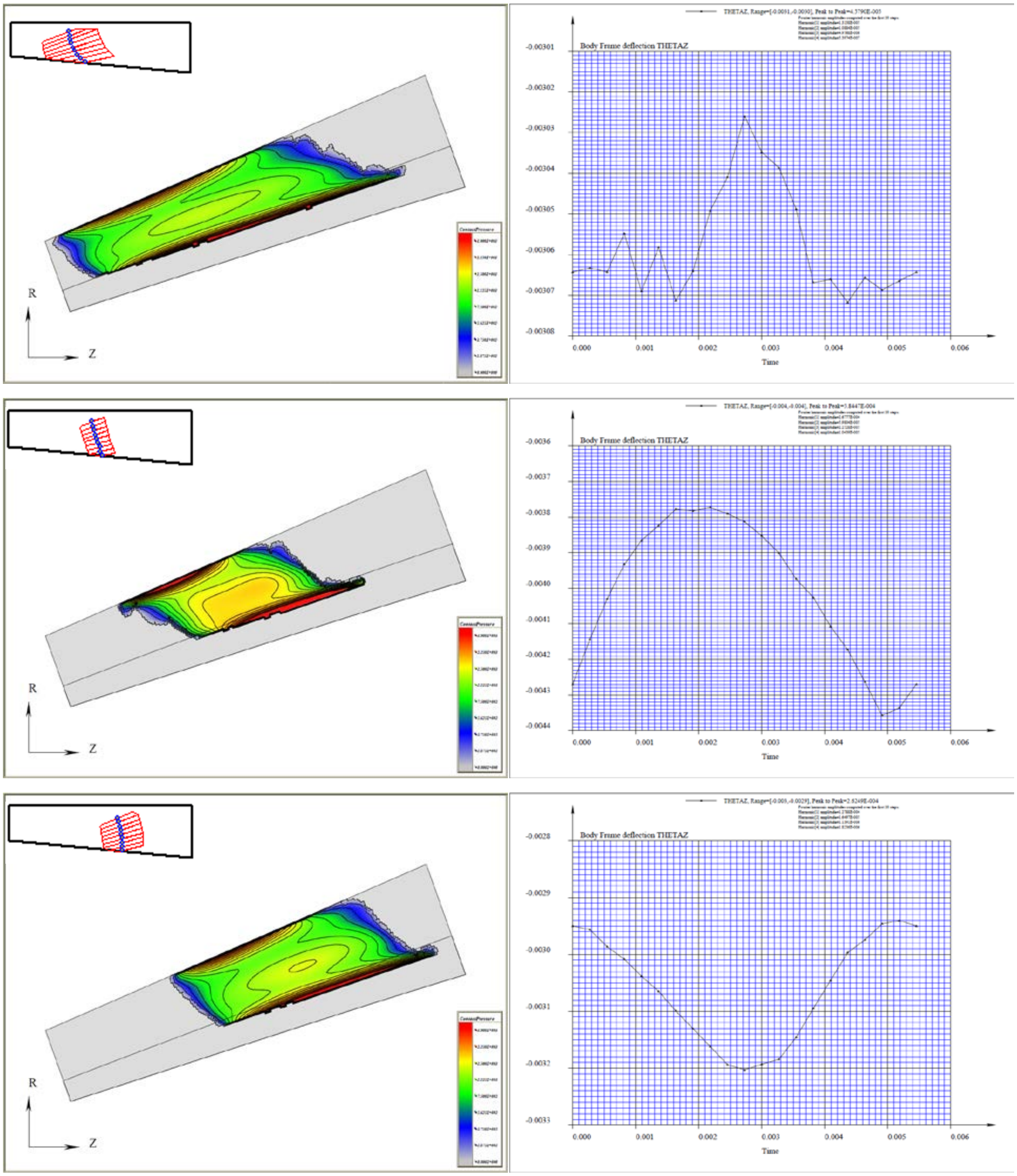

Figure 63 The loaded contact patterns and transmission errors from LTCA for the three cases

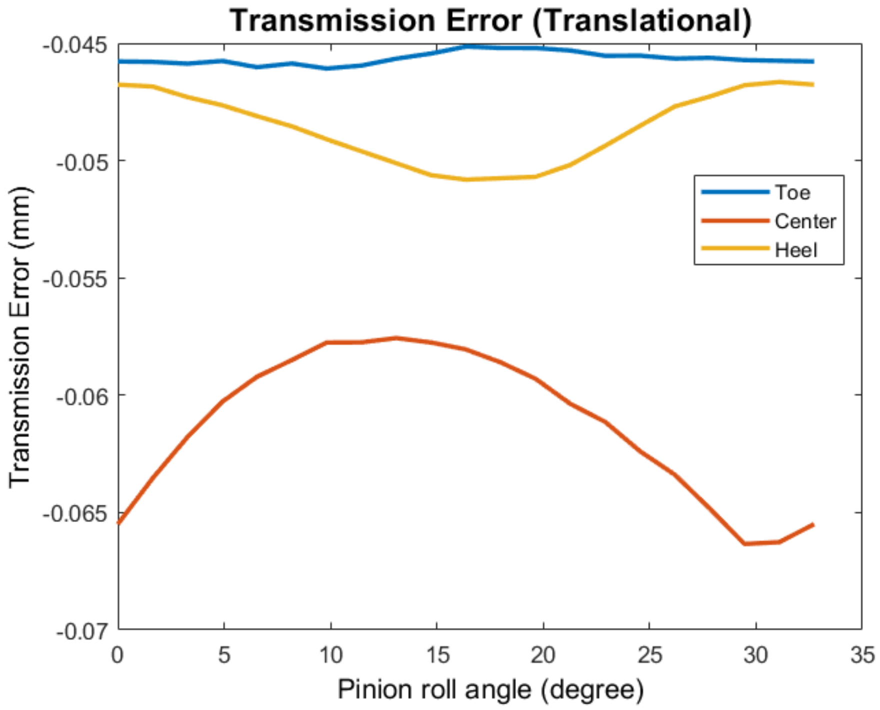

Figure 64 The translational transmission error of the three cases

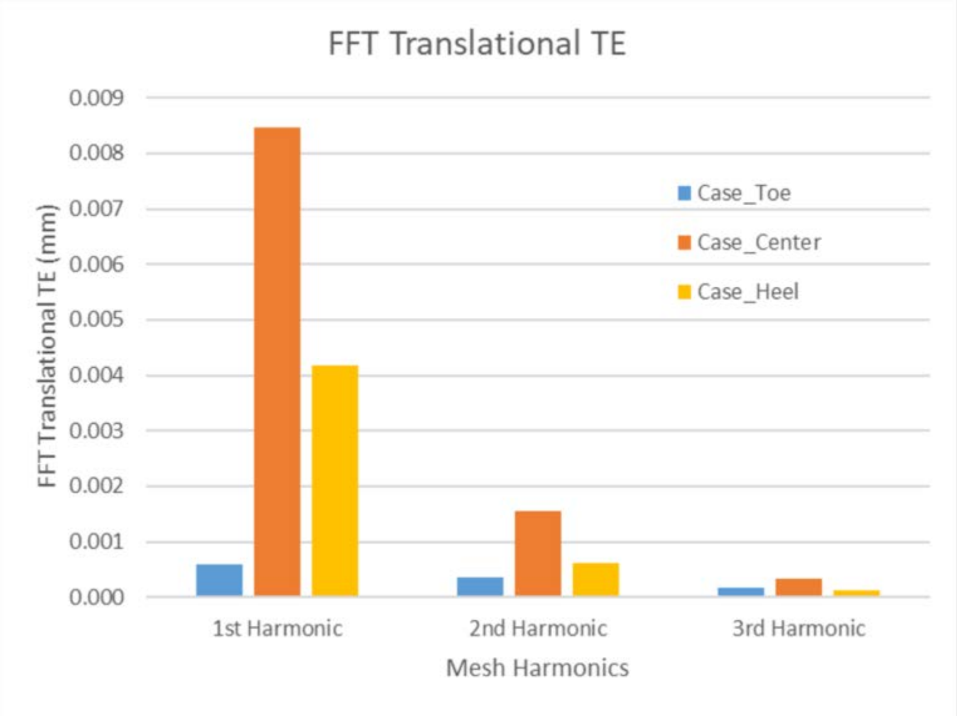

Figure 65 The TE harmonic comparison of the three cases

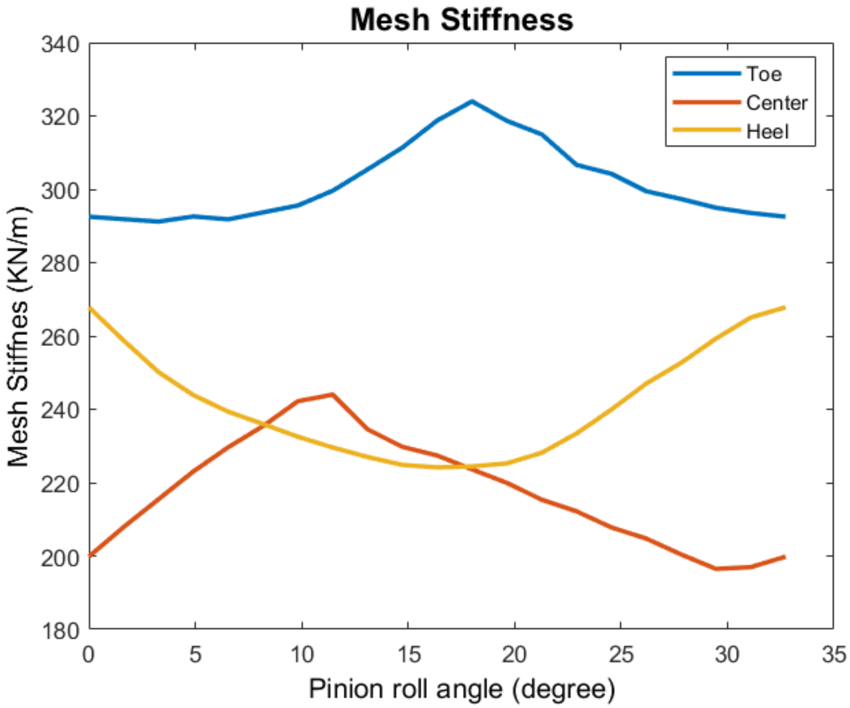

Figure 66 The Mesh Stiffness of the three cases

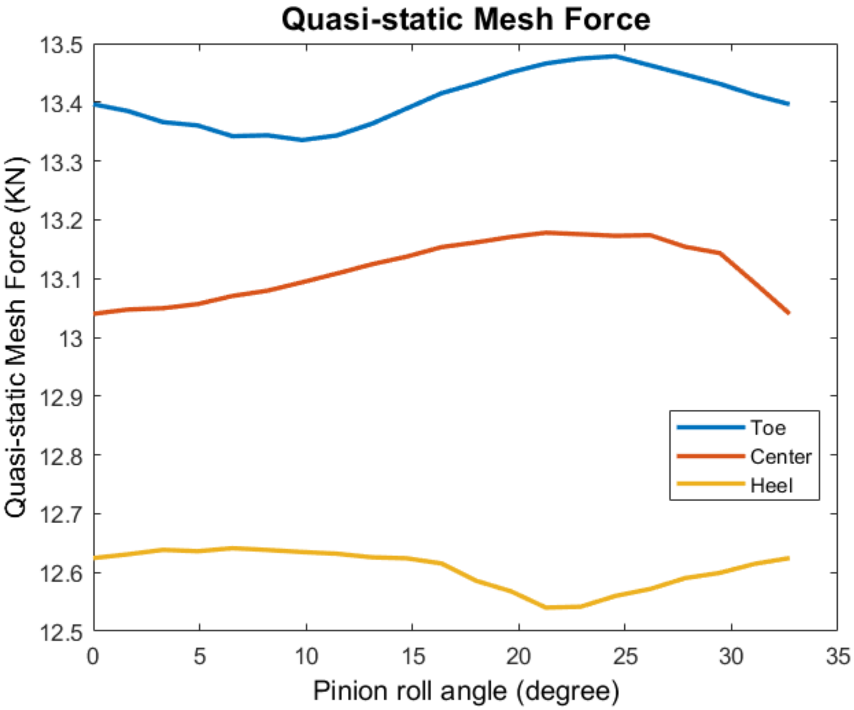

Figure 67 The quasi-static mesh force of the three cases

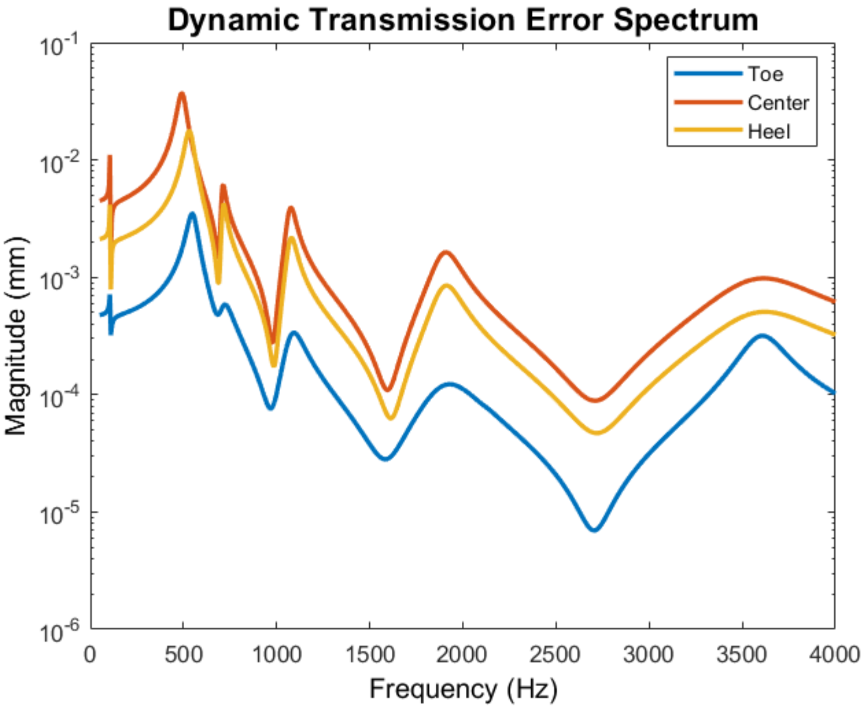

Figure 68 The dynamic transmission error of the three cases

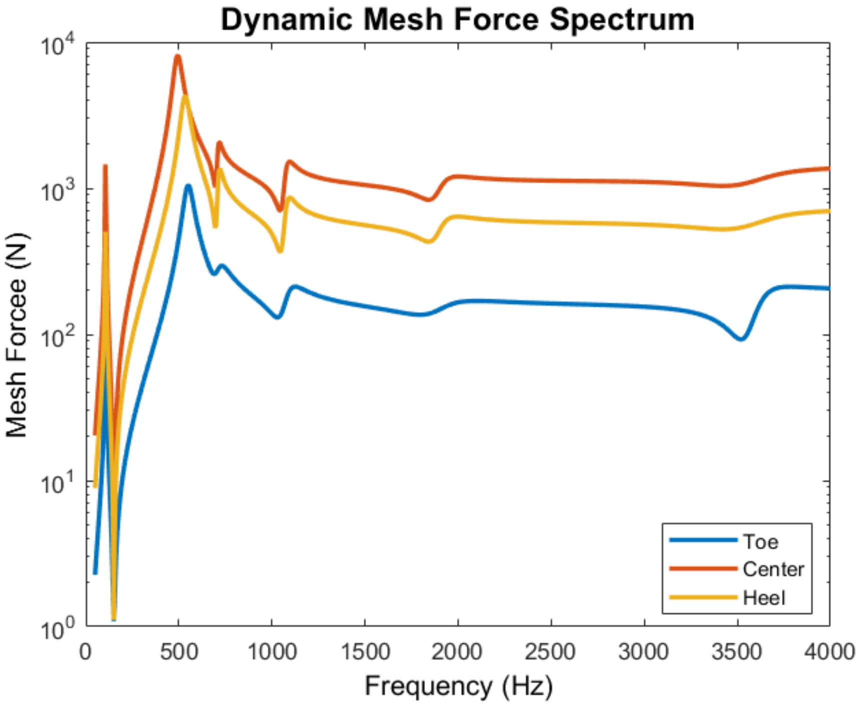

Figure 69 The dynamic mesh force spectrum of the three cases

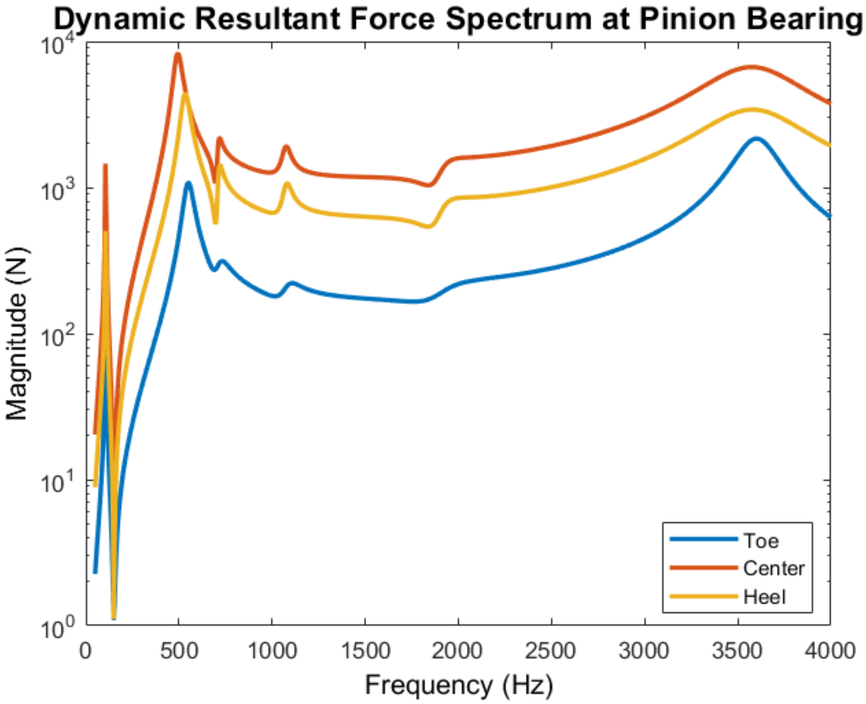

Figure 70 The dynamic bearing force at pinion of the three cases

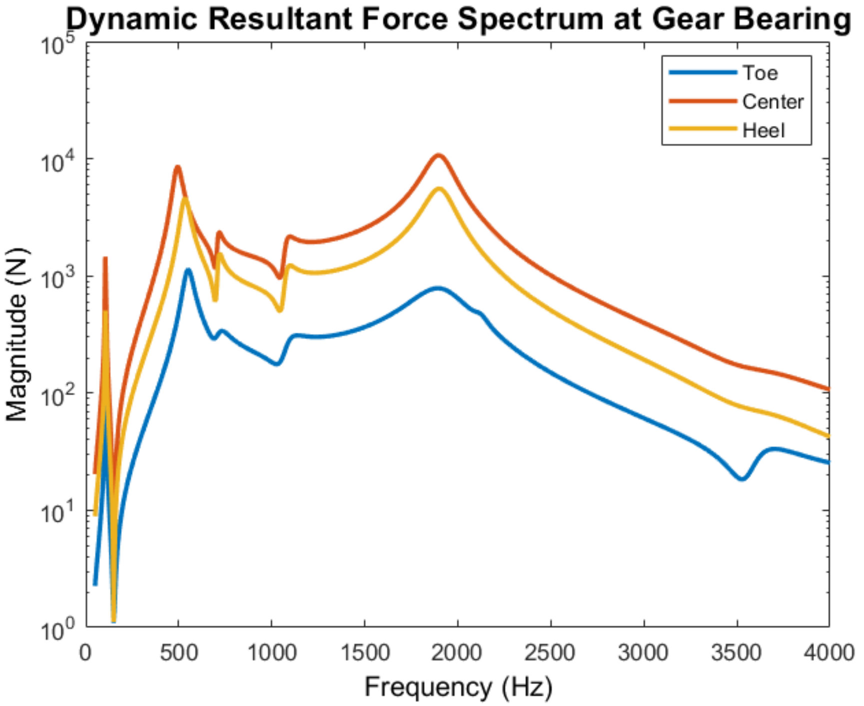

Figure 71 The dynamic bearing force at gear of the three cases

The loaded contact patterns and loaded transmission error from LTCA are plotted as Figure 63. The toe case has the smallest loaded transmission error. The results are synthesized to the mesh model and the translational transmission error, TE harmonics, and mesh stiffness can be calculated as Figure 64 to Figure 66. The toe case has smaller TE variation and mesh stiffness variation. The dynamic responses of the geared-rotor system model are calculated and plotted as Figure 68 to Figure 71. The toe case has the lowest response of the dynamic transmission error, dynamic mesh force, and also the dynamic bearing force on pinion and gear position. The dynamic bearing forces at the four actual bearing positions are used as input excitations on the axle housing model with rigid body elements coupled with the surface elements. The bearing force applied position is shown in Figure 72.

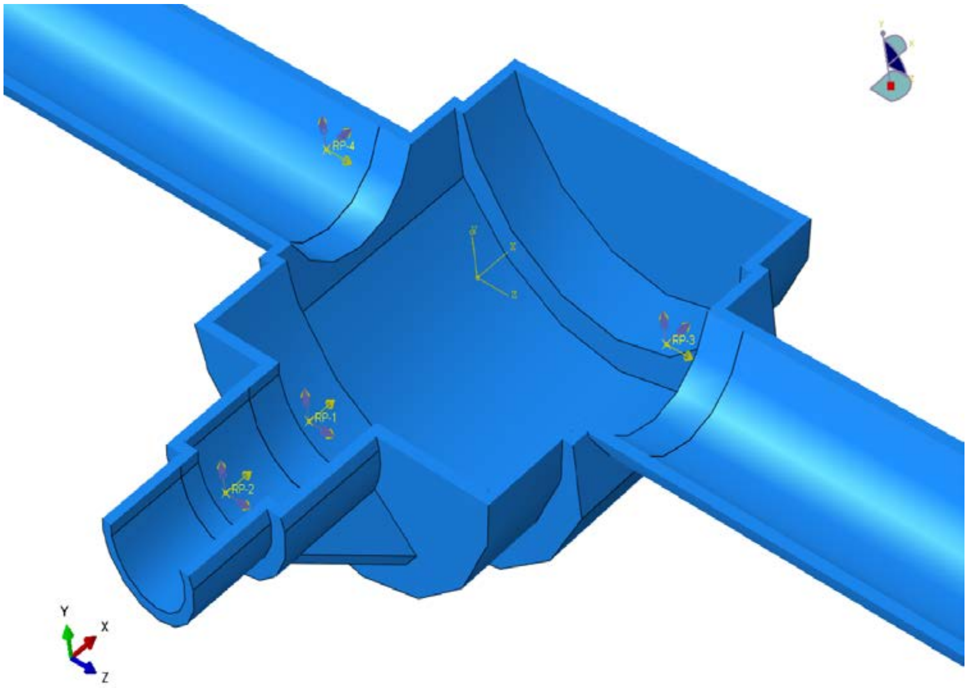

Figure 72 The applied position of bearing locations of dynamic bearing force

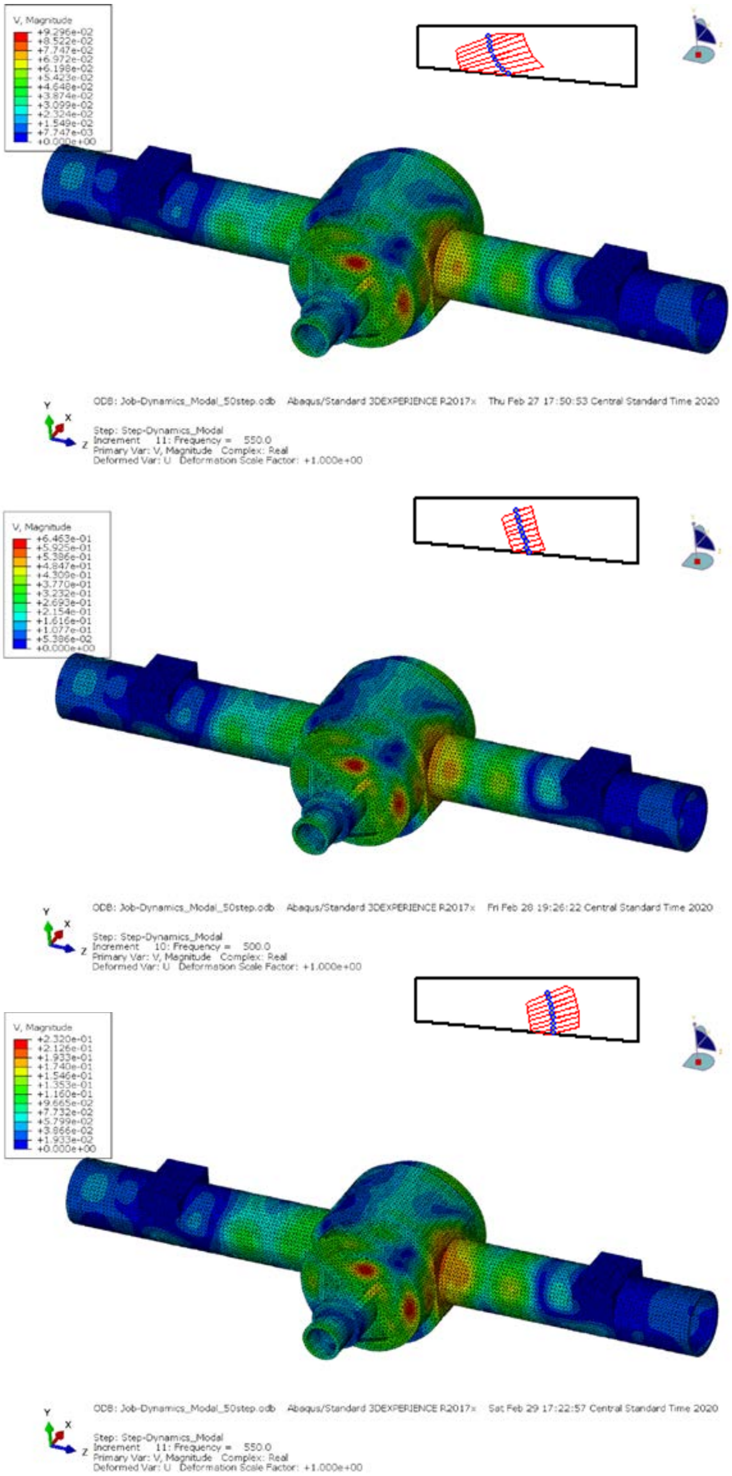

Figure 73 The velocity distribution of the axle housing of the three cases

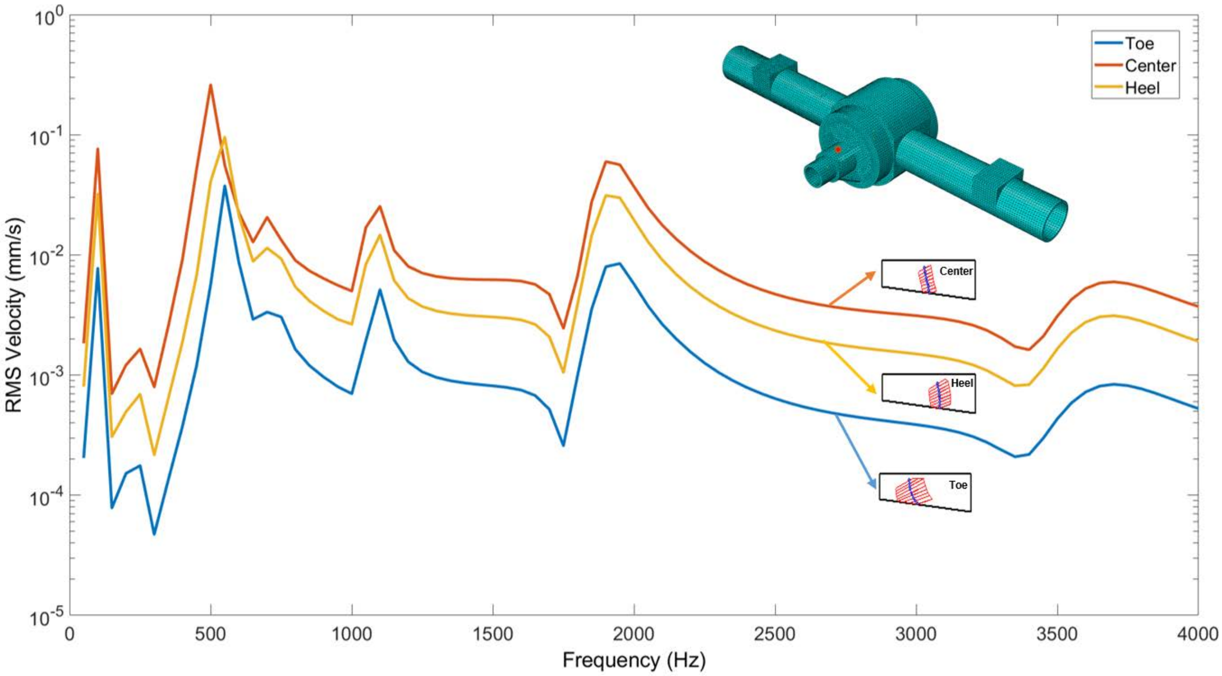

Figure 74 RMS velocity on pinion nose position comparison of the three cases

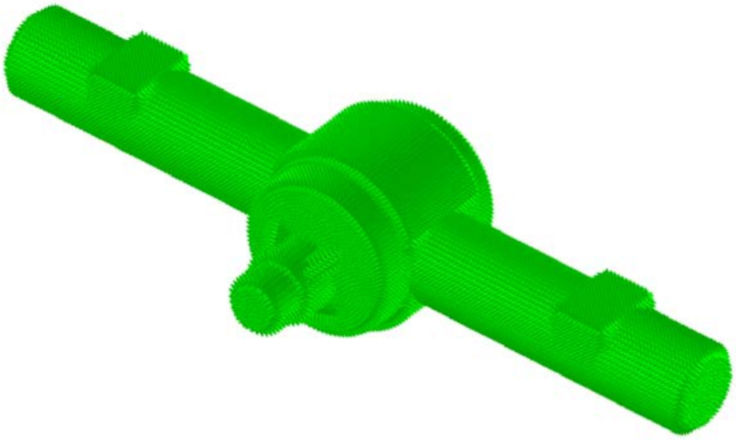

Figure 75 The boundary element model for the vibro-acoustic analysis

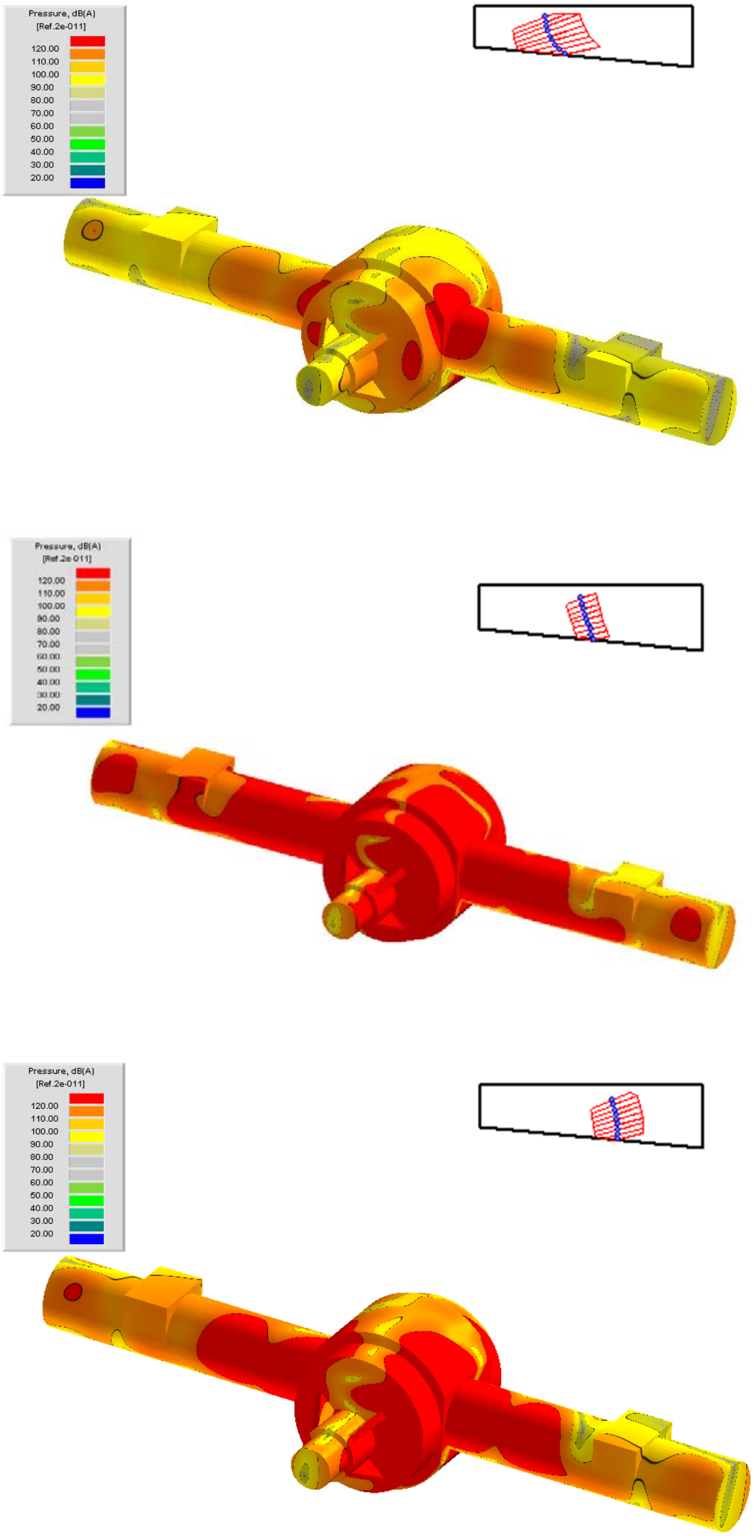

Figure 76 The sound pressure distributions on the axle housing surface of the three cases

The steady-state dynamic vibration analysis is performed on the axle finite element model. The axle housing velocity surface distributions are plotted in Figure 73. The RMS velocity comparison is plotted in Figure 74. The toe case has the smallest max value of surface velocity and the lowest response of the RMS velocity for all the frequency range.

The boundary element model is generated from the structure mesh as Figure 75. The vibro-acoustic analysis is performed. The sound pressure distributions on the axle housing surface and the far-field sphere mesh with a 1-meter radius from the axle center are plotted as Figure 76 to Figure 78. The toe case has the lowest response among all cases. The sound pressure level (SPL) and sound power level (SWL) based on ISO 3745 are compared and plotted as Figure 79 and Figure 80. The toe case has the lowest response for all the frequency range.

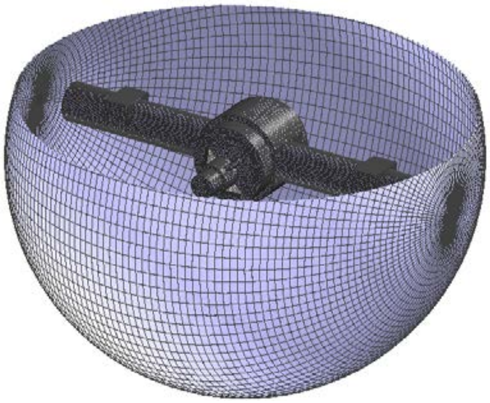

Figure 77 The far-field sphere mesh of 1-meter radius from the axle center

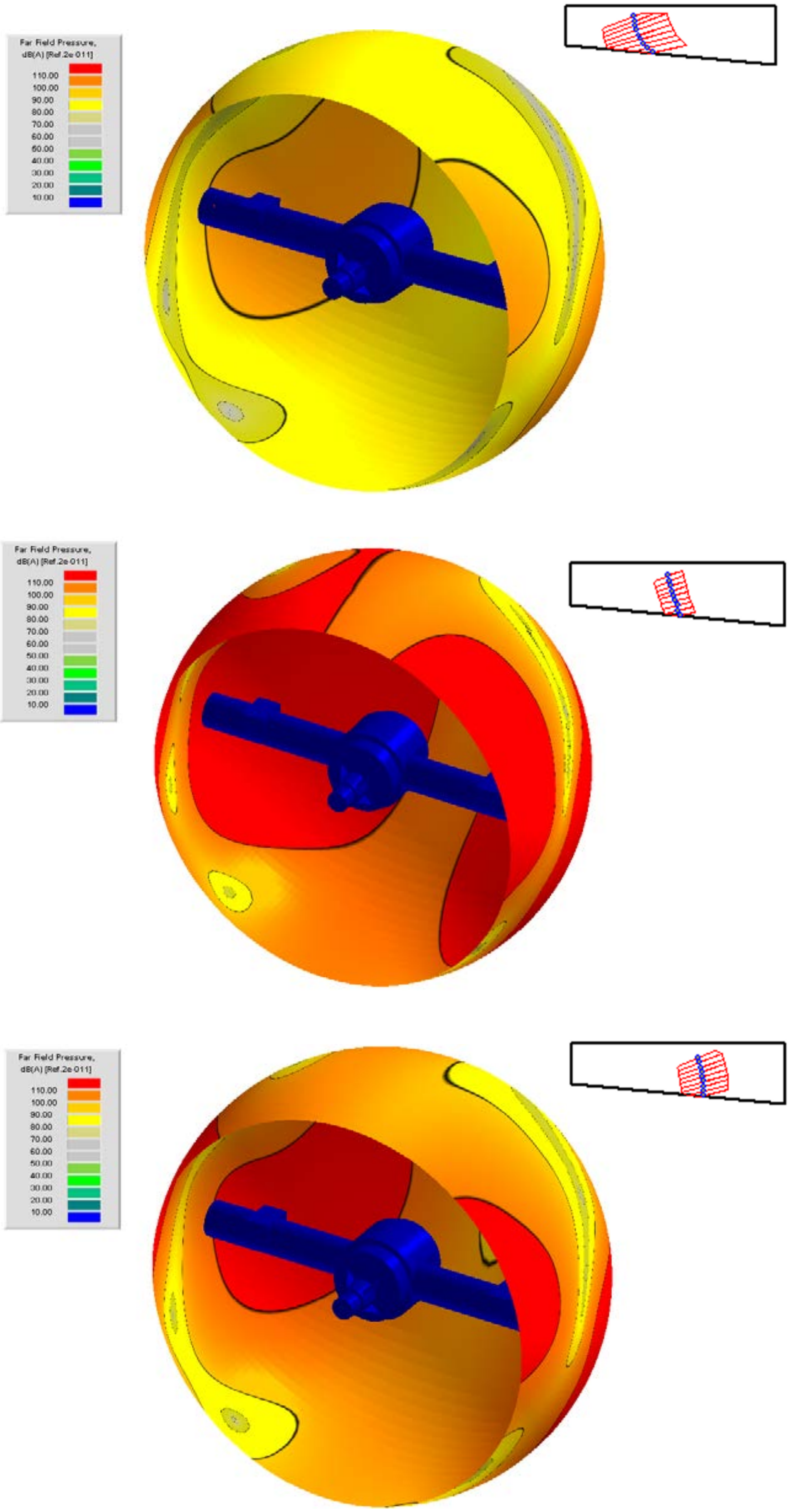

Figure 78 The sound pressure distributions on the far-field sphere of the three cases

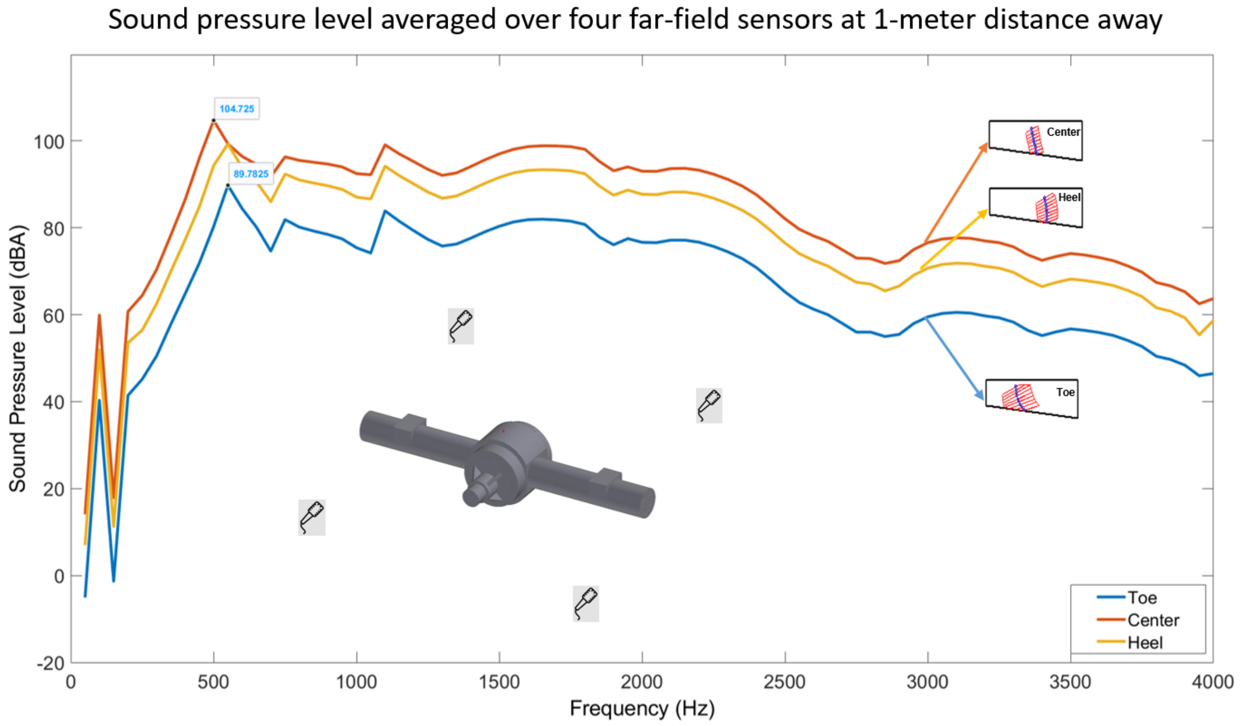

Figure 79 The SPL averaged over 4 microphones for the three cases

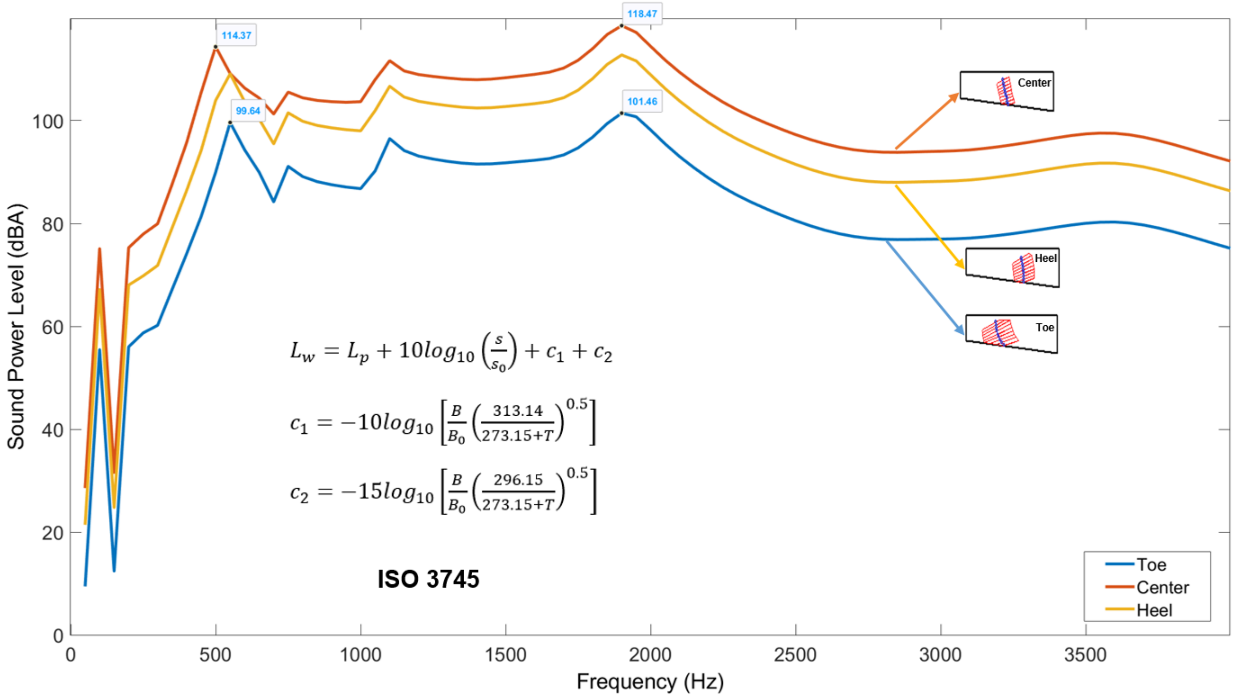

$$L_w = L_p + 10log_{10}\left(\frac{s}{s_0}\right) + c_1 + c_2$$

$$c_1 = -10log_{10}\left[\frac{B}{B_0}\left(\frac{313.14}{273.15+T}\right)^{0.5}\right]$$

$$c_2 = -15log_{10}\left[\frac{B}{B_0}\left(\frac{296.15}{273.15+T}\right)^{0.5}\right]$$

ISO 3745

Figure 80 The sound power level (SWL) of ISO 3745 for the three cases

6.4 Conclusion

A comprehensive approach to analyze noise and vibration response of the rear axle system is discussed. A machine setting parameters calculation method is proposed, which can directly control the contact characteristic of hypoid gears. The contact characteristics of the hypoid gear pairs have considerable influence on the NVH performance of the rear axle system. The surface velocity and noise pressure distribution on the housing surface are reduced. The sound power level and sound pressure level averaged over four far-field sensors at a 1-meter distance away are improved up to 10 dBA.

Chapter 7 Experimental Validation

7.1 Introduction

The Design of a quiet and reliable driveline system is highly desirable for the automotive industry. The reduction of the gear whine noise is always the design requirement for an axle system manufactory. Chung [35] presented a systematic approach to gear element design to optimize the gear blank design of the transmission error and system dynamics on operating noise. Sun [36] presented the principles of the robustness design of axle system dynamics to reduce vehicle system-related axle gear whine. Lee[37] presented practical work on the reduction of gear whine that transfer paths are searched and analyzed by operational deflection shape analysis and experimental modal analysis. The main objective of this study is to develop a comprehensive modeling process from gear design to vibro-acoustic analysis. The end-to-end solution can be used to control the noise and vibration level of the axle system application by control the excitation source of hypoid gear transmission error and tuning the system parameters to make the system less sensitive to the dynamic mesh force. The experimental validation has been developed including the hypoid gear single flank test for gear contact patterns and transmission errors and the NVH testing for vibration measurements of accelerometers and sound pressure measurements for microphones.

The entire simulation validation process can be observed in Figure 81. The basic design parameters and operating conditions are given. By performing the ease-off surface modification on the tooth surface of the hypoid gear pair and integrating the coordinate measuring machine (CMM) data on the tooth surface, the modified cutter and machine settings can be calculated. The design case A with original design parameters is compared with the design case B with the different design parameters.

The two hypoid gear sets are performed the rolling test on the Gleason single flank testing machine. The results of the contact pattern, transmission error, and its harmonics are compared between the simulation and the testing.

The loaded tooth contact analysis is performed to calculate the load distribution on the tooth surface and loaded transmission error. The load distribution is synthesized for the mesh model. The axle system models including gear shafts, bearings, and housing are created in the Transmission 3D software to have the bearing load and displacement as input to calculate the bearing stiffness.

With the axle dynamic parameters, the gear-rotor system model is created and simulated the dynamic response for the interesting frequency range. The dynamic bearing forces on the actual bearing positions are used as excitation forces to the finite element axle housing. The results of housing surface velocities are interpolated with boundary surface elements of the housing surface.

The vibration analysis and vibro-acoustic analysis are performed to validate the measurements of the accelerometers and microphones on the NVH testing for both the design case A and the design case B.

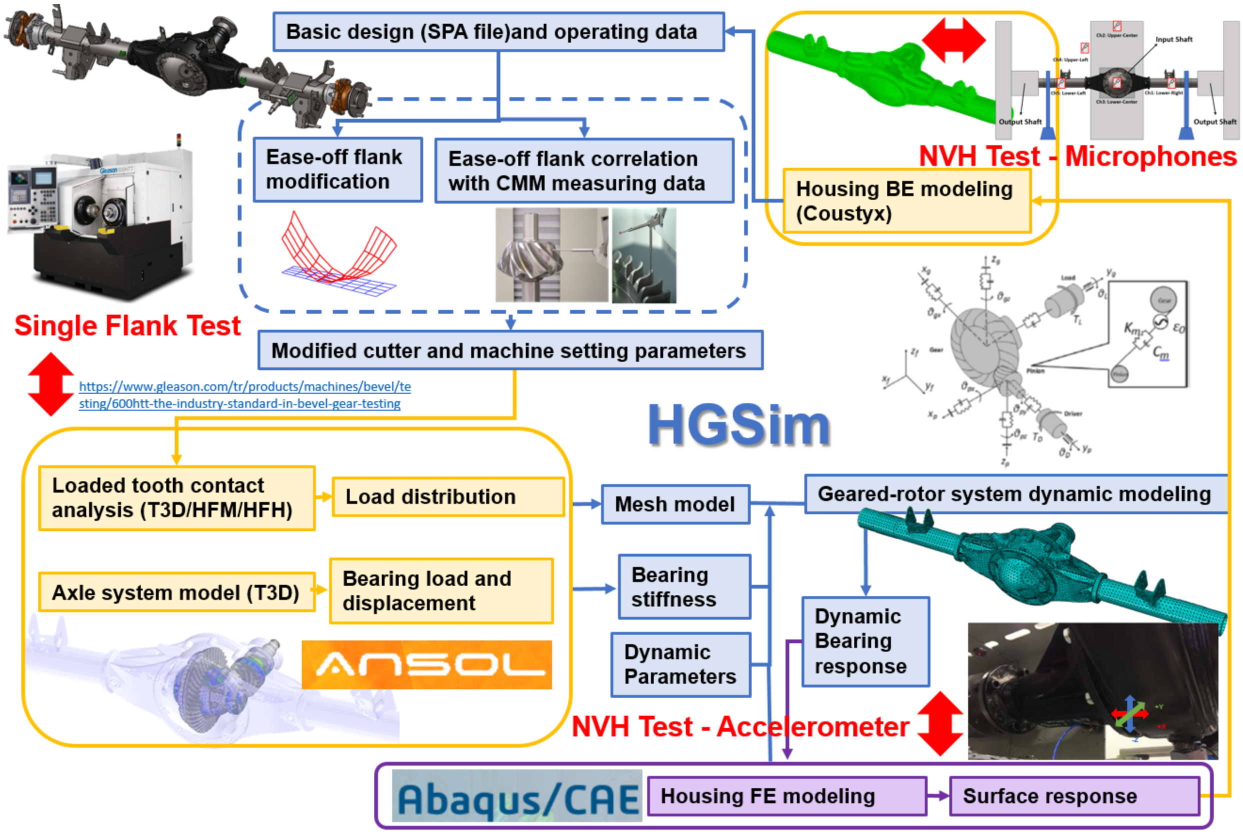

Figure 81 Simulation Validation Flow Chart

7.2 Single Flank Test

A single flank tester is a machine that measures the transmission error of a gear set one flank at a time. The single flank test is a rotational test of a gear and a pinion rolling together at their proper mounting position, with proper backlash, and one flank of the tooth in contact while optical encoders measure the angular displacement relative to a perfect gear. An SFT test includes the collection of the transmission error data and the resulting analysis [38]. The paint can be applied to the contact flank surface to have the contact pattern. The single flank test conditions for this comparison are 5 Nm torque and 60 RPM.

The hypoid gear set used on this axle product is a face-hobbed gear set with left-hand pinion and right-hand ring gear. For the drive condition, the input pinion shaft is driving the output ring gear shaft. On the other hand, the coast condition, the output ring gear shaft is driving the input pinion shaft.

The result of the contact pattern on the ring gear for the drive condition is on the gear convex side. The design case A contact pattern from the SFT is shown in Figure 82. The paint thickness is the factor to influence the contact pattern area. The design case A contact pattern from the simulation of loaded tooth contact analysis is shown in Figure 83. The contact patterns of both test and simulation results are closed to the inner toe side with a thin shape in the middle of the tooth profile. The contact stress distribution of the simulation result is also plotted on the tooth surface as Figure 84. The contact area near the tooth tips has some stress concentration and the position is still near the inner toe side. It may because of the profile variation on the tooth surface with the integration of the CMM surface data from the manufactural error or hear treatment distortion.

Figure 82 Contact pattern of design A test case on the drive condition

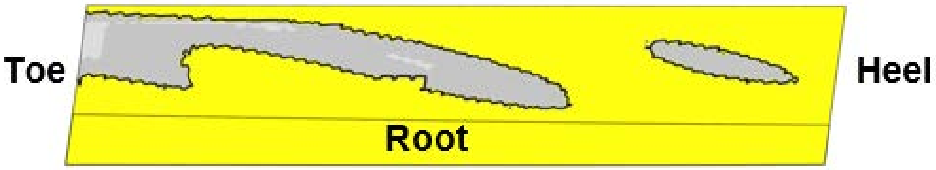

Figure 83 Contact pattern of design A simulation case on the drive condition

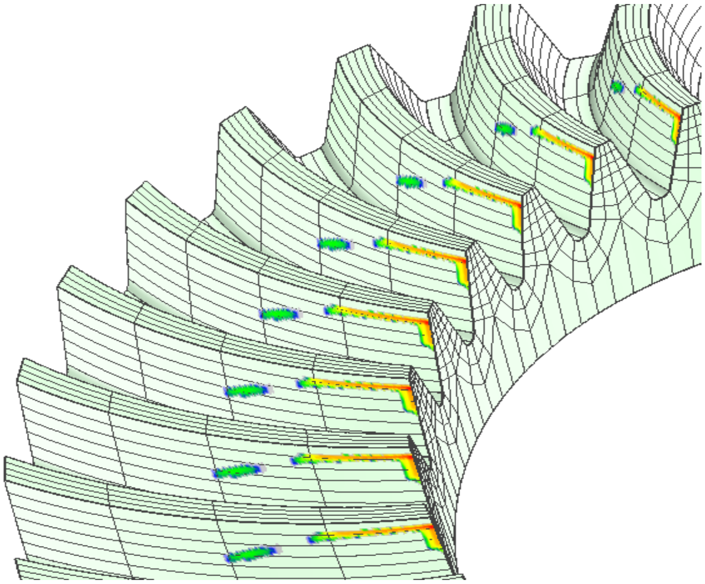

Figure 84 Contact stress distribution of design A simulation case on the drive condition

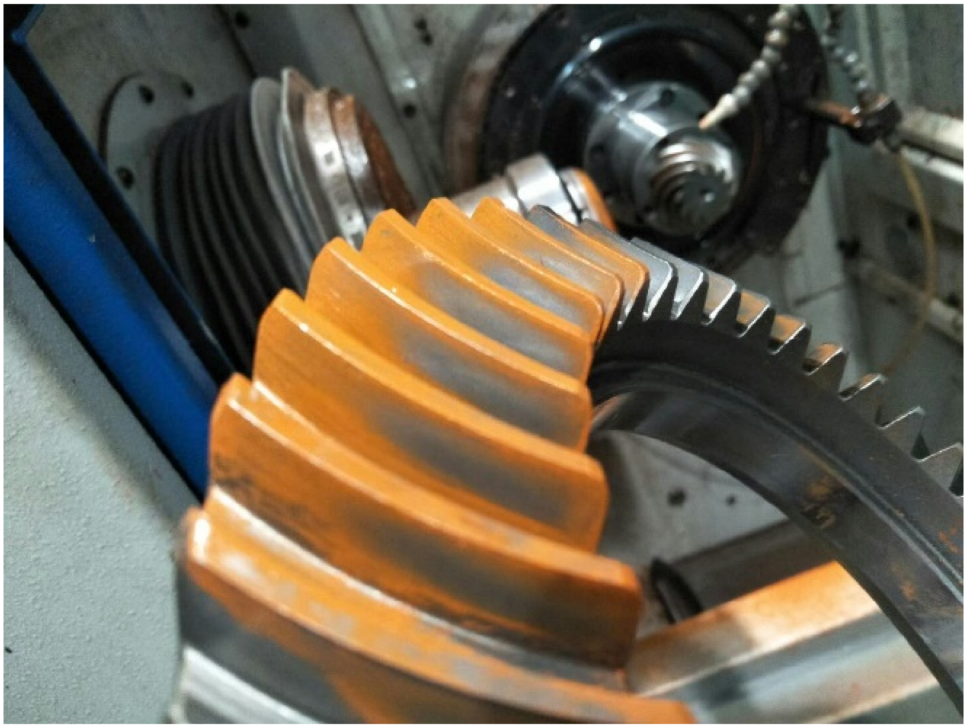

Figure 85 Contact pattern of deign B test case on the drive condition

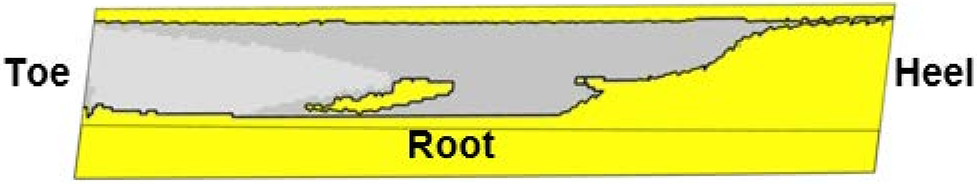

Figure 86 Contact pattern of design B simulation case on the drive condition

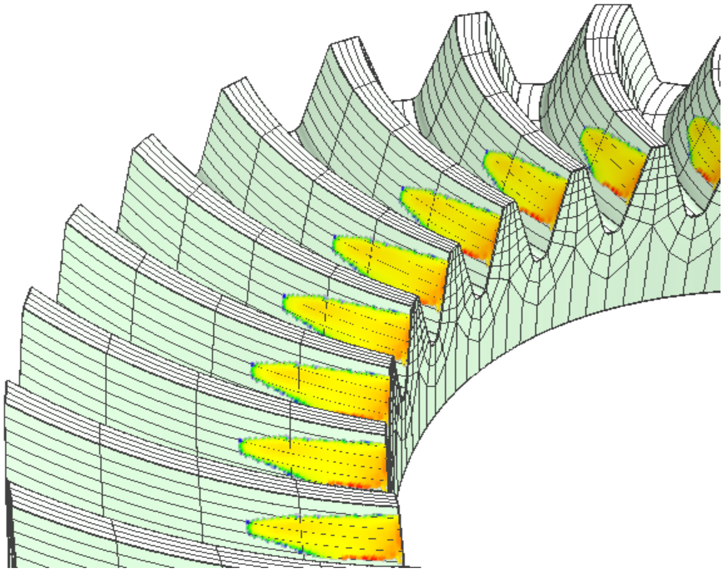

Figure 87 Contact stress distribution of design B simulation case on the drive condition

The design case B contact pattern from the SFT is shown in Figure 85. The design B case contact pattern from the simulation of loaded tooth contact analysis is shown in Figure 86. The contact patterns of both test and simulation results are closed to the inner toe side with the closed shape. The contact stress distribution of the simulation result is also plotted on the tooth surface as Figure 87. The contact stress distribution is more evenly and the shape is also closed to the test contact pattern.

The transmission error of the peak-to-peak value and the first third harmonic are plotted and compared as Figure 88. The transmission errors of the design B case are lower than the design A case in the test and simulation. The error of the design A case between the test and simulation is larger than the design B case.

The result of the contact pattern on the ring gear for the coast condition is on the gear concave side. The design A case contact pattern from the SFT is shown in Figure 89. The design A case contact pattern from the simulation of loaded tooth contact analysis is shown in Figure 90. The contact patterns of both test and simulation results are closed to the inner toe side with a thin shape in the middle of the tooth profile. The contact stress distribution of the simulation result is also plotted on the tooth surface as Figure 91. The contact area near the tooth tips has some stress concentration and the position is still near the inner toe side.

The design B case contact pattern from the SFT is shown in Figure 92. The design B case contact pattern from the simulation of loaded tooth contact analysis is shown in Figure 93. The contact patterns of both test and simulation results are closed to the inner toe side with the closed shape. The contact stress distribution of the simulation result is also plotted on the tooth surface as Figure 94. The contact stress distribution is more evenly and the shape is also closed to the test contact pattern.

The transmission error of the peak-to-peak value and the first third harmonic are plotted and compared as Figure 95. The transmission errors of the design B case are lower than the design A case in the test, but the design B case is higher than the design A case in simulation. The error for peak-to-peak TE between the test and simulation is quite large. It may because of the light torque load, 5Nm. The simulation results are highly sensitive with input torque load for the loaded tooth contact analysis.

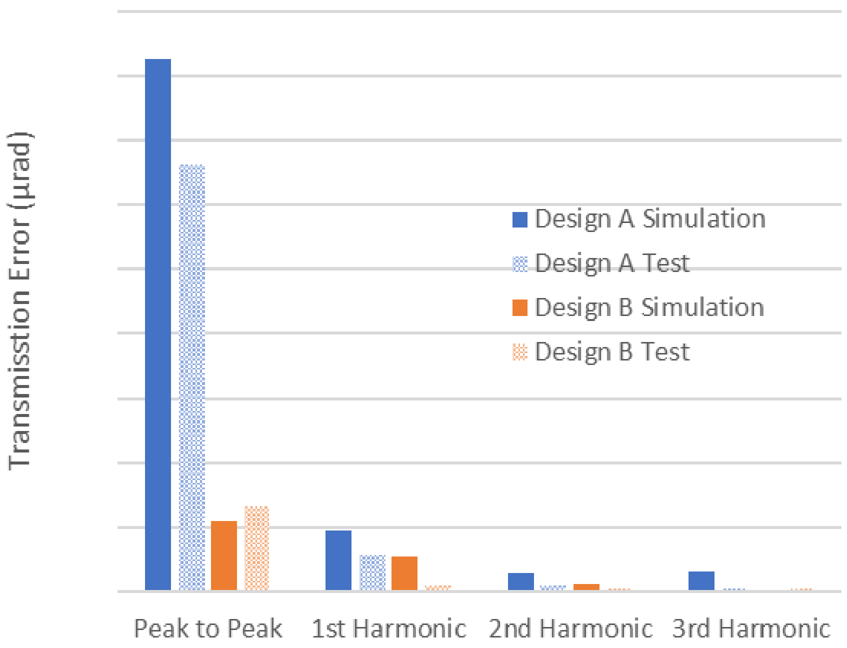

Figure 88 Transmission error comparison of drive condition for the design A and design B case

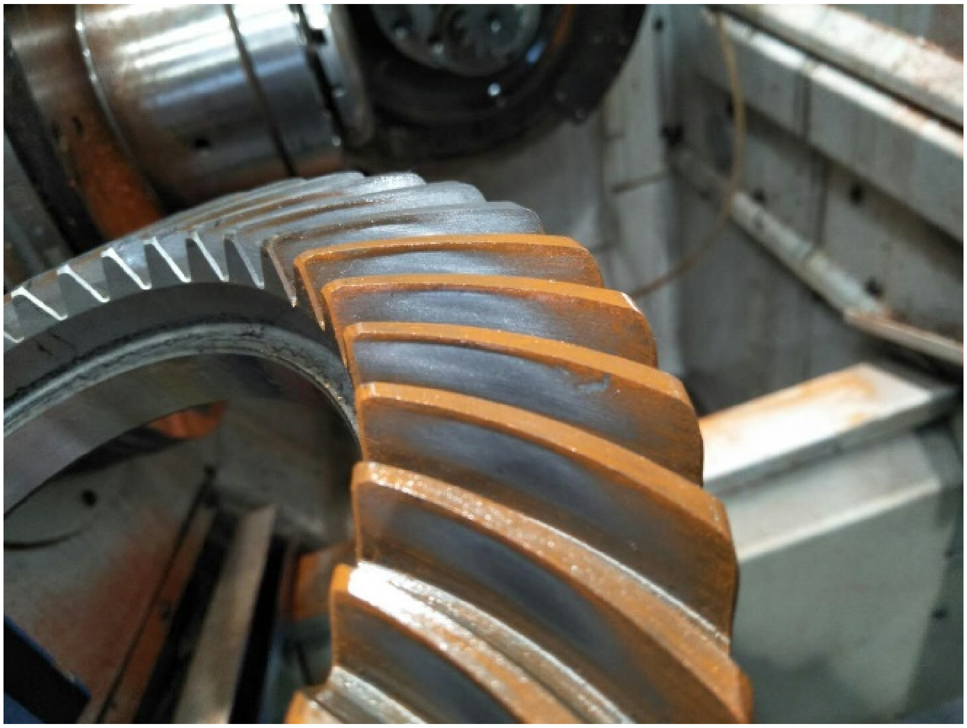

Figure 89 Contact pattern of design A test case on the coast condition

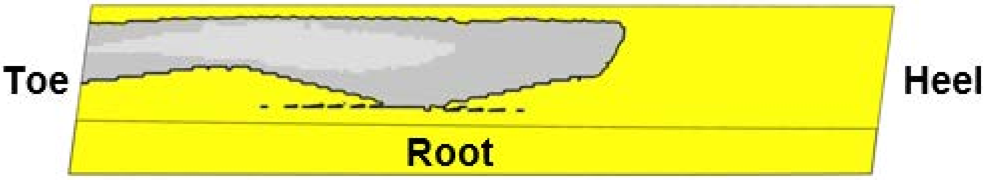

Figure 90 Contact pattern of design A simulation case on the coast condition

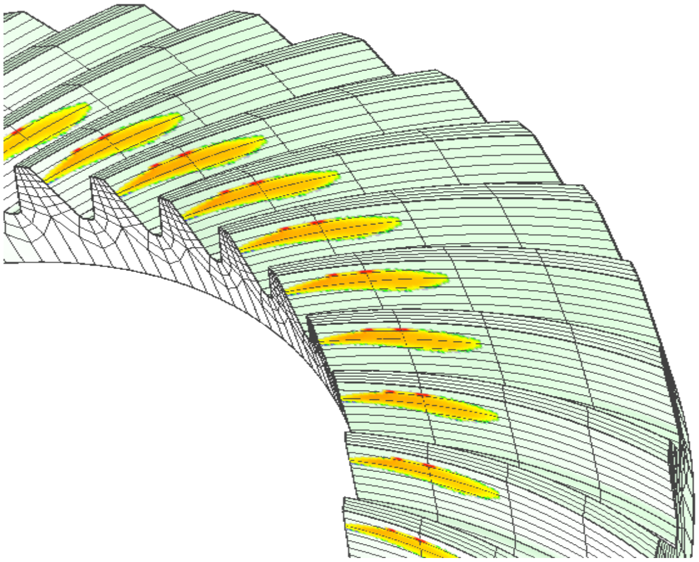

Figure 91 Contact stress distribution of design A simulation case on the coast condition

Figure 92 Contact pattern of design B test case on the coast condition

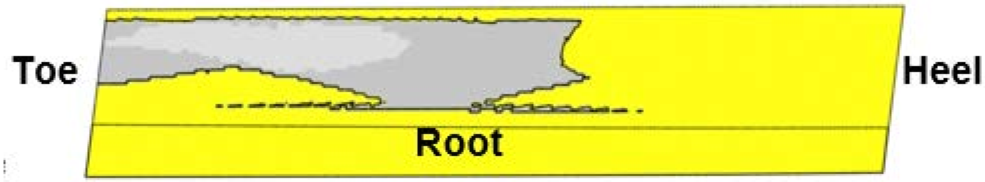

Figure 93 Contact pattern of design B simulation case on the coast condition

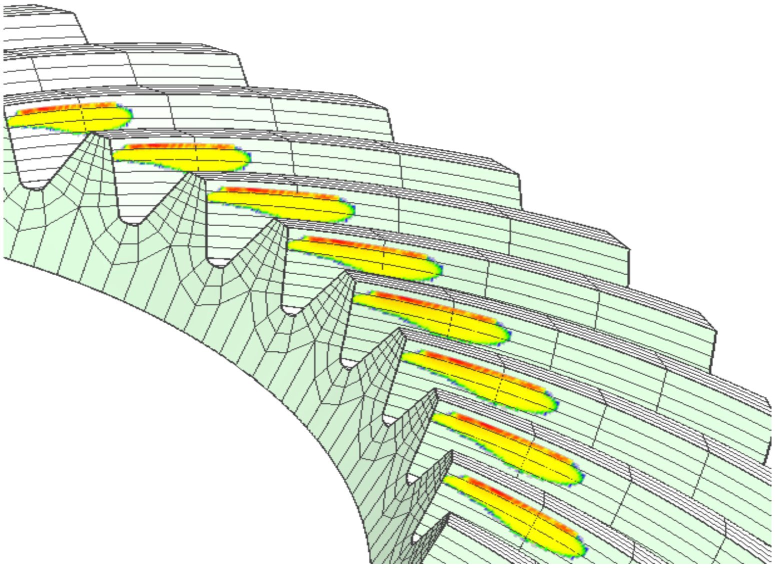

Figure 94 Contact stress distribution of design B simulation case on the coast condition

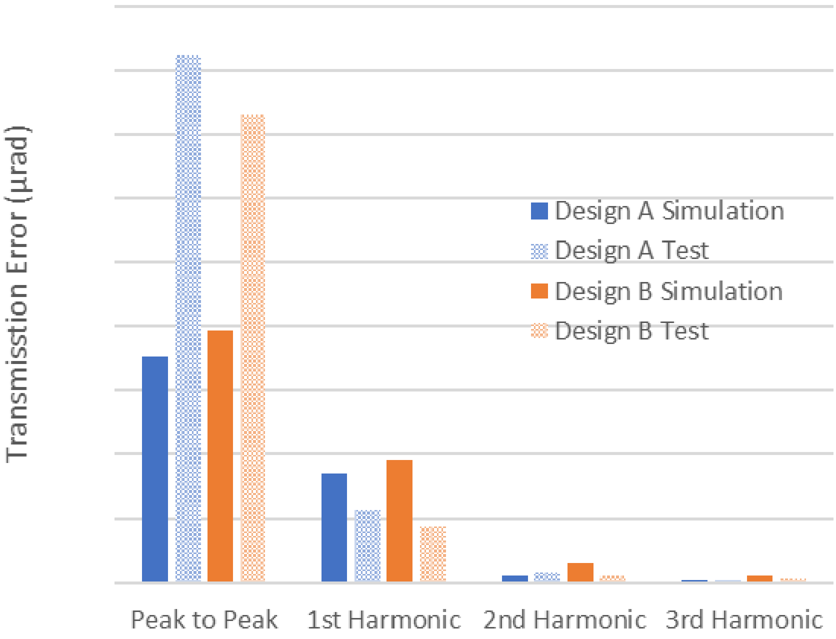

Figure 95 Transmission error comparison of coast condition for the design A and design B case

7.3 Loaded Tooth Contact Analysis

Loaded tooth contact analysis (LTCA) is the first step of gear analysis and the basis of gear mesh modeling for dynamic simulation. In the current study, a well-developed 3-dimensional quasi-static LTCA package for hypoid and spiral bevel gears (Calyx) (Vijayakar, 2003) is applied. All the basic gear design and machine settings are extracted from the Gleason SPA supplied by the gear designer. Gear tooth surface and body solid geometry generation, finite element (FE) modeling, and static/quasi-static loaded gear meshing simulations are performed and given the nominal operating torque load and speed. In the current study, the target torque load is selected as the most critical case in the practical product operation from the gear noise point of view. The target torque for the drive condition is 150 Nm and the coast condition is 98 Nm.

The loaded tooth contact analysis of the hypoid gear set is performed for both drive and coast conditions. The pinion and ring gear models are created in the HypoidFaceHobbed (HFH) software as Figure 96 from the design SPA file and CMM surface measurement data for the design A case and the design B case. The results of the contact pattern on pinion and ring gear tooth surface for the drive and coast condition are compared as Figure 97. The contact pattern of the design B case for the drive condition is more evenly distributed than the design A case and no stress concentration area. For the coast condition, the two cases are almost the same. The transmission error including the peak-to-peak value and the first third harmonics are compared and plotted in Figure 98. The design B case has a transmission error reduction for both drive and coast conditions.

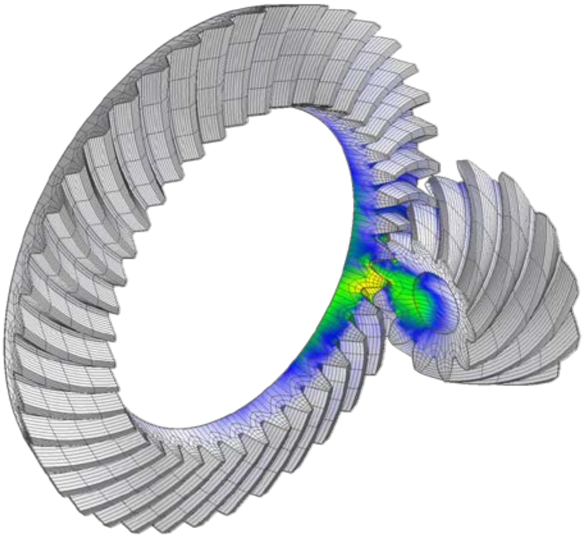

Figure 96 LTCA model for pinion and ring gear

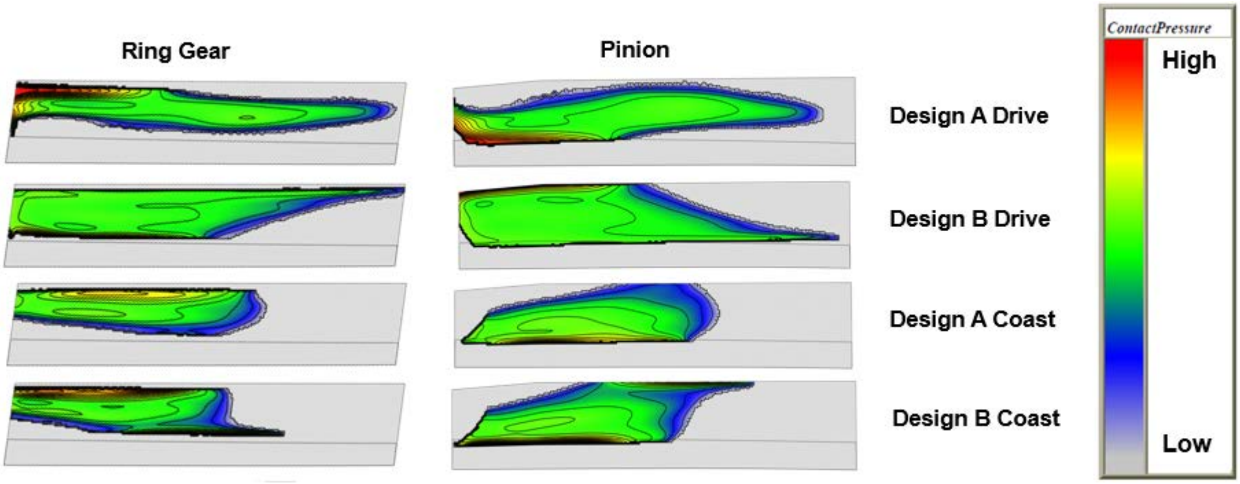

Figure 97 Gear pair contact patterns comparison between the design A and design B case on pinion and ring gear tooth surface for the drive and coast conditions

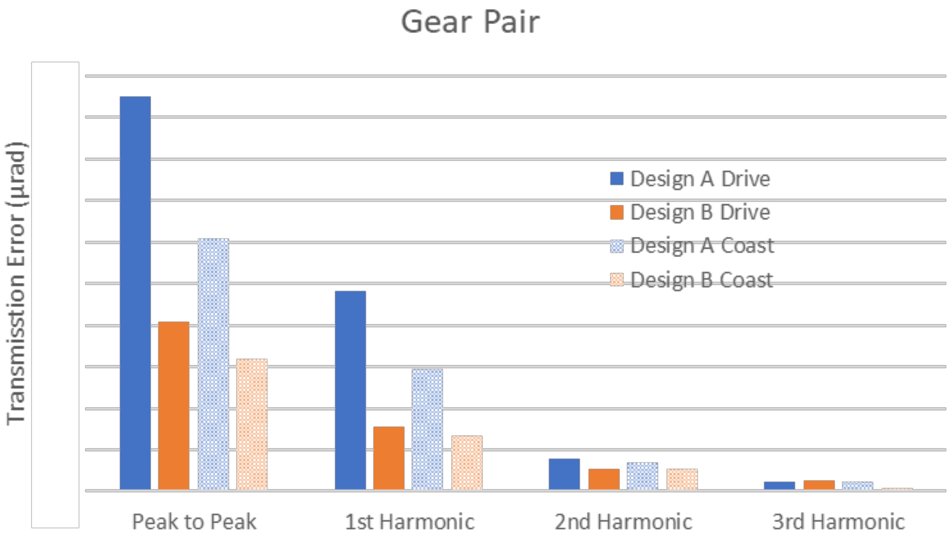

Figure 98 Transmission error of gear pair model comparison between design A and design B cases for the drive and coast conditions.

The loaded tooth contact analysis of the axle system model is performed for both drive and coast conditions. The axle system models including shafts, bearings, and housing are created in the Transmission 3D software as Figure 99 from the design SPA file and CMM surface measurement data for the design A case and design B case. The results of the contact pattern on pinion and ring gear tooth surface for the drive and coast condition are compared as Figure 100. The contact pattern of the design B case for the drive condition is more evenly distributed than the design A case and no stress concentration area. For the coast condition, the two cases are almost the same. The transmission error including the peak-to-peak value and the first third harmonics are compared and plotted in Figure 101. The design B case has transmission error reduction for drive condition, but the design A case has lower transmission error of the peak to peak value, first, and second harmonics.

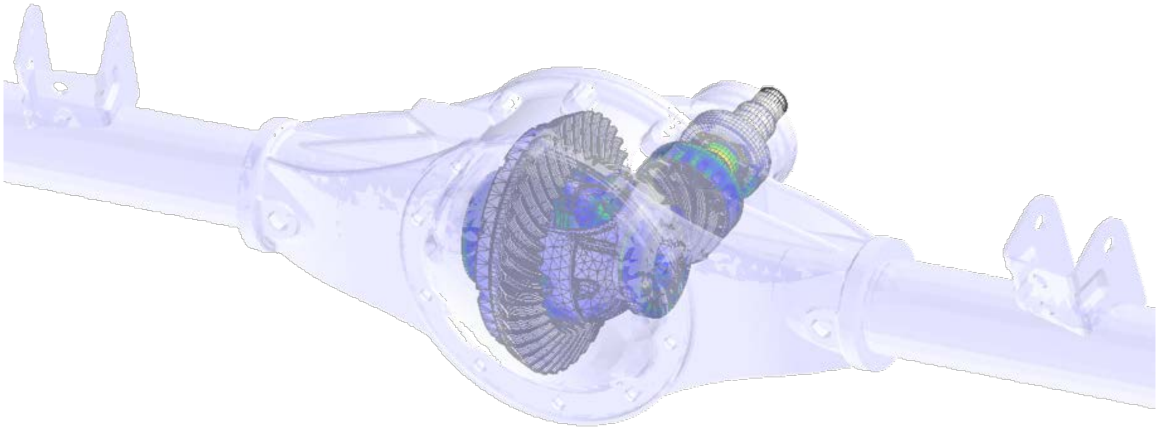

Figure 99 LTCA model for the axle system

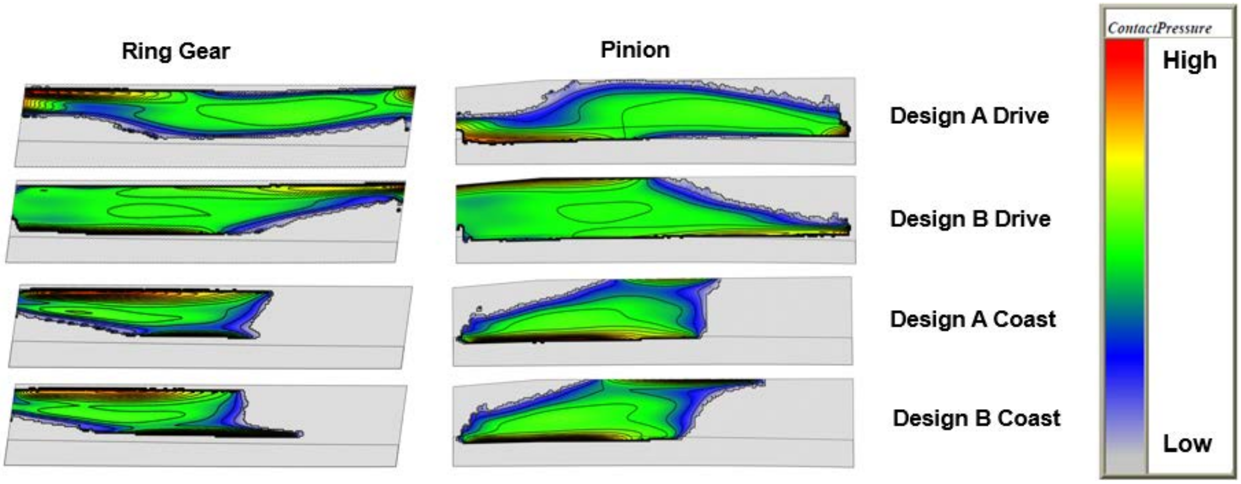

Figure 100 Axle system contact patterns comparison between design A and design B case on pinion and ring gear tooth surface for the drive and coast condition

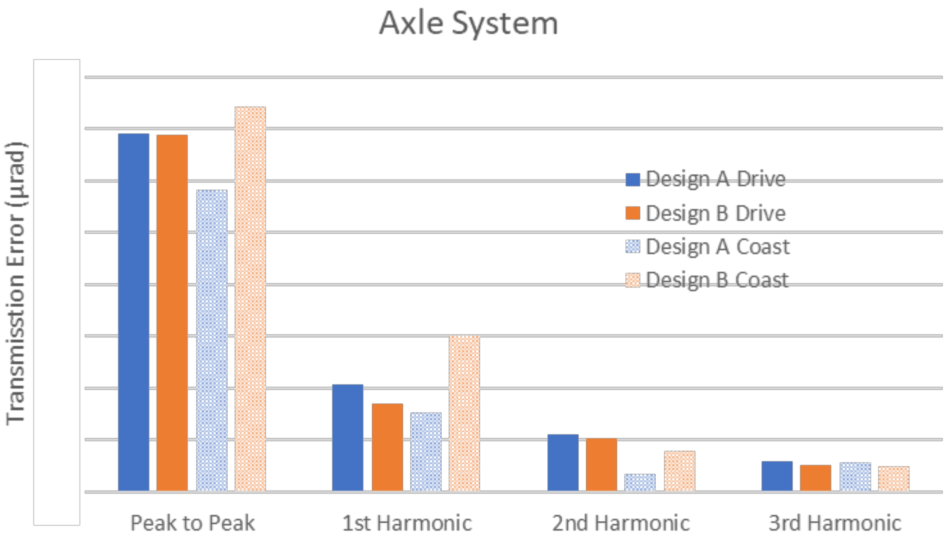

Figure 101 Transmission error of axle system model comparison between design A and design B cases for the drive and coast condition

7.4 Gear Mesh and Dynamic Results

The quasi-static LTCA results are necessary to be synthesized to the effective lumped parameter gear mesh model featuring the effective spring-damper elements to represent the gear mesh coupling in the lumped parameter dynamic analysis as Figure 102. The modeling approach has been developed and presented in previous studies. It is noted that the resultant mesh model parameters and translational TE are torque load and pinion roll angle dependent, and varying with a period of mesh cycle. The simulation is performed on 150 Nm for drive condition. The translational transmission error is compared in Figure 103. The design B case has a smaller peak to peak transmission error and variation. The mesh stiffness and the quasi-static mesh force are also compared as Figure 104 and Figure 105. The design B case also has a smaller variation for the mesh stiffness and quasi-static mesh force.

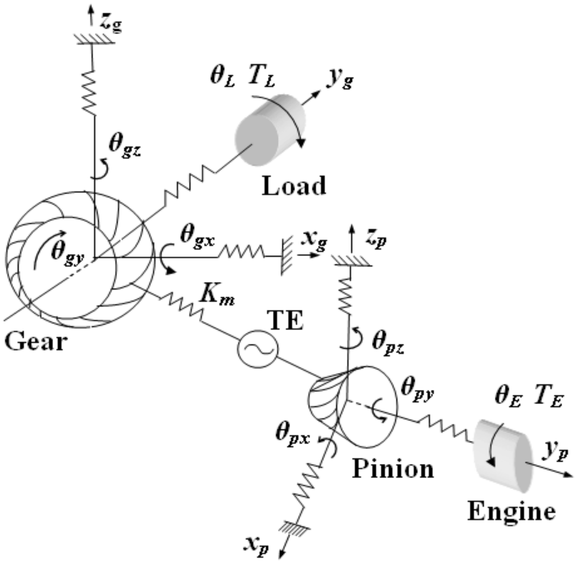

Figure 102 A lumped parameter model of the hypoid geared rotor system

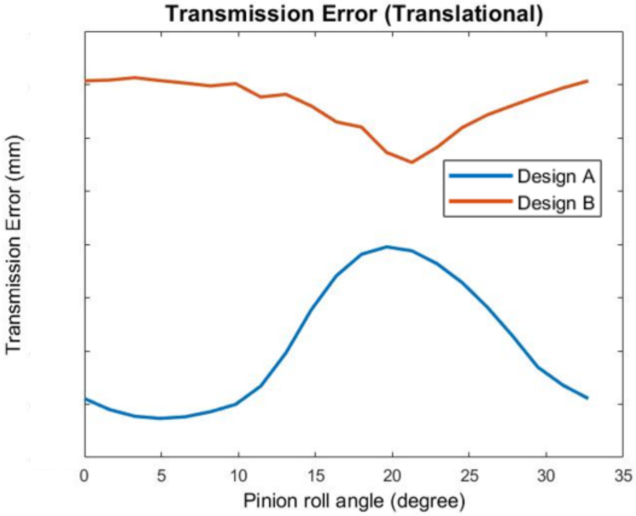

Figure 103 Time-varying translational transmission error for design A and design B cases

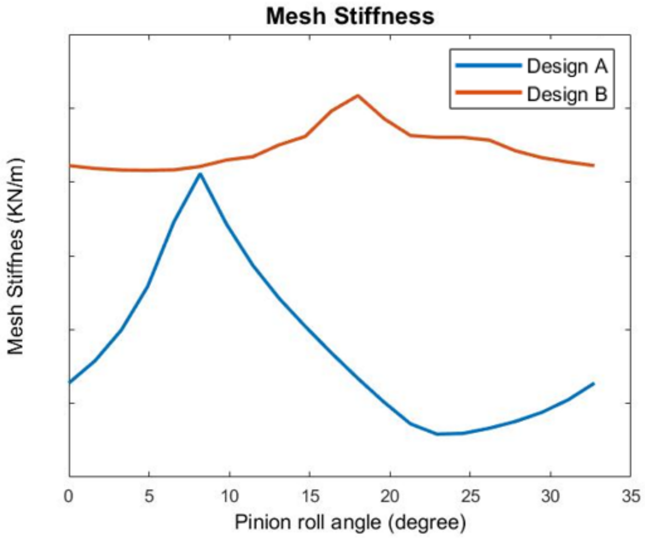

Figure 104 Time-varying mesh stiffness for design A and design B cases

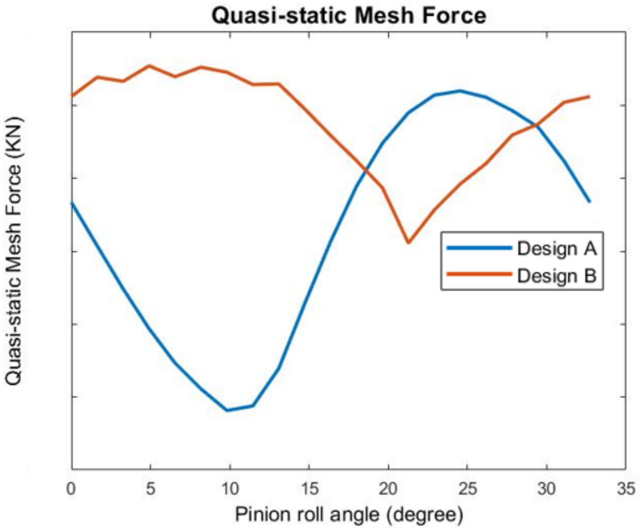

Figure 105 Time-varying quasi-static mesh force for design A and design B cases

The multi-body multi-DOF lumped parameter dynamic model of a hypoid or spiral bevel geared rotor system proposed in the previous study is directly applied. The out-of-phase gear pair torsion modes for pinion and ring gear are the main source of excitation for the geared-rotor dynamics from the previous research. The natural frequencies of out-of-phase gear pair torsion mode for design A and design B cases are compared as Figure 106. The first two peaks of gear mesh mode for the design A case are 690 and 852 Hz. The same modes for the design B case are 751 and 875 Hz because of the higher mean mesh stiffness. These natural frequencies are the main response region for the dynamic response.

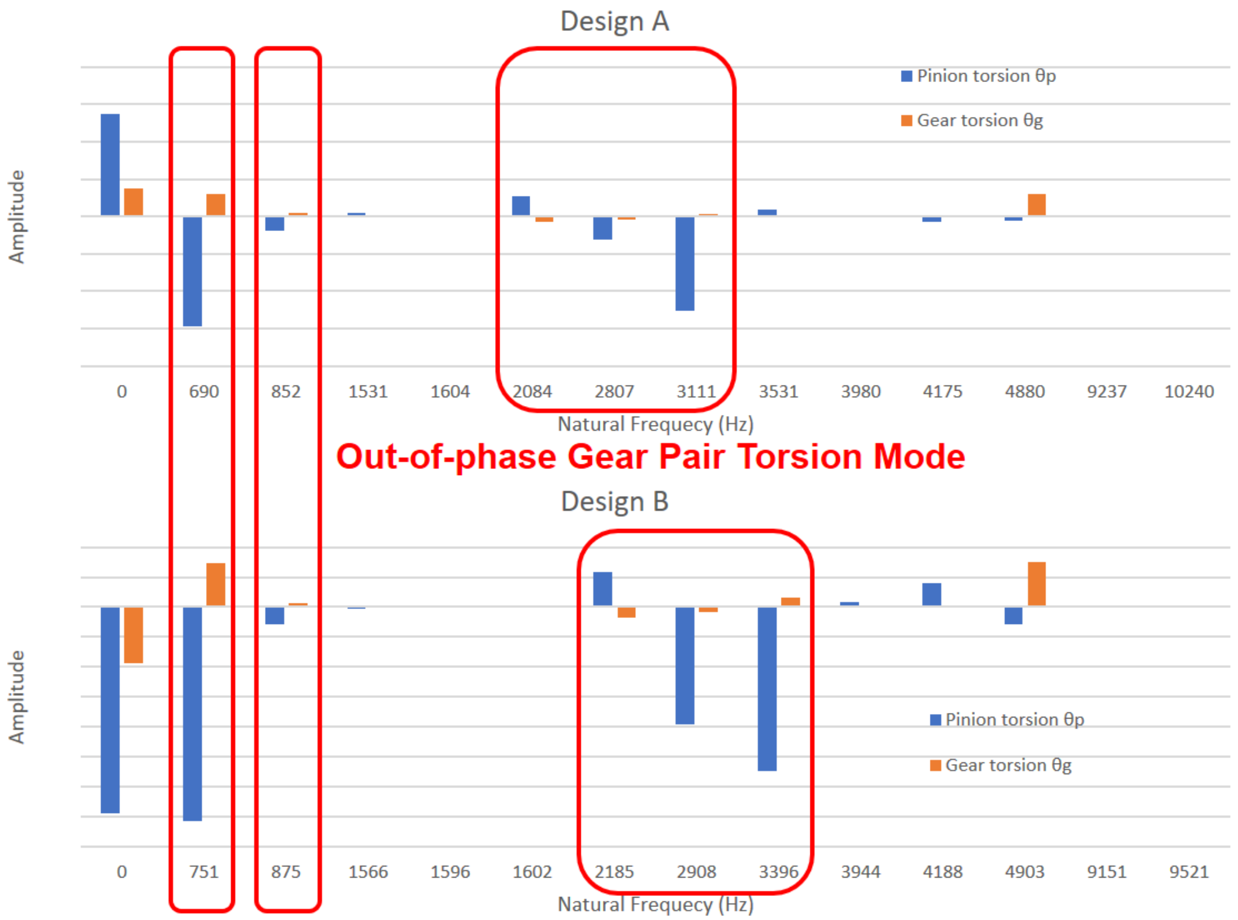

Figure 106 14 DOF gear-rotor system out-of-phase torsion mode and natural frequencies comparison for design A and design B cases

The dynamic responses of dynamic transmission error spectrum and dynamic mesh force spectrum are compared and plotted as Figure 107 and Figure 108. The design B case has a lower response both on the dynamic transmission error and dynamic mesh force for all frequency range from 50 to 4000 Hz. The first peak mode is the first gear pair torsion mode for the 14 DOF geared-rotor system around 700 Hz for design A and design B cases.

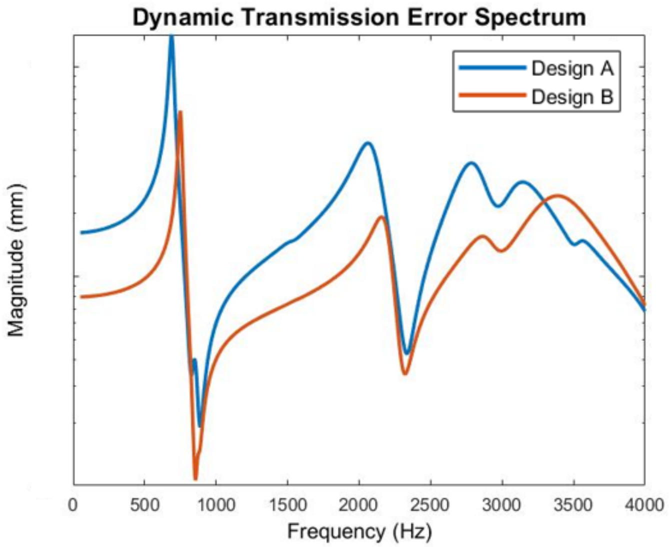

Figure 107 Dynamic transmission error spectrum for design A and design B case

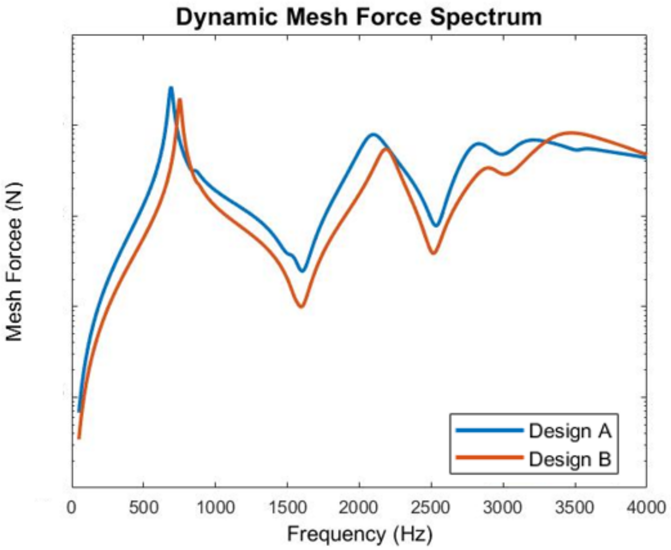

Figure 108 Dynamic mesh force spectrum for design A and design B case

The dynamic responses of dynamic bearing force spectrum at pinion and gear are compared and plotted as Figure 109 and Figure 110. The design B case has a lower response both on the dynamic bearing force spectrum at pinion and gear for all frequency range from 50 to 4000 Hz.

The first peak mode is the first gear pair torsion mode for the 14 DOF geared-rotor system around 700 Hz for design A and design B cases.

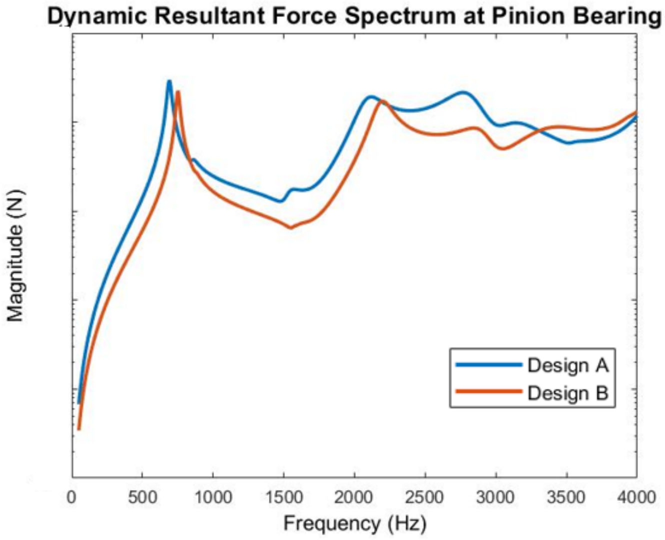

Figure 109 Dynamic bearing force spectrum at pinion bearing for design A and design B case

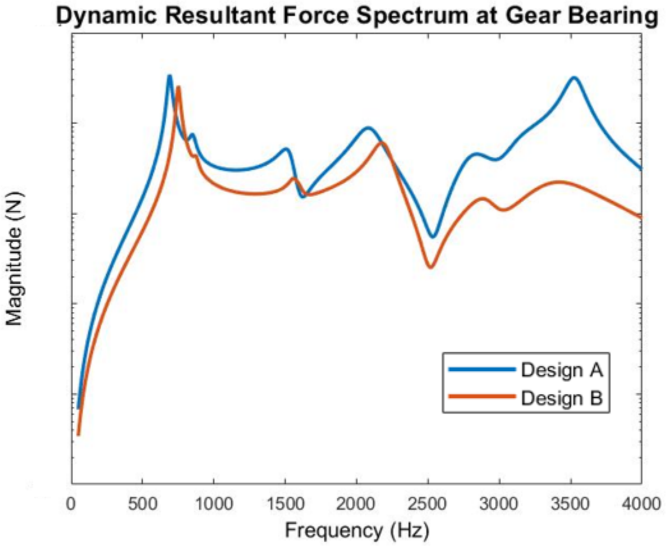

Figure 110 Dynamic bearing force spectrum at gear bearing for design A and design B case

The dynamic responses of the axle system combine all the component contributions inside the axle assembly including gear mesh, shafts, bearings, and housing. The modal analysis for the axle housing is performed to identify the structural modes on the dynamic response. The mode shapes and natural frequencies for the axle housing under 1000 Hz are shown in Figure 111. The mode with 750.07 Hz natural frequency is closed to the first gear mesh mode around 700 Hz. The dynamic response of the housing and gear mesh excitation will have a coupled reaction.

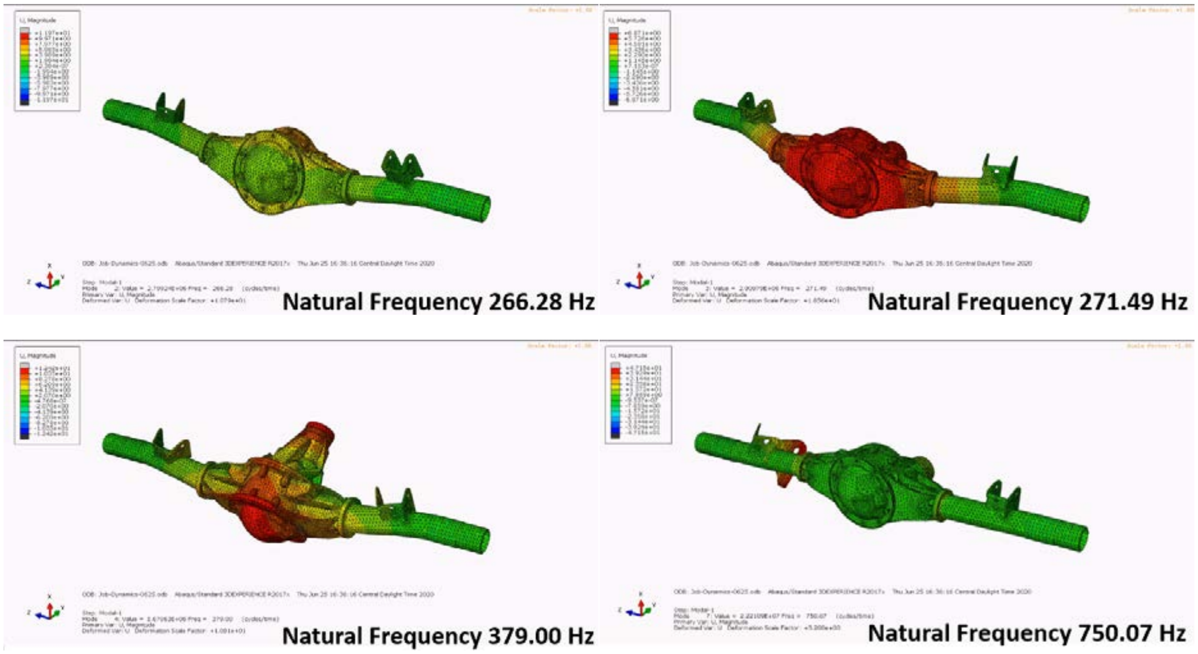

Figure 111 The mode shapes and natural frequencies for the axle housing structure

7.5 NVH Testing of vibration measurement

The NVH test is performed as the testing set in Figure 112. The test operational condition is speed sweep from 1100 to 3800 rpm with the approximate constant torque 150 Nm for the drive condition. The dynamic responses on the housing surface are measured for the design A and design B surface on the position of the bottom surface of the pinion head bearing as shown in Figure 113. The comparison node on the finite element housing model is placed in the same location. The steady-state dynamic vibration analysis is performed for both the design A and design B cases. The acceleration on the measurement point is compared for the input speed frequency range.

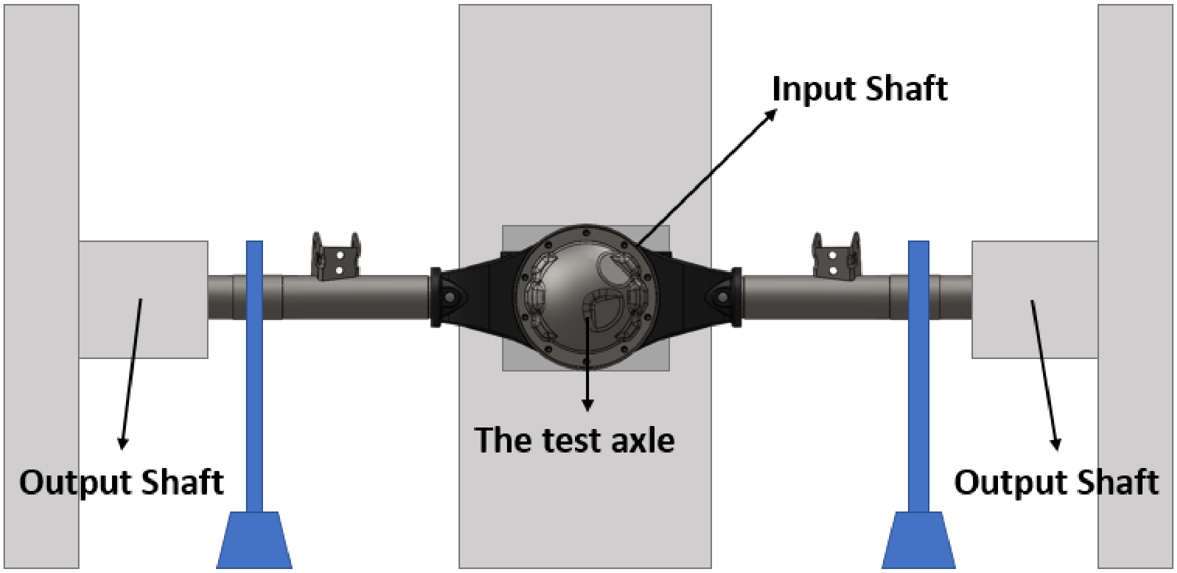

Figure 112 The axle system testing set

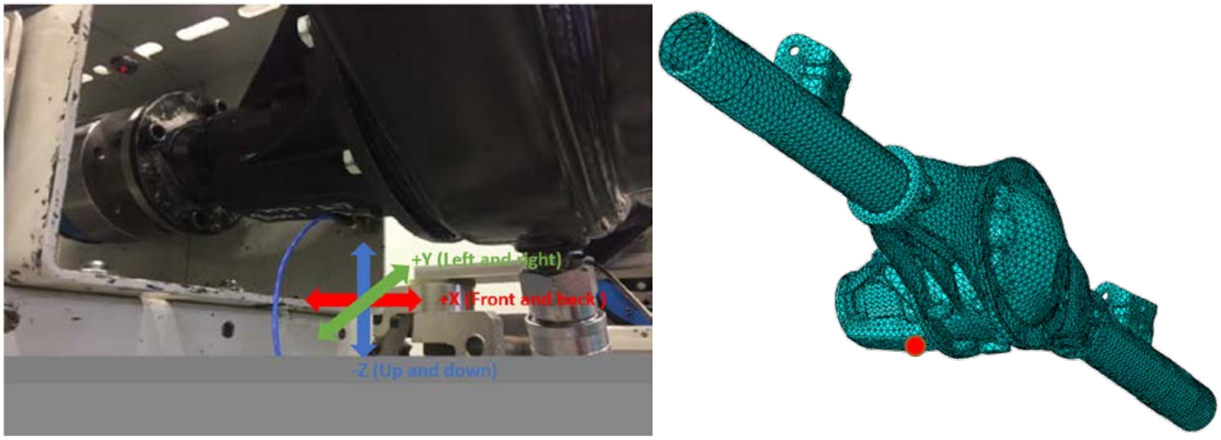

Figure 113 The position of the accelerometer on the housing bottom surface

The directions of the tri-axis accelerometer are x-direction on the front and back direction, y-direction on the left and right direction, and z-direction on the up and down as Figure 113. The results can be analyzed through the response map, frequency spectrum, Campbell plots, order tracking, etc. In the discussion, the speed sweep results from the experimental test and the dynamic simulation will be examined. The results of the accelerometer for the design A case are plotted on the waterfall plot as Figure 114 and the spectrogram as Figure 115. The mesh order excitations can be observed as the inclination lines across the frequency range from input mesh frequency from around 200 to 700 Hz as input speed sweep from 1100 to 3800 rpm. The structural modes can also be seen as the vertical lines on the specific frequency which are the fundamental frequencies for the structural modes and do not change with the speed sweep. The results of the accelerometer for the design B case are plotted on the waterfall plot as Figure 116 and the spectrogram as Figure 117.

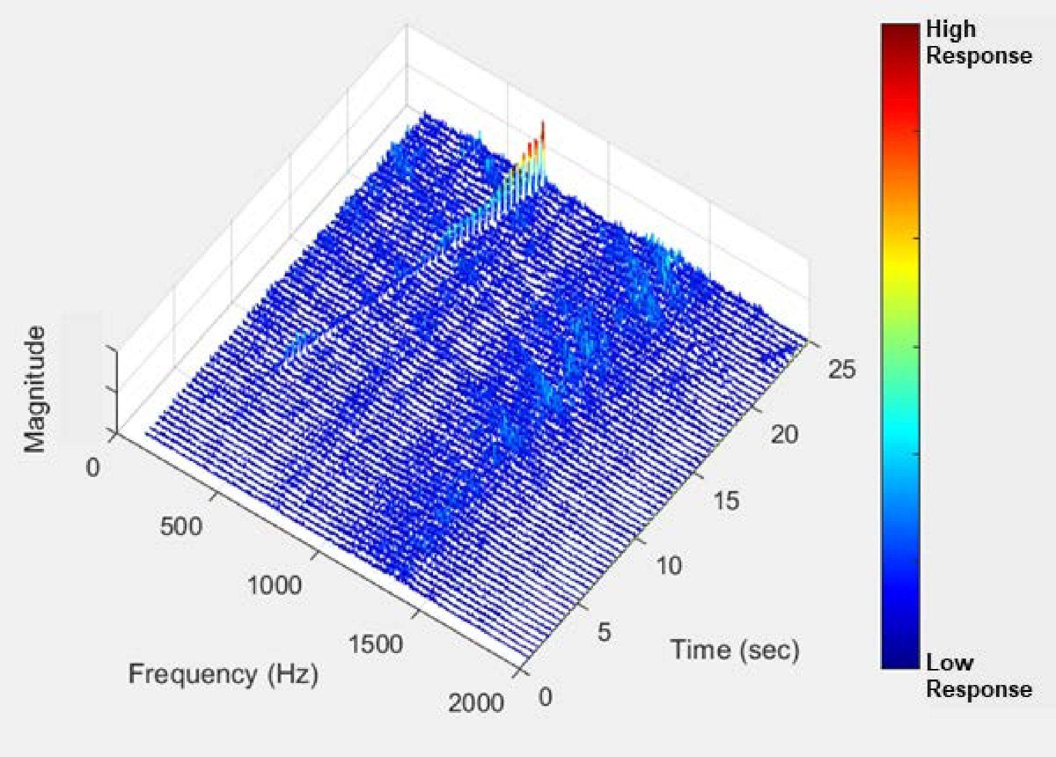

Figure 114 Waterfall plot for design A case acceleration measurement (Unit: g)

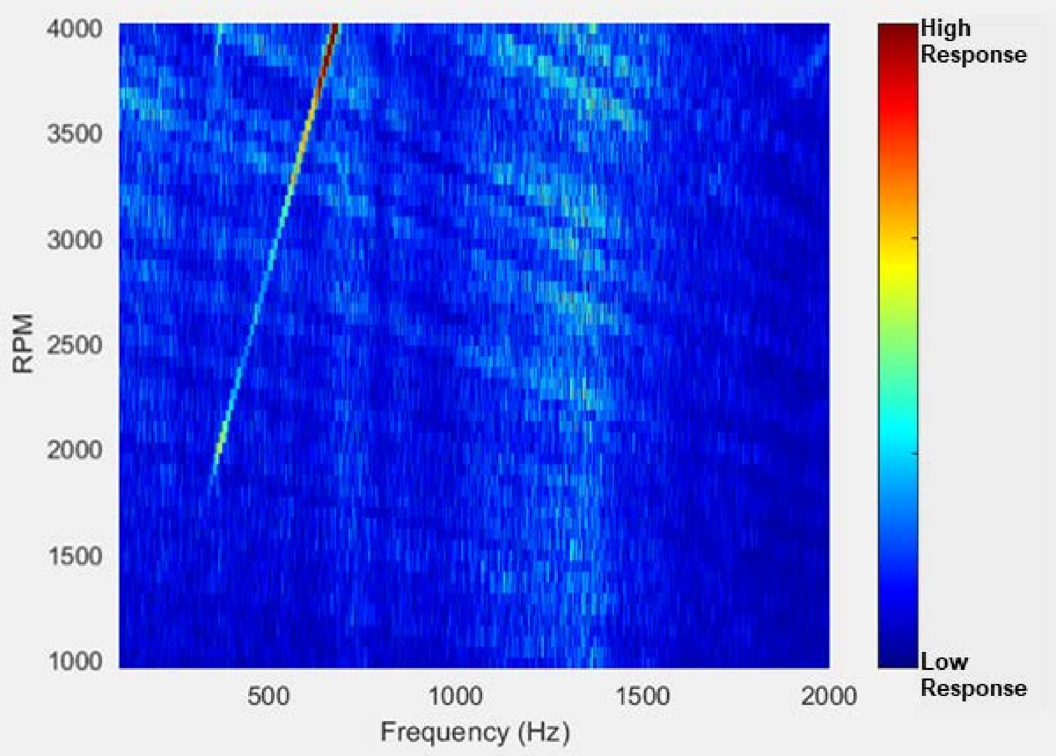

Figure 115 Spectrogram for the design A case acceleration measurement (Unit: g)

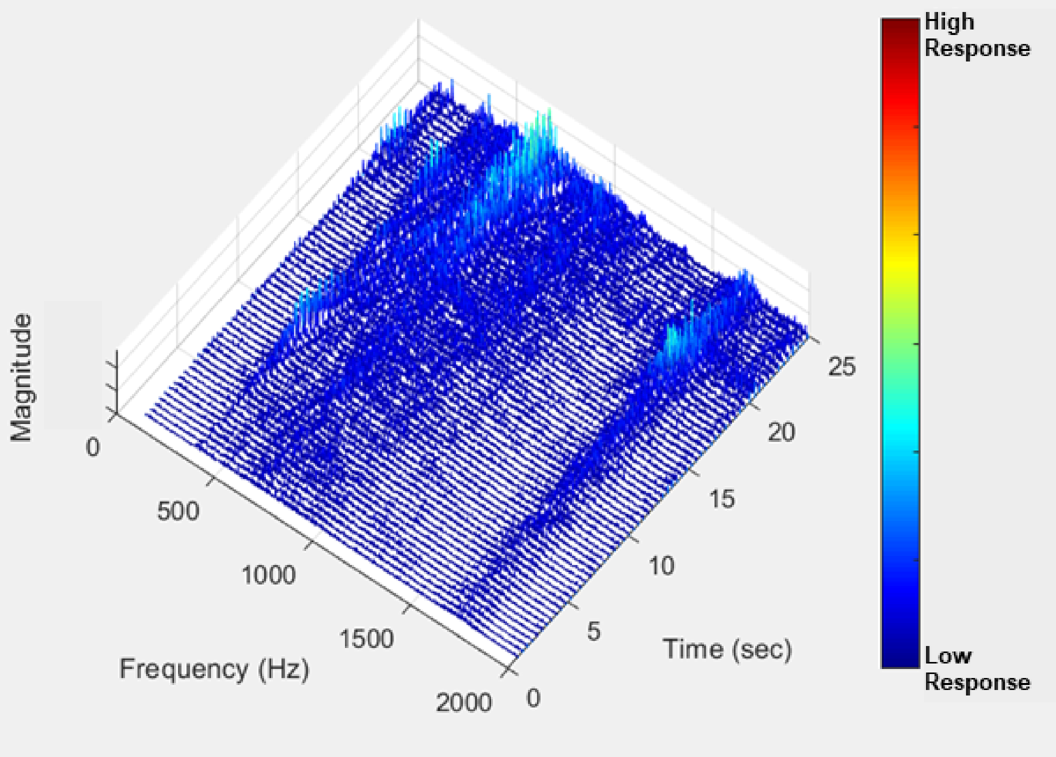

Figure 116 Waterfall plot for design B case acceleration measurement (Unit: g)

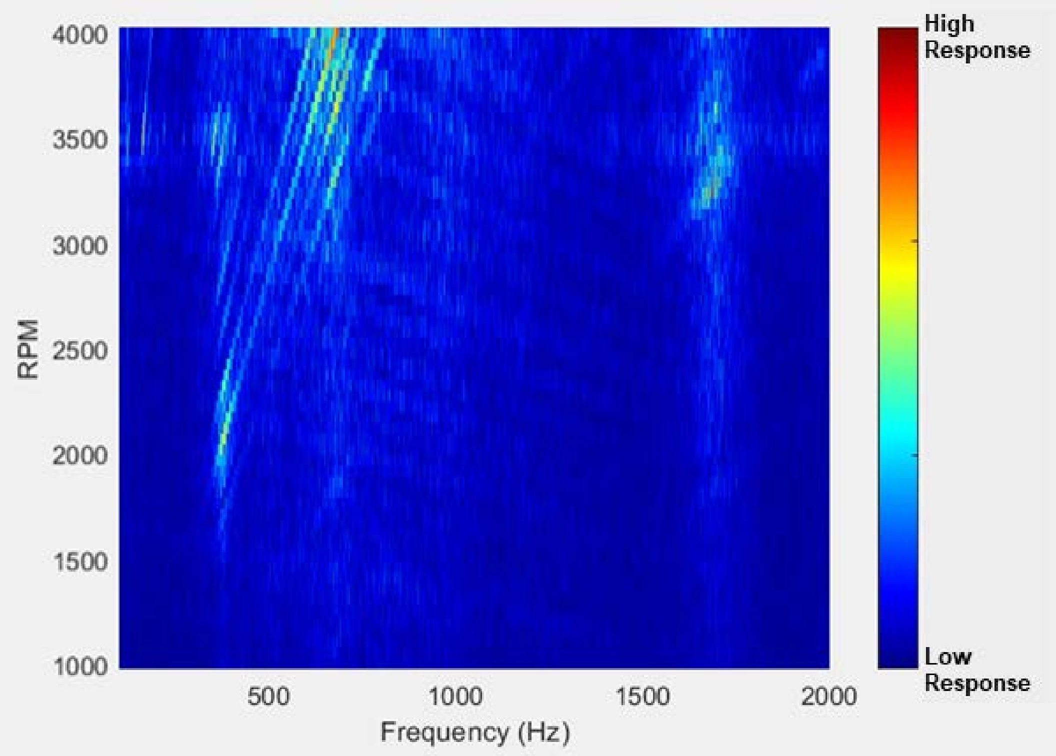

Figure 117 Spectrogram for the design B case acceleration measurement (Unit: g)

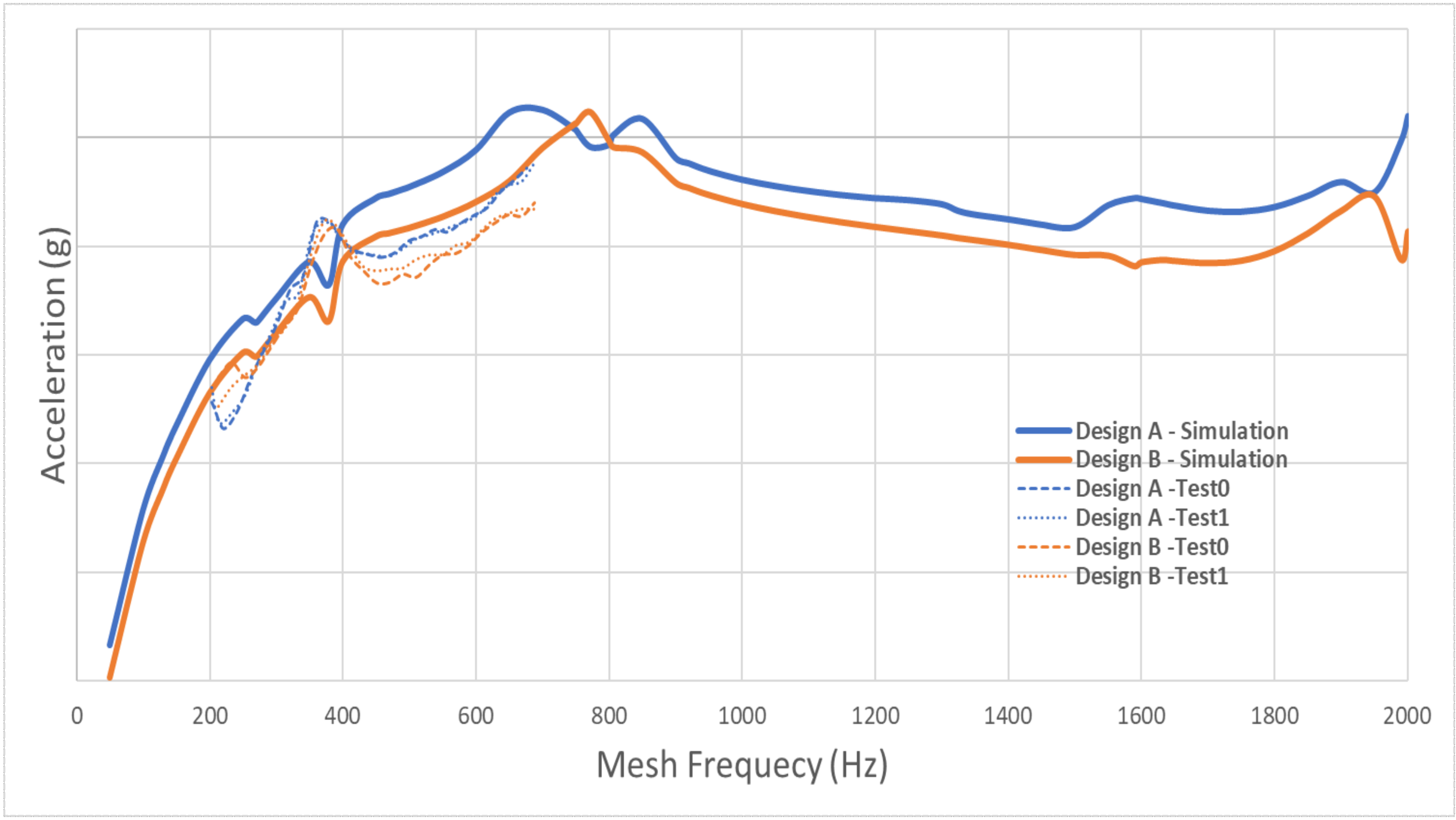

Figure 118 Comparison of acceleration response of design A and design B case between simulation and test results

The response of the acceleration magnitude for the design B case is lower than the design A case. The comparison of the acceleration response of the design A and design B case between the simulation and test results are plotted as Figure 118. Each case has two testing data that are plotted as dosh lines on the figure. The simulation is calculated from 100 to 2000 Hz while the test is performed only 200 to 700 Hz. The same trend can be observed for both simulation and test on the frequency range from 200 to 700 Hz. The reduction of the vibration can also be seen in both simulation and test results.

7.6 NVH Testing of sound pressure measurement

The test operational condition is speed sweep from 1100 to 3800 rpm with the approximate constant torque 150 Nm for the drive condition. The dynamic responses for the sound pressure are measured for the design A and design B case on five microphone positions as shown in Figure 119. Two microphones are on the upper left and lower left side. The other two microphones are on the upper center and lower center side. The last microphone is on the lower right side. The five microphones have the same distance of 0.5 m from the center of the axle. The five virtual microphones on the boundary element model are placed on the same location as Figure 120. The vibro-acoustic analysis is performed for both the design A and design B cases. The sound pressure level on the measurement point is compared for the input speed frequency range.

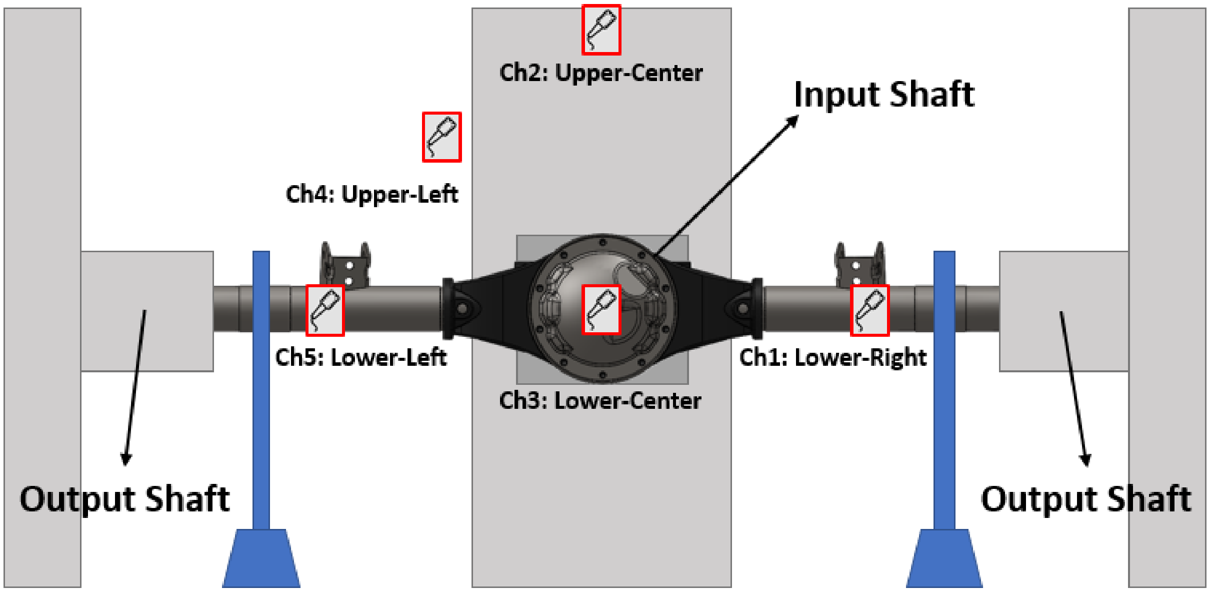

Figure 119 The microphone positions of the sound pressure measurements

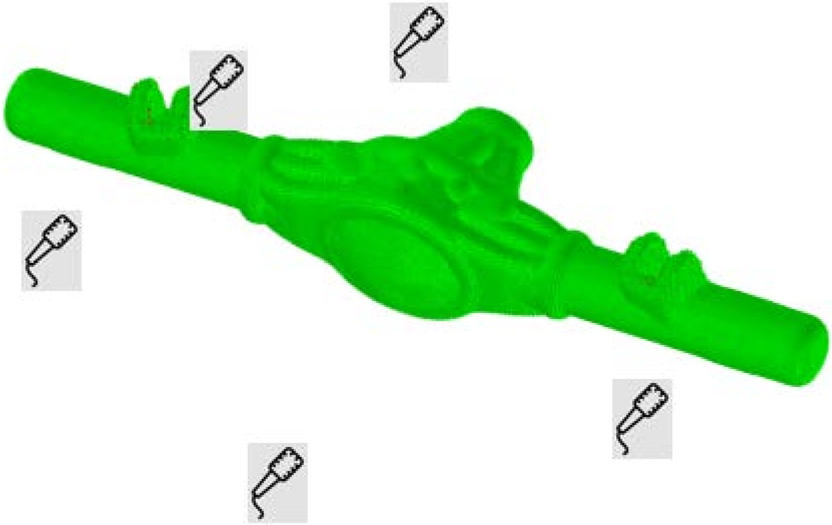

Figure 120 The virtual microphone positions (sensors) of the noise radiation simulation

The results of the averaged of five microphones for the design A case is plotted on the waterfall plot as Figure 121 and spectrogram as Figure 122. The mesh order excitations can be observed as the inclination lines across the frequency range from input mesh frequency from around 200 to 700 Hz as input speed sweep from 1100 to 3800 rpm. The structural modes can also be seen as the vertical lines on the specific frequency which are the fundamental frequencies for the structural modes and do not change with the speed sweep. The results of the averaged of five microphones for the design B case are plotted on the waterfall plot as Figure 123 and spectrogram as Figure 124.

The response of the SPL magnitude for the design B case is lower than the design A case. The comparison of the SPL response of the design A and design B case between the simulation and test results are plotted as Figure 125. Each case has two testing data that are plotted as dosh lines on the figure. The simulation is calculated from 100 to 2000 Hz while the test is performed only 200 to 700 Hz. The same trend can be observed for both simulation and test on the frequency range from 200 to 700 Hz. The reduction of the noise level can also be seen in both simulation and test results.

The sound pressure distribution on the axle housing surface and the far-field sphere surface of the 1-meter radius is shown in Figure 126 and Figure 127. The design B case has better noise performance on both the axle surface and far-field sphere surface for sound pressure distribution.

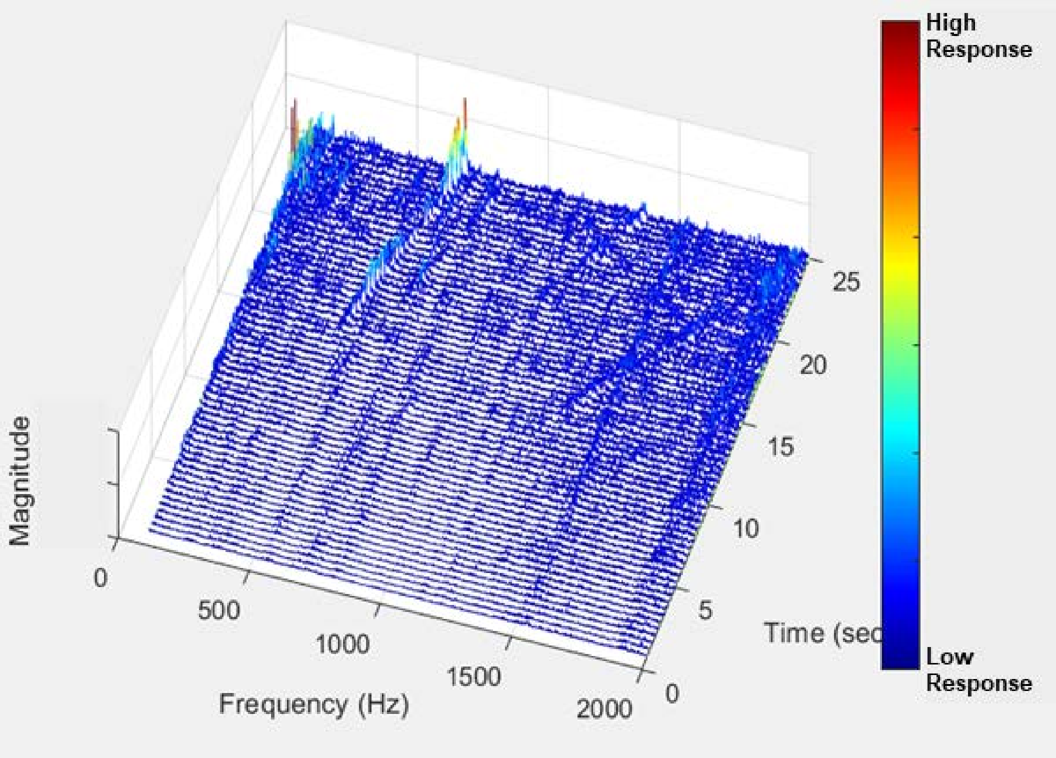

Figure 121 Waterfall plot for design A case sound pressure measurement (Unit: Pa)

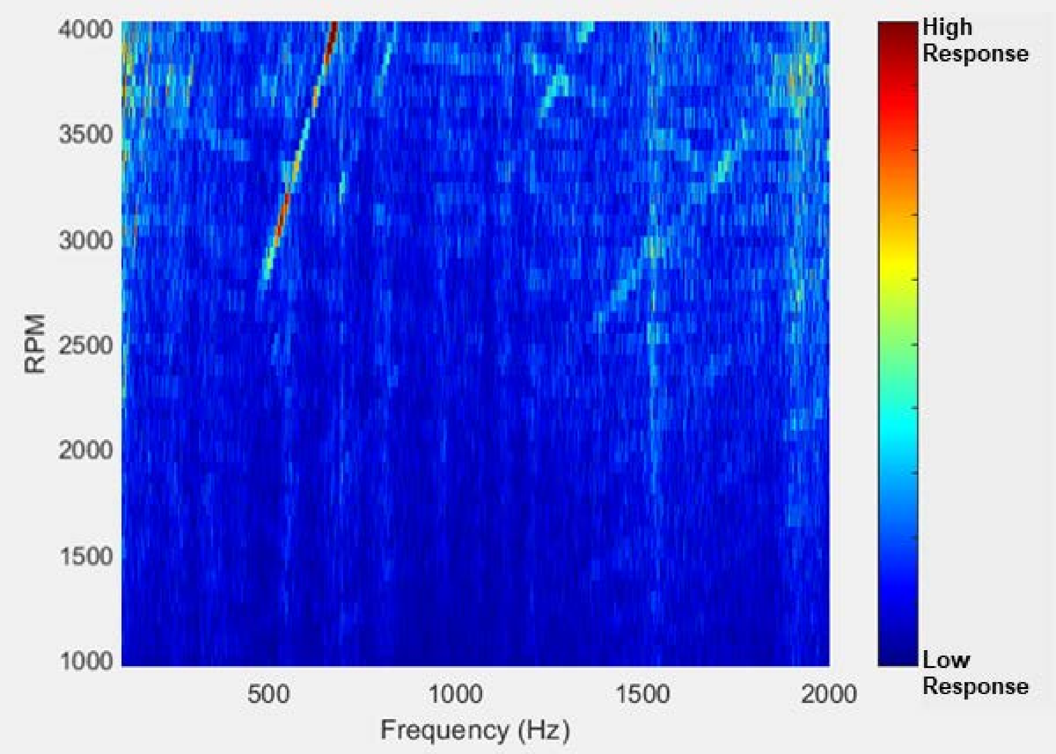

Figure 122 Spectrogram for the design A case sound pressure measurement (Unit: Pa)

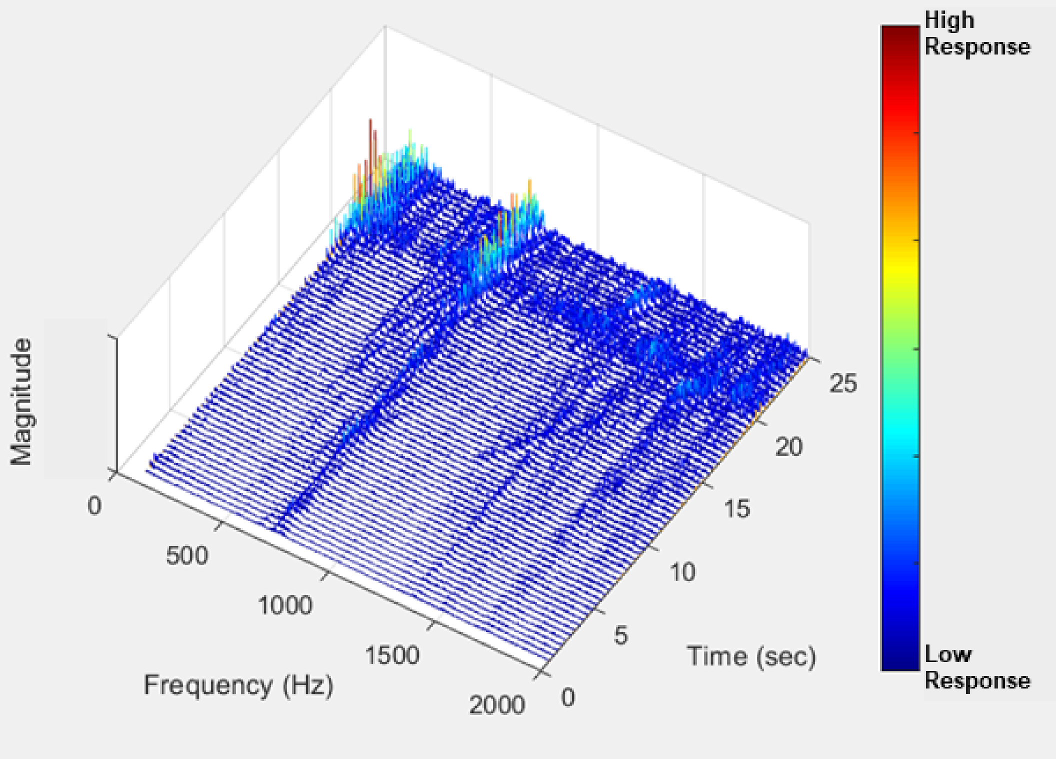

Figure 123 Waterfall plot for design B case sound pressure measurement (Unit: Pa)

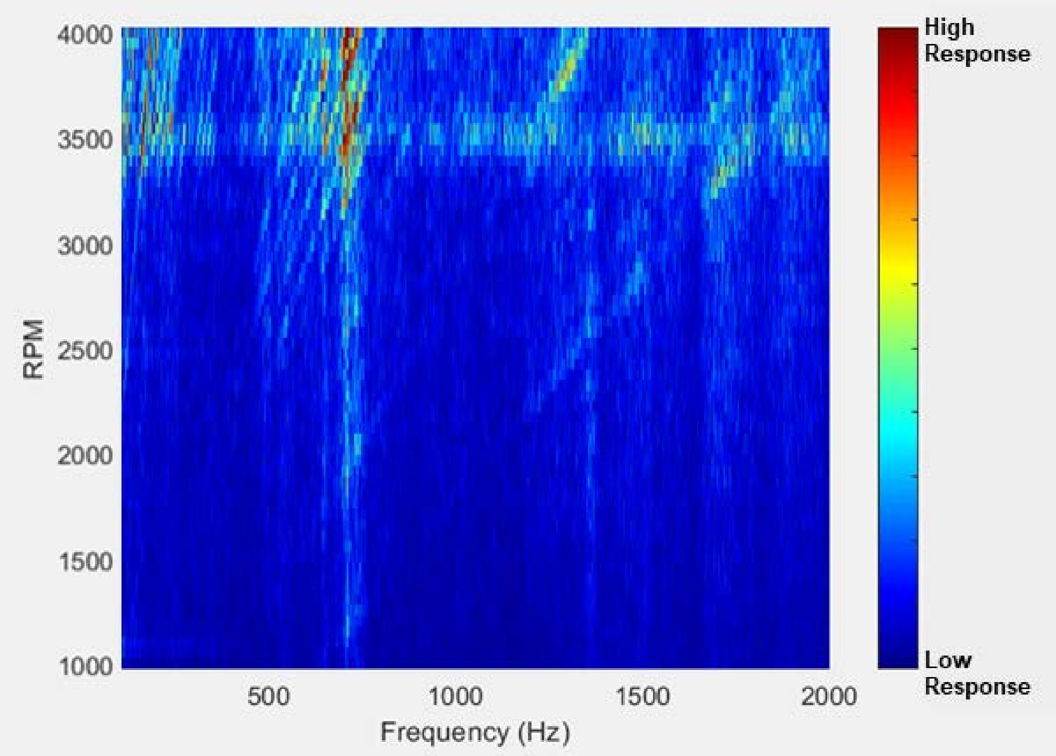

Figure 124 Spectrogram for the design B case sound pressure measurement (Unit: Pa)

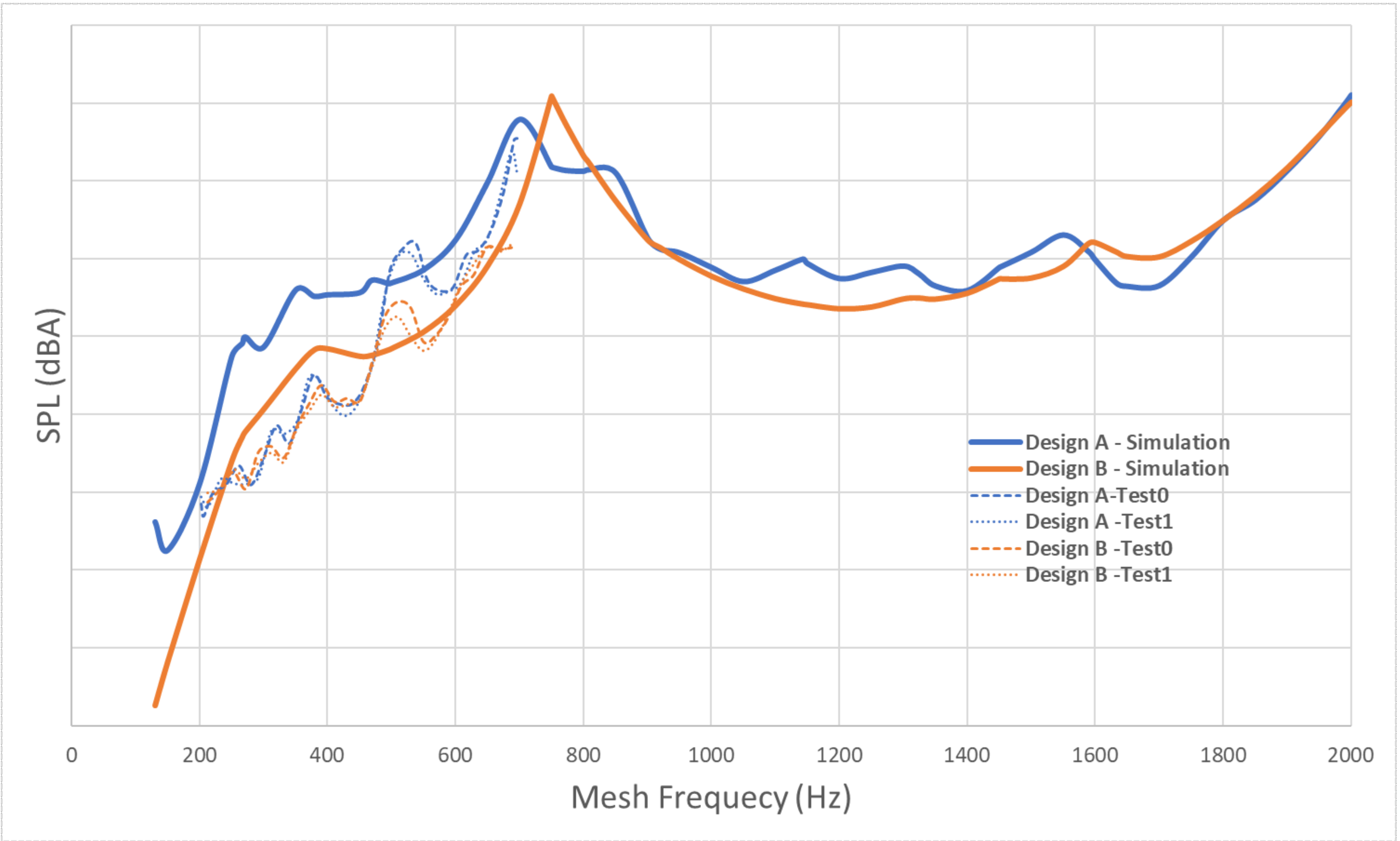

Figure 125 Comparison of SPL response of design A and design B case between simulation and test results

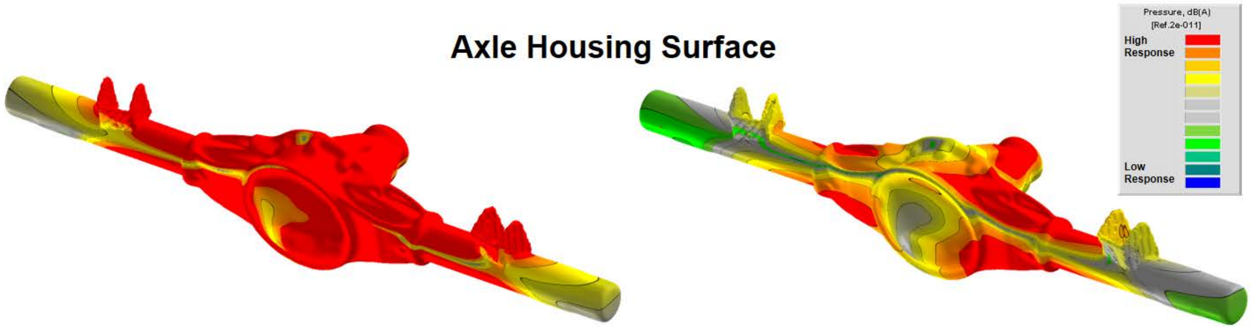

Figure 126 Sound pressure distribution on the axle housing surface for the design A and design B case

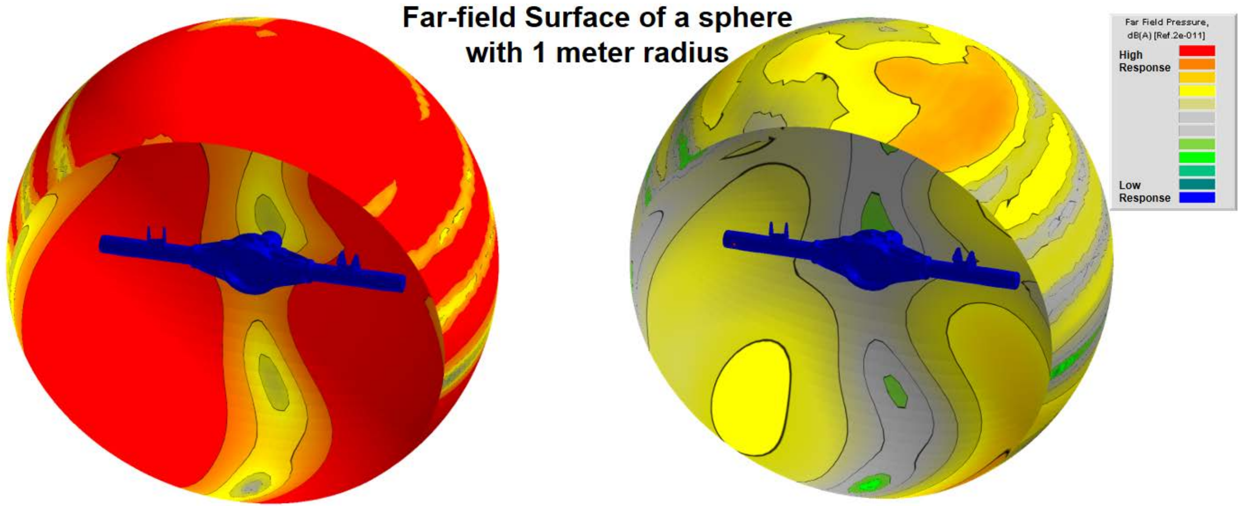

Figure 127 Sound pressure distribution on the far-field sphere surface with a 1-meter radius for the design A and design B

7.7 Conclusion

The end to end simulation approach is applied to the real axle product design process. The axle system model for the tooth contact analysis, geared-rotor dynamic analysis, steady-state housing vibration analysis, and vibro-acoustic analysis are developed. The relevant gear static and dynamic experiments have been set up and performed to generate the necessary data to guide and validate simulation models. The single flank test for gear pair and the NVH test for vibration and sound pressure measurements are compared between the simulation and test results. The design B case with the ease-off modification has a better performance on the noise and vibration on both simulation and testing results. The experimental validation is partial but still adds great confidence to the previous analytical studies.

Chapter 8 Conclusion

8.1 Summary

In this study, the effect of optimal tooth profile modification on the vehicle axle system is discussed. An approach with IPSO-BP neural network algorithm to obtain minimum transmission error and improved dynamic response with optimal tooth profile modification parameters is presented. A case study of a hypoid gear pair with specified design parameters and working condition is calculated and compared with optimized TPM cases. The results revealed that by using tooth profile modifications obtained through the proposed method, the following improvements can be identified when compared to the baseline case:

1) Lower maximum contact pressure contributed by the prevention of edge contact situations, which is the main cause of stress concentration.
2) Reduction of the variance of zero-to-peak transmission error, which is the source of vibration in the axle system.
3) An overall decrement in the magnitude of dynamic responses, including dynamic transmission error, dynamic mesh force, and dynamic bearing resultant force, that are commonly used to evaluate the vibration response in system dynamics.
4) A comprehensive approach to analyze noise and vibration response of the rear axle

system is proposed.

5) A robust method with the neural network model and ease-off modification to optimize the gear design parameters and noise performance are proposed.
6) The methodology is validated with experimental data.

The results conclude that optimal tooth profile modification parameters acquired by minimizing TE can improve the overall NVH behavior. The proposed approach provides a better understanding of the effects of optimal tooth profile modification on vehicle axle system dynamics.

8.2 Conclusions

- The contact characteristics of the hypoid gear pairs have considerable influence on the NVH performance of the rear axle system.
- The surface velocity and noise pressure distribution on the housing surface are reduced by the proposed model.
- An end-to-end simulation solution can be provided to the gear designers and NVH engineers to have a closed-loop design process for the rear axle systems.

Reference

1. Qatu, M.S., “Recent research on vehicle noise and vibration.” *Int. J. Vehicle Noise and Vibration*, Vol. 8, No. 4: pp. 289 – 301, 2012.
2. Qatu, M.S., Abdelhamid, M.K., Pang, Jian, and Sheng, Gang, “Overview of automotive noise and vibration.” *Int. J. Vehicle Noise and Vibration*, Vol. 5**,** No. 1/2: pp. 1 – 35, 2009.
3. Wang, Y., Li, X., Qiao, G., and Lim, T., "Effect of Component Flexibility on Axle System Dynamics," *SAE Int. J. Veh. Dyn., Stab., and NVH*, 1(2), 2017, doi:10.4271/2017-01-1772.
4. Wang, Y. "Vibration and Sound Radiation Analysis of Vehicle Powertrain Systems with Right-Angle Geared Drive." Ph.D. diss., University of Cincinnati, 2017.
5. Wang, Y., Yang, J., Li, X., Sun, G. et al., "Interaction of Gear-Shaft Dynamics Considering Gyroscopic Effect of Compliant Driveline System," *SAE Int. J. Passeng. Cars - Mech. Syst.*, 8(2), 2015, doi:10.4271/2015-01-2182.
6. Chen, Z., and Shao, Y., "Mesh stiffness calculation of a spur gear pair with tooth profile modification and tooth root crack." *Mechanism and Machine Theory*, 62: 63-74, 2013.
7. Simon, V., "Optimization of face-hobbed hypoid gears." *Mechanism and Machine Theory*, 77: 164-181, 2014.
8. Simon, V., "Optimal Machine Tool Settings for the Manufacture of Face-Hobbed Spiral Bevel Gears," *Journal of Mechanical Design*, Vol. 136, 081004:1-8, 2014.
9. Simon, V., "Influence of tooth modifications on tooth contact in face-hobbed spiral bevel gears." *Mechanism and machine theory* 46, no. 12: 1980-1998, 2010.
10. Simon, V., "Head-cutter for optimal tooth modifications in spiral bevel gears." *Mechanism and Machine Theory*, 44, no. 7: 1420-1435, 2009.

11. Simon, V. "Design and manufacture of spiral bevel gears with reduced transmission errors." *Journal of Mechanical Design,* 131, no. 4, 041007:1-11, 2009.
12. Simon, V., "Optimal tooth modifications in hypoid gears." *Journal of Mechanical Design,* 127, no. 4: 646-655, 2005.
13. Simon, V., "Optimal machine tool setting for hypoid gears improving load distribution." *Journal of Mechanical Design,* 123, no. 4: 577-582, 2001.
14. Shih, Y., "A novel ease-off flank modification methodology for spiral bevel and hypoid gears." *Mechanism and Machine Theory,* 45, no. 8: 1108-1124, 2010.
15. Shih, Y., and Fong Z., "Flank modification methodology for face-hobbing hypoid gears based on ease-off topography." *Journal of Mechanical Design,* 129, no. 12: 1294-1302, 2007.
16. Fan, Q., Ronald D., and John S., "Higher-order tooth flank form error correction for face-milled spiral bevel and hypoid gears." *Journal of Mechanical Design,* 130, no. 7, 072601:1-7, 2008.
17. Mu, Y., Li, W., Fang Z., and Zhang X., "A novel tooth surface modification method for spiral bevel gears with higher-order transmission error." *Mechanism and Machine Theory,* 126: 49-60, 2018.
18. Litvin, F.T. and Gutman, Y., “Methods of Synthesis and Analysis for Hypoid Gear-Drives of “Formate” and “Helixform” Part 1-3.” Journal of Mechanical Design, Vol. 103 (1981): pp. 83-113.
19. Yu, W., Chris M., and Markus T., "Influence of the addendum modification on spur gear back-side mesh stiffness and dynamics." *Journal of Sound and Vibration,* 389: 183-201, 2017.

20. Ghosh, S., and Chakraborty G., "On optimal tooth profile modification for reduction of vibration and noise in spur gear pairs." *Mechanism and Machine Theory,* 105: 145-163, 2016.
21. Ma, H., Pang, X., Feng, R., and Wen, B., "Evaluation of optimum profile modification curves of profile shifted spur gears based on vibration responses." *Mechanical Systems and Signal Processing,* 70: 1131-1149, 2016.
22. Hu, Z., Tang, J., Zhong, J., Chen, S., et al., "Effects of tooth profile modification on dynamic responses of a high speed gear-rotor-bearing system." *Mechanical Systems and Signal Processing,* 76: 294-318, 2016.
23. Xun, C., Long, X., and Hua, H., "Effects of random tooth profile errors on the dynamic behaviors of planetary gears." *Journal of Sound and Vibration,* 415: 91-110, 2018.
24. Bahk, C., and Parker, R. "Analytical investigation of tooth profile modification effects on planetary gear dynamics." *Mechanism and machine theory,* 70: 298-319, 2013.
25. Sun, S, Wang, S., Wang, Y., Lim, T. et al. "Optimization of hypoid gear design and tooth contact analysis." Proceedings of the ASME 2017 International Design Engineering Technical Conferences and Computers and Information in Engineering Conference IDETC/CIE 2017. 2017. August 6-9, 2017, Cleveland, Ohio, USA.
26. Peng, T. "Coupled multi-body dynamic and vibration analysis of hypoid and bevel geared rotor system." Ph.D. diss., University of Cincinnati, 2010.
27. Vijayakar, S., and Abad, S., "Hypoid Face Milled User's Manual." *Advanced Numerical Solutions LLC,* 2003.
28. Vijayakar, S. "A combined surface integral and finite element solution for a three-dimensional contact problem." *International Journal for Numerical Methods in Engineering,* 31, no. 3: 525-545, 1991.

29. Guo, Y., Eritenel, T., Ericson, T. M. and Parker, R. G., "Vibro-acoustic propagation of gear dynamics in a gear-bearing-housing system," Journal of Sound and Vibration, 333(22), pp. 5762-5785, 2014.
30. Gunda, R., "Boundary element acoustics and the fast multipole method (FMM)," Sound and Vibration, 42(3), pp. 12, 2008.
31. Liu, S., Song, C., Zhu, C., Liang, C., Yang, X., "Investigation on the influence of work holding equipment errors on contact characteristics of face-hobbed hypoid gear." *Mechanism and Machine Theory*, Vol.138 (2019): pp.95-111.
32. Kolivand, M., Kahraman, A.," A load distribution model for hypoid gears using ease-off topography and shell theory." *Mechanism and Machine Theory*, Vol.44 (2009): pp.1848-1865.
33. Kolivand, M.," Development of tooth contact and mechanical efficiency models for face-milled and faced-hobbed hypoid and spiral bevel gears" Ph.D. diss., The Ohio State University, 2009.
34. W. Zhang, Y. Wang, C.-C. Lin, T.C. Lim, et al., "Improvement of Hypoid Gears Dynamics Performance Based on Tooth Contact Optimization," Proceedings of the SAE Noise and Vibration Conference and Exposition, Grand Rapids, Michigan, Paper 2019-01-1563.
35. C.-H. Chung, G. Steyer, T. Abe, M. Clapper, C. Shah, "Gear Noise Reduction through Transmission Error Control and Gear Blank Dynamic Tuning", SAE Transactions Vol. 108, SECTION 6: *JOURNAL OF PASSENGER CARS*, PART 2 (1999), pp. 2829-2837.
36. Z. Sun, G. Steyer, G. Meinhardt, M. Ranek, "NVH Robustness Design of Axle Systems", SAE Transactions Vol. 112, Section 6: *JOURNAL OF PASSENGER CAR: MECHANICAL SYSTEMS JOURNAL* (2003), pp. 1746-1754.

37. Lee, S., Go, S., Yu, D., Lee, J. et al., "Identification and Reduction of Gear Whine Noise of the Axle System in a Passenger Van," SAE Technical Paper 2005-01-2302, 2005, https://doi.org/10.4271/2005-01-2302.
38. DeSantis, A.,” Understand single flank testing” The Gleason Works.